A DAMAGE MECHANICS APPROACH TO THE THREE DIMENSIONAL CONSTITUTIVE MODELLING OF ICE DEFORMATION

by

KYUNGSIK CHOI

B.S. in Naval Architecture
Seoul National University, KOREA (1980)

M.S. in Naval Architecture
Seoul National University, KOREA (1983)

Submitted to the Department of
Ocean Engineering
in Partial Fulfillment of the Requirements
for the Degree of

DOCTOR OF PHILOSOPHY

at the

MASSACHUSETTS INSTITUTE OF TECHNOLOGY

February 1989

Signature of Author: _____
Department of Ocean Engineering
October 28, 1988

Certified by: _____
Dale G. Karr
Associate Professor, Ocean Engineering
Thesis Supervisor

Accepted by: _____
A. Douglas Carmichael
Chairman, Departmental Committee
on Graduate Students

A DAMAGE MECHANICS APPROACH TO THE THREE DIMENSIONAL CONSTITUTIVE MODELLING OF ICE DEFORMATION

by

KYUNGSIK CHOI

Submitted to the Department of Ocean Engineering
on Oct. 28, 1988, in partial fulfillment of the requirements
for the Degree of Doctor of Philosophy

ABSTRACT

Uncertainties in existing ice models come primarily from the incomplete modelling of the deformation behavior of ice in various loading states. In this study constitutive equations characterizing microcrack damage behavior of polycrystalline ice are developed based on continuum damage mechanics. The principal goal of the thesis is the formulation of a three dimensional damage model for the description of ice deformation, where damage evolution is formulated on the basis of a mathematical description of the physical aspects of microcracking.

The specific objectives include: 1)Development of rate-dependent constitutive equations describing ice deformation for uniaxial and multiaxial stress states. Total strain is composed of three components, instantaneous elastic, delayed elastic and viscous strain. Each strain component is incorporated with material damage growth through a damage parameter. The mathematical nature of damage parameter is selected as a tensor based on the anisotropic behavior of microcrack fields. 2)Development of a physically based damage model associated with two microcracking mechanisms, grain boundary and transgranular cracking. The main contribution of the thesis lies in the formulation of damage evolution laws where the damage growth rate is expressed by resolved normal strain, normal stress, and strain-rate for each damage mechanism.

Applications are directed to constant stress and constant strain-rate tests under uniaxial, biaxial, and confining pressure conditions. Cyclic behavior is also examined. The constitutive modelling is compared with available experimental results. The model is capable of predicting several important features of ice deformation behavior over a wide range of deformation regimes. The difference in tensile and compressive behavior and damage induced anisotropy can be predicted.

Thesis Supervisor: Prof. Dale G. Karr

Title: Associate Professor of Ocean Engineering

Acknowledgements

I would like to express my deep gratitude to Professor Dale G. Karr, the chairman of my thesis committee for his encouragement and advice through my graduate work. He provided me an opportunity for studying this rare field of ice mechanics and showed a great patience during the course of this work. I am truly indebted.

I also would like to thank Professor T. Wierzbicki, Professor S. Shyam Sunder and Professor D.M. Parks for their invaluable comments and recommendations which improved this thesis a lot.

Thanks are given to the Ministry of Education of Korea whose Government Scholarship made it possible for me to study at M.I.T. This research was partly supported by the Office of Naval Research Grant. I appreciate their interest and financial support.

Finally I would like to make special thanks to my family and colleagues for their encouragement and friendship throughout my stay at M.I.T. Thank you.

Table of Contents

Abstract 2

Acknowledgements 3

Table of Contents 4

List of Figures 7

Notations 10

Chapter 1 Introduction 13

1.1 Background 13

1.2 Objectives of the Research 14

1.3 Organization 19

Chapter 2 Review of Ice Properties 20

2.1 Formation and Types of Ice 20

2.1.1 Fresh Water Ice 21
2.1.2 Sea Ice 22
2.1.3 Glaciers and Icebergs 23

2.2 Mechanical Properties of Ice 23

2.2.1 Elastic Moduli and Poisson's Ratio 24
2.2.2 Failure Strength 25

2.3 Deformation and Failure Mechanisms 27

2.3.1 Constant Strain-rate Deformation 28
2.3.2 Constant Stress Deformation 28

Chapter 3 Literature Survey 33

3.1 A Review of Continuum Damage Models 33

3.1.1 Scalar Damage Models 35
3.1.2 Vectorial Damage Models 41
3.1.3 Tensorial Damage Models 44

3.2 A Review of Continuum Damage Theory in Ice Modelling 48

Chapter 4 Modelling of Ice Deformation 51

4.1 Ice Modelling without Damage Description 51

4.2 Material Damage 53

4.2.1 Basic Concepts 53
4.2.2 Microcrack Systems 57
4.2.3 Measure of Damage 61

4.3 Continuum Damage Mechanics 63

4.3.1 Theory of Internal Variables 63
4.3.2 Thermodynamic Restrictions 65
4.3.3 Helmholtz Free Energy Function 68

4.4 Multiaxial Deformation Modelling 72

4.4.1 Delayed Elastic Strain 72
4.4.2 Viscous Strain 76

4.5 Damage Evolution 79

4.6 Summary of Formulation 87

Chapter 5 Constitutive Model in Simple Deformation Modes 90

5.1 Formulation of Simple Deformation Modes 90

5.2 Calibration of Material Parameters 99

5.3 Solution Algorithms 101

Chapter 6 Applications 103

6.1 Uniaxial Deformation Responses 103

6.1.1 Constant Strain-rate Deformation 103
6.1.2 Constant Stress Deformation 109
6.1.3 Cyclic Stress Deformation 113

6.2 Multiaxial Deformation Responses 115

6.2.1 Axial Deformation under Confining Pressure 115
6.2.2 Biaxial Plane Stress Deformation 116

Chapter 7 Conclusions and Recommendations for Future Study 153

7.1 Summary of the Constitutive Model 153

7.2 Conclusions 155

7.3 Recommendations for Future Research 159

References 161

Appendix 174

A.1 Genetic Classification of Ice 174

List of Figures

Figure 1.1 The Arctic Regions. 15

Figure 2.1 Effect of Strain-rate on the Compressive and Tensile Strength of Non-saline Ice. 26

Figure 2.2 Typical Stress-strain Curves for Ice under Simple Compression. 31

Figure 2.3 Typical Creep Curves in Log-scale. 32

Figure 4.1 Delayed Elastic Strain for Formation of First Visible Cracks in Columnar S2 Ice at -10°C. 55

Figure 4.2 Strain Dependence of Crack Density in Columnar S2 Ice for Compressive Stress at -9.5°C. 56

Figure 4.3 A System of Parallel Microcrack Field. 59

Figure 4.4 Definition of Axial Vectors in a Rectangular Coordinate. 59

Figure 4.5 A Mechanical Spring-Dashpot Model for Delayed Elastic Strain. 73

Figure 4.6 Concept of Effective Stress. 78

Figure 4.7 Orthogonal Coordinate Transformation with Successive Rotations of Axes. 78

Figure 4.8 Mohr's Circle Representation of the Favored Microcrack Orientations for Uniaxial Loading. 85

Figure 4.9 Mohr's Circle Representation of the Favored Microcrack Orientations for General Triaxial Loading. 85

Figure 4.10 Combination of Damage with Conventional Viscoelastic Model. 89

Figure 5.1 Uniaxial Compression with Confining Pressure. 91

Figure 5.2 a) Damage Orientation under Uniaxial Compression. 93

Figure 5.2 b) Damage Orientation under Uniaxial Tension. 93

Figure 6.1 Predictions of Stress-strain Plots under Uniaxial Compression. 118

Figure 6.2 a) Stress-strain Plots for Uniaxial Tension. 119

Figure 6.2 b) Stress-strain Plots for Uniaxial Compression and Uniaxial Tension at Constant Strain-rate. 120

Figure 6.3 Strength of Ice in Strain-rate Variations. 121

Figure 6.4 Failure Strains against Strain-rates. 122

Figure 6.5 a) Damage Evolution Curves for Uniaxial Compression. 123

Figure 6.5 b) Damage Evolution Curves for Each Damage Mechanisms in Uniaxial Compression. 124

Figure 6.6 a) Strain Ratio Variation for Uniaxial Compression. 125

Figure 6.6 b) Strain Ratio Variation for Uniaxial Tension. 126

Figure 6.7 a) Stress versus Volumetric Strain Plots for Uniaxial Compression. 127

Figure 6.7 b) Stress versus Volumetric Strain Plots for Uniaxial Tension. 128

Figure 6.8 a) Conventional Linear Scale Plots for Creep Strain vs. Elapsed Time. 129

Figure 6.8 b) Conventional Linear Scale Plots for Creep Strain vs. Elapsed Time. (continued) 130

Figure 6.8 c) Log-scale Plots for Creep Strain-rate vs. Elapsed Time. 131

Figure 6.8 d) Log-scale Plots for Creep Strain-rate vs. Strain. 132

Figure 6.9 Comparison of Damage Accumulation with Macroscopic Damage Measure (Crack Density) at Constant Stresses. 133

Figure 6.10 Correspondence of Constant Stress Curve and Constant Strain-rate Curve. 134

Figure 6.11 Strain-rate plotted against Time using Dimensionless

Variables [Ashby and Duval, 1985]. 135

Figure 6.12 a) Strain-rate plotted against Time using Dimensionless Variables to Mellor and Cole's [1982] data. 136

Figure 6.12 b) Strain plotted against Time using Dimensionless Variables to Mellor and Cole's [1982] data. 137

Figure 6.12 c) Strain-rate plotted against Strain using Dimensionless Variables to Mellor and Cole's [1982] data. 138

Figure 6.13 a) Cyclic Stress History for Maximum Stress 2.0 MPa. 139

Figure 6.13 b) Creep Strain plotted against Time under Cyclic Stress. 140

Figure 6.14 a) Stress-strain Plot at Initial Stage for Maximum Cyclic Stress 2.0 MPa. 141

Figure 6.14 b) Stress-strain Plot at Intermediate Stage. 142

Figure 6.15 Damage Evolution Curve for Cyclic Loading. 143

Figure 6.16 a) Creep Strain versus Time Plots. 144

Figure 6.16 b) Mean Strain-rate vs. Time Plots in Linear Scale. 145

Figure 6.17 Failure Stress plotted against Confining Pressure for Different Strain-rates [Jordaan, 1986]. 146

Figure 6.18 Stress-strain Curves for Different Confining Pressures. 147

Figure 6.19 Deviatoric Failure Strength plotted against Confining Pressure. 148

Figure 6.20 Effect of Confining Pressure on the Creep Responses. 149

Figure 6.21 Prediction of the Biaxial Failure Envelopes for Polycrystalline Ice under Constant Strain-rate. 150

Figure 6.22 Failure Envelopes suggested by Timco and Frederking [1984] for Various Types of Ice. 151

Figure 6.23 I_1- $\sqrt{J_2}$ Plots for Constant Strain-rate. 152

NOTATIONS

A	Material constant in delayed elastic strain
C	Parameter in Ashby and Duval's creep model [1985]
C_1, C_2	Damage effect parameters in free energy function
D, D_{ij}	Damage parameters
D_t, D_c	Damage notations associated with tension and compression respectively [Mazars, 1986]
E	Young's modulus
$\tilde{E}$	Apparent tangent modulus
G	Shear modulus
G_0	Reference magnitude in shear modulus
I_i	Invariants for irreducible integrity basis
I_1	First invariant of stress tensor
J_2	Second invariant of deviatoric stress tensor
$\underline{\dot{J}}$	Thermodynamic flux vector
K	Material constant in delayed elastic strain
K_1, K_2	Damage effect parameters in free energy function
K_n	Material constant in viscous strain
$\underset{\sim}{N}$	Unit normal vector
N_{kl}	Dyadic product of two axial vectors N_k and N_l
R_i	Thermodynamic forces
S	Specific entropy
S_{ij}	Deviatoric stresses
$\tilde{S}_{ij}$	Effective deviatoric stresses

T	Absolute temperature
$\underline{X}$	Conjugate vector of generalized thermodynamic forces $\underline{J}$
a, b	Constants
a_T, b	Constants in Sinha's [1978] delayed elastic strain
b_j	Body force per unit mass
$b_j^{(k)}$	Relative displacement separated by crack surface
c_1, d_1	Constants in Sinha's [1979] delayed elastic strain
d	Grain size
m, n	Constants
$n_i^{(k)}$	Unit normal vector to crack surface $S_{(k)}$
q_i	Heat flux vector
r	External heat supply
s	Constant
t	Time
$\bar{t}$	Dimensionless time
u	Internal energy per unit mass
α_1, α_2	Damage parameters
α_t, α_c	Constants associated with damage parameters D_t, D_c
β_1, β_2	Damage parameters
γ_1, γ_2	Damage parameters
δ	Kronecker delta
ϵ, ϵ_{ij}	Strains (total)
ϵ_{ij}^e, ϵ_{ij}^d, ϵ_{ij}^v	Instantaneous elastic, delayed elastic, and viscous strains
ϵ_0	Reference strain
$\bar{\epsilon}$	Dimensionless strain

$\dot{\epsilon}$, $\dot{\epsilon}_{ij}$	Strain-rates
$\dot{\epsilon}_0$	Reference strain-rate
$\bar{\dot{\epsilon}}$	Dimensionless strain-rate
η_1, η_2	Damage parameters
λ, μ	Lame's constants
ψ	Helmholtz free energy function
ν	Poisson's ratio
θ	Microcrack orientation angle
ξ_1, ξ_2	Damage parameters
$\underline{\xi}$	Microcrack vector
ρ	Mass density
σ, σ_{ij}	Stresses
σ_0	Reference stress
$\bar{\sigma}$	Von Mises equivalent stress
$\tilde{\sigma}_{ij}$	Effective stresses
ϕ	Microcrack orientation angle
ω, ω_{ij}	Damage parameters
ω_0	Reference magnitude of damage
Ω	$2\pi f$, f is frequency of applied cyclic loading

CHAPTER 1

INTRODUCTION

1.1 BACKGROUND

The Arctic is a new and extremely severe frontier environment for most of us. Conventional engineering methods are faced with new challenges. Arctic engineering differs from the engineering practice in the temperate zones due to the unique environmental conditions, especially the presence of ice [Polar Research Board, 1985].

In the last decade or so, the Arctic has become an important technical challenge. This awareness was stimulated primarily by discoveries of large oil and gas reserves, which are expected to lie in offshore areas which are seasonally ice-covered. Recent studies indicate that of all the regions of the world, the Arctic area has the greatest potential for new oil and gas discoveries. The U.S. Arctic (Alaska) is expected to contribute as much as 40% of U.S. future oil and gas production (based on National Petroleum Council estimates). This new awareness was also influenced by the development of submarine technologies which made navigation under the polar ice possible.

The Arctic nations neighboring the Arctic Ocean are becoming increasingly aware of the importance of the region in which they have a shared interest. (Figure 1.1 and Table 1.1) National policy of the U.S. (as well as other Arctic interest nations) concerning the Arctic, has focused on a number of key objectives. Among them are:

1) Support for resource and energy development while preserving the environment,
2) Promotion of scientific research to increase knowledge on the Arctic environment,
3) Maintenance of essential national security and safe marine transportation.

The developments along the Arctic coasts created a great demand for more understanding of ice since it is the largest obstacle to exploitation of energy and mineral resources. Although significant achievements have been realized to date, there are many problems to solve in associated with ice.

1.2 OBJECTIVES OF THE RESEARCH

Ice in general is a very complex material. Complexities of ice behavior are due mainly to the dependence on the loading-rate, temperature, and internal structure such as grain size, fabrics, salinity, etc. Simultaneous occurrence of ductile and brittle deformation modes adds complicated features to ice deformation behavior. Uncertainties in existing ice models come primarily from the incomplete modelling of the mechanical behavior of ice in various loading states. In order to understand these uncertainties and to better predict load-deformation relations, proper constitutive modelling is necessary especially for the computer simulation of ice-structure interaction processes.

To date, constitutive models of ice have been developed on the

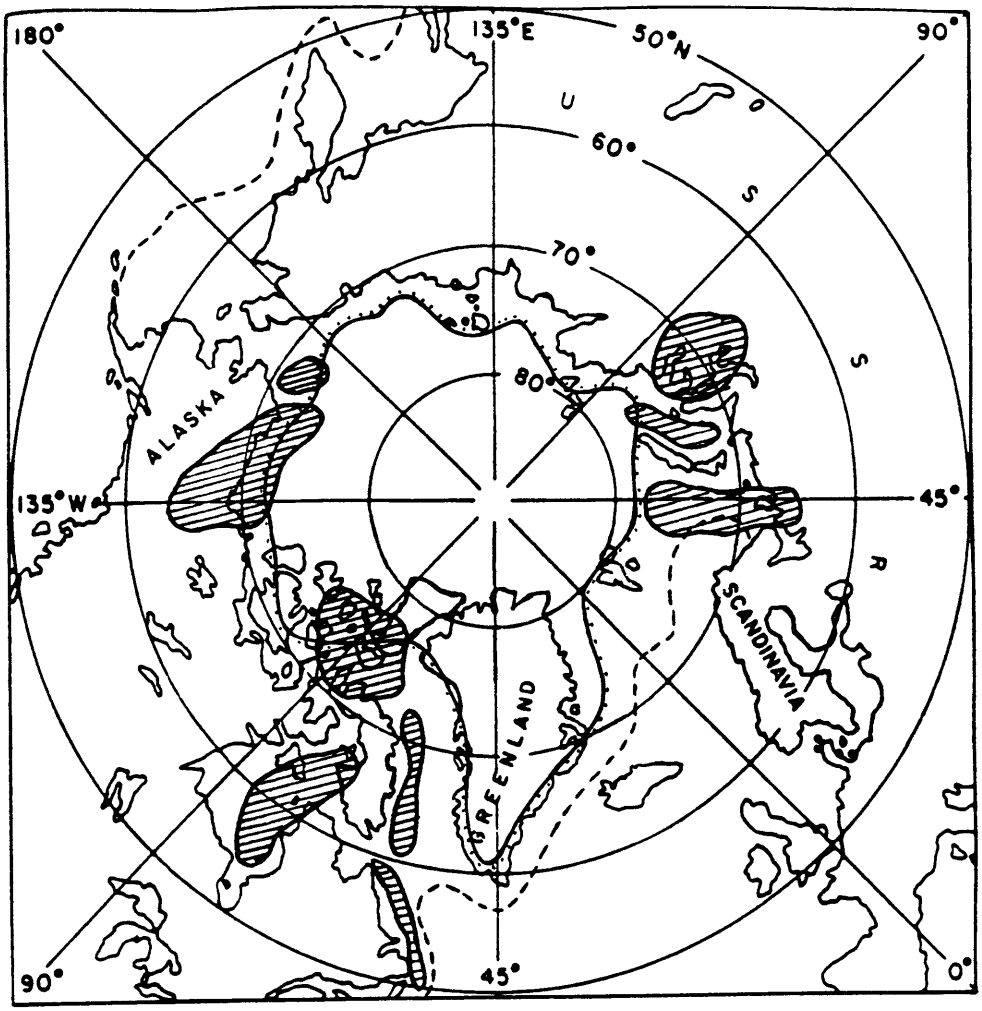

Figure 1.1 The Arctic Regions.

Table 1.1 National Interests in the Arctic [from Kildow, 1984].

	Issue Areas / National Interest	Jurisdiction Claims	National Defense	Oil, Gas & Minerals	Transportation & Navigation	Oceanic & Atmospheric Research	Resources & Environment	Native Interests
Arctic Interest Nations — Arctic Environment Nations; Arctic Nations;	USSR	■	■	■	■	■	■	
	CANADA	■	■	■	■	■	■	■
	GREENLAND(DENMARK)	■	□	■	■	■	■	■
	USA	■	■	■	■	■	■	■
	NORWAY	■	□	■	■	■	■	□
	ICELAND	□	□	□	■	□	■	
	SWEDEN		□		□	□		□
	FINLAND				□	□		□
	GREAT BRITAIN	□	■	□	□	■	□	
	FRANCE		□			□		
	WEST GERMANY		□		□	□	□	
	JAPAN	□	■	□	□	□	■	

High Interest ■ Low Interest □ No Interest (blank)

basis of more or less independent approaches. Basically the brittle behavior of ice is a result of the nucleation of microvoids and the growth of existing microvoids. Microcracking affects the response of a solid in a substantially different manner from ductile deformation in which dislocation movements play a major role. In view of the physical differences existing between two microstructural processes, microcracking can not be explained by the conventional plasticity theory alone [Krajcinovic and Fonseka, 1981]. In addition, since the test data are generally limited to simple deformation modes, the empirical methods based on curve fitting procedure can not easily be extended to general cases of loading and geometry. Theoretical efforts to describe, explain and predict the observed response of ice require a physically motivated constitutive model which can describe the behavior of ice over a broad range of deformation regimes.

The **principal goal of the research** is the formulation of a three dimensional constitutive model of ice deformation. The need for a general approach becomes evident by considering the conventional rheological models such as viscoelastic, elasto-plastic models which are applicable only for limited ranges of response. Bearing in mind that the accumulation of microcracks throughout the material volume is one of the primary sources of material nonlinearity, it appears that a reasonable constitutive model for the mechanical behavior of ice should be based on continuum damage theory, a newly developing branch of continuum mechanics.

The specific objectives of the thesis include:

1) Development of three dimensional, rate-dependent constitutive

equations describing ice deformation for various loading conditions.

2) Development of a physically-based damage model which is able to account for various microcracking mechanisms.
3) Formulation of damage evolution equations and their application to uniaxial and multiaxial deformation tests.

The **main contribution of the thesis** lies in the formulation of damage evolution laws where damage growth is expressed by strain, stress, and strain-rate for each damage mechanism. A key aspect in the development of constitutive models is the selection of a damage parameter. The mathematical nature of the damage parameter is selected as a tensor based on the anisotropic behavior of microcrack fields.

The development of constitutive models needs accurate and consistent experimental data on ice, associated with uniaxial loading, multiaxial loading, cyclic loading, material anisotropy, microcracking and fracture. Although limited to simple deformation modes, recent test results have provided much needed experimental data for various ice deformation regimes.

The complexity of the substructure of ice may vary from a nearly isotropic material with very low salinity to a very complicated anisotropic material containing entrapped air and brine pockets. Since sea ice may be appropriately regarded as a variation of pure fresh water ice, an understanding of pure polycrystalline ice will therefore be considered first.

1.3 ORGANIZATION

Chapter 2 introduces a review of the basic experimental properties of the polycrystalline ice and describes the fundamental mechanisms of ice deformation. Material behaviors of ice in tension, compression, and flexure are presented. Some significant results which serve a pivotal role in the development of a constitutive model are discussed. In Chapter 3, a comprehensive literature survey about continuum damage mechanics and its application to the modelling of ice is presented. The basic concepts and methodology for the mathematical modelling of ice deformation are presented in Chapter 4. The constitutive model, based on a second order tensorial damage variable, is characterized by its ability to present (a)uniaxial and multiaxial loading problems, (b)rate-dependent behavior in constant stress and constant strain-rate tests, (c)strain softening and brittle-to-ductile transition behavior in compression and tension. The constitutive equations for some simple response modes are described in Chapter 5. Calibration of the model is achieved with experimental data for polycrystalline ice. In Chapter 6, the constitutive model is tested for uniaxial and multiaxial deformation responses in constant stress and constant strain-rate. Multiaxial applications include axial compression with confining lateral pressure test and biaxial plane stress test. The results are compared with several individual test data. Brief discussion on the constitutive model and its application problem is also presented. Finally Chapter 7 contains conclusions and some remarks on future research.

CHAPTER 2

REVIEW OF ICE PROPERTIES

2.1 FORMULATION AND TYPES OF ICE

Ice in nature is a very complex material which may have many different crystalline structures which account for a wide diversity of physical and mechanical properties. In order to determine the various properties of ice it is necessary to have some fundamental knowledge on the formation and types of ice structures. The summary presented in this chapter is extracted mainly from Michel [1978b] and Mellor [1983].

If we cool water to a temperature below its melting point, we find that the crystallization temperature is always lower than the melting point [Heverly, 1949]. Although a certain amount of cooling is required to nucleate the first ice crystal, the condition of supercooling alone is not a sufficient cause for water to begin to crystallize. Before crystals can initiate there must exist in the water a number of minute centers of crystallization known as seeds or nuclei. Nucleation may occur spontaneously or it may be induced by some external stimulants. Seeding is frequently used in industrial crystallization to control the product size and grain size distribution.

Hexagonal symmetric structure is commonly found in natural ice. The structure is stable down to very low temperature at normal

pressures. The hexagonal shape is related to its continuous molecular arrangement. The molecules are arranged as a series of parallel planes known as the basal planes. The normal to the basal planes is called the c-axis of the crystal [Michel, 1978b].

2.1.1 Fresh Water Ice

There are essentially three ways in which the first ice (primary ice) may appear in a river or lake water. Ice may start to grow at the surface of a calm water or in slow laminar flow induced by large temperature gradient with depth. When the supercooled top layer will attain the nucleation temperature the first ice crystal will appear in the form of needles. The individual ice needles grow to form a thin continuous ice plate at the surface. Ice may also initiate by the dynamic accumulation of ice crystals to form frazil nucleation when surface currents induce a turbulent mass and heat exchange. The ice cover formation in large northern rivers is mainly due to the dynamic ice formation from frazil slush and ice floes. Another way to initiate ice crystals is by introducing seeds from the atmosphere when the water temperature is close to the freezing point. A heavy snowfall often initiates the ice formation when the floating snow particles refreeze at the top of the existing ice cover.

The initial needle type ice crystals tend to grow parallel to the heat flow, which has preferred or random c-axis orientations (secondary ice). They will interlock with each other before they have time to develop large crystals and the resulting structure will be more complex. The classification of ice based on the nucleation

mechanisms by Michel and Ramseier [1971] is summarized in Appendix A.1.

2.1.2 Sea Ice

Sea ice is an important feature of the Arctic ocean and adjoining seas. The major difference between sea ice and fresh water ice is the amount of salts, in the form of brine pockets squeezed within the ice structure. Because of the salt content in the sea water, the freezing point of sea water is lower than that of fresh water. For standard sea water with a salinity of 34.5 $^{0}/_{00}$, the freezing temperature is -1.8°C. As the temperature drops, the salts in sea ice precipitate in the brine pockets.

The appearance of a first crystal of sea ice is similar to what is observed in fresh water ice. Once ice crystals initiate and grow, the salt in sea water plays a major role in structuring of ice and the structure of sea ice becomes quite different from that of fresh water ice. One major difference is the nonuniform growth of sea ice crystals at the ice-water boundary. Sea ice tends to form columnar shape crystals and the brine is trapped between the vertical planes. This columnar structure of sea ice causes an anisotropic behavior.

Multi-year polar sea ice attains an equilibrium thickness as the ice and snow which melt or evaporate at the top during the summer periods is compensated by sea ice growth underneath during the colder periods. Since the melt water is essentially fresh, the salinity of multi-year ice is relatively low and the structure is fairly strong compared to the first-year sea ice.

2.1.3 Glaciers and Icebergs

One of the most important features of glacier ice is the creeping movement of a huge ice mass down a mountain slope. Although the velocity is very slow, this movement affects the morphology of the glacier ice. Because of huge mass and slow velocity, the glacier ice behaves like a visco-plastic material. Substructures of a glacier ice are characterized by their air bubble and debris contents. In general glacier ice is made up of a pile-up of layers of different types of ice, originating from snow. When a glacier front reaches the sea or lake, ice floes detatch from the ice shelf (icebergs).

2.2 MECHANICAL PROPERTIES OF ICE

For estimating ice strength, the compressive, tensile, and bending failure strengths together with Young's modulus and Poisson's ratio are important properties. Concerning the strength of ice, it is necessary to distinguish two different meanings for this property of ice, i.e., the fracture strength and the yield strength (these are commonly called the failure strength), which correspond to completely different failure modes [Michel, 1978b].

The brittle behavior of polycrystalline ice is characterized by elastic deformation followed by a sudden fracture which occurs when a brittle crack is formed and propagates across an ice sample. The elastic deformation is caused primarily by changes in intermolecular distances under applied stresses and there is no permanent plastic deformation. When the stress level is high enough the stored elastic

strain energy will be released to produce microcracks in the grain, that propagate and fail the ice sample.

However, in ductile condition, ice may fail by yielding instead of fracture and this yield strength corresponds to the maximum stress that the ice can resist during deformation. Ice is a material similar to a metal at high temperatures (the temperature of ice in nature is close to that at which it melts and its homologous temperature is usually greater than 0.9) and the controlling mechanism in the ductile deformation is dislocation movement [Michel, 1978b]. At low strain-rates, the viscous properties are remarkable along the basal plane. The stress needed for fracture is much higher than the stress required to make the ice glide on the basal plane.

2.2.1 Elastic Moduli and Poisson's Ratio

Since the properties of ice are sensitive to the rate of loading, the apparent elastic moduli of the polycrystalline ice vary within a wide range depending on the prevailing conditions. A conventional stress-strain curve does not give an accurate measure of Young's modulus, E. The highest values are obtained when loads are applied dynamically. Under static condition, it takes a certain time to apply a load and the ice sample shows considerable delayed elasticity and this added with the instantaneous deformation gives a much lower apparent elasic modulus [Michel, 1978b].

The effect of the temperature on the elastic moduli of ice is not very important, however the porosity of the ice has a major importance. Young's modulus, in general, slightly increases with

decreasing temperature [Traetteberg et al., 1975]. The porosity of ice is derived from air bubbles, brine pockets, or initially existing microcracks. For ice of low porosity (density ρ = 0.917 g/cm^3), high frequency vibrational methods give values of E approximately 9.0 to 9.5 GPa in the temperature range -5°C to -10°C. Measurements of the initial tangent slope in uniaxial compression tests give values close to the dynamic modulus 9.0 to 10.0 GPa [Mellor, 1983].

The values of Poisson's ratio ν for fresh water ice of very low porosity is approximately 0.30 to 0.35. As material response becomes more ductile by increasing temperature or decreasing loading-rate, the apparent Poisson's ratio increases up to a limit of 0.5, which represents incompressible flow [Murat and Lainey, 1982].

2.2.2 Failure Strength

The strength of polycrystalline ice depends on a number of factors which include temperature, internal structure, and loading conditions. At very low strain-rate where deformation occurs mainly by viscous flow and recrystallization, there is no significant difference between the compressive strength and the tensile strength. However at high rate of loading where brittle fracture occurs, the compressive strength is much larger than the tensile strength. Once the condition of ductile-to-brittle transition has been established, there is little change of tensile strength as strain-rate increases, although the compressive strength continues to increase with strain-rates (Figure 2.1).

Uniaxial compressive strength is an important parameter and it is

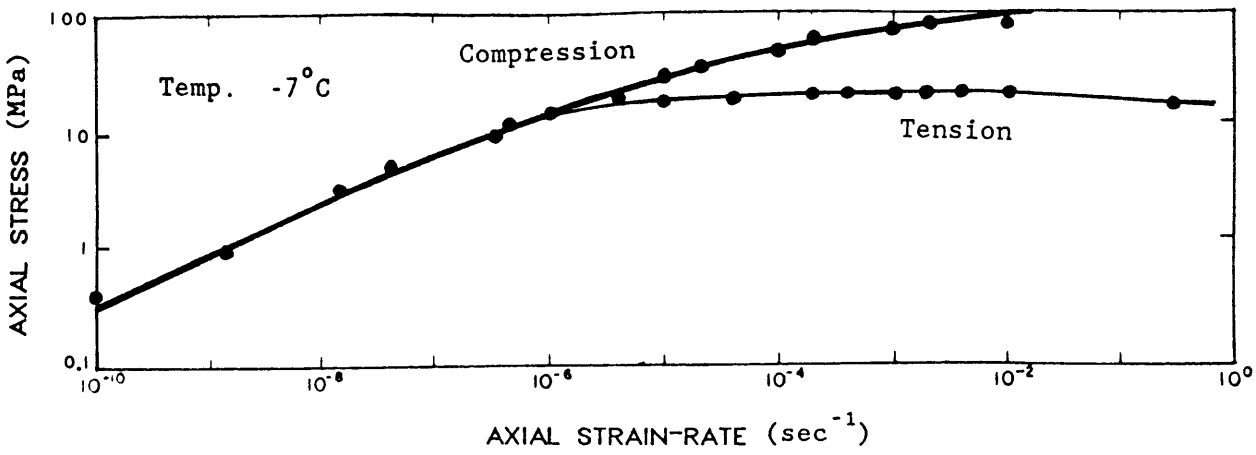

Figure 2.1 Effect of Strain-rate on the Compressive and Tensile Strength of Non-saline Ice [Hawkes and Mellor, 1972].

relatively easy to measure. Uniaxial compressive strength is regarded as the maximum stress that can be developed at a specific strain-rate. At low strain-rates, the strength has about one-third power relationship with strain-rate while for higher strain-rates the strength has a slightly lower power relation with strain-rate. For strain-rate greater than $10^{-3}sec^{-1}$, the rate of compressive strength decreases as strain-rate increases because of brittle behavior. At this strain-rate range, there is not much variation of strength with temperature, since the loading process is nearly elastic. On the other hand, at the very low strain-rates, where ice fails by ductile

rupture, the strength varies with temperature significantly.

Uniaxial tensile strength is often obtained from indirect tests such as three-points beam bending tests with an assumption of pure elastic process, however the values from indirect test can be misleading since they do not measure purely elastic uniaxial tensile strength. For most brittle materials the tensile strength from bending tests is greater than the purely uniaxial tensile strength [Hawkes and Mellor, 1972].

2.3 DEFORMATION AND FAILURE MECHANISMS

As previously mentioned, ice is a highly nonlinear brittle material which is sensitive to loading-rate, temperature, impurity contents and other factors such as grain size and orientation of microstructures. Material tests performed with different types of ice in nature show that there is simultaneous occurrence of ductile and brittle modes of deformation depending on these factors. Material anisotropy also leads to strength variation.

The mechanisms of ice deformation include lattice and grain boundary diffusion, dislocation slip, grain boundary sliding and microcracking [Langdon, 1973; Ashby and Frost, 1975; Sinha, 1977, 1982a]. In many cases ice exhibits an interaction of brittle and ductile processes. The correspondence between creep curves and strength curves has been discussed by Mellor and Cole [1982]. The strain at minimum strain-rate on the creep curve is coincident to the strain at peak stress on a stress-strain curve. The significance of

this correspondence is that the data from creep tests can be supplemented by data derived from strength test with some limitations at higher strain-rates. This will be discussed later in Chapter 6.

2.3.1 Constant Strain-rate Deformation

A selection of typical stress-strain curves is shown in Figure 2.2 for uniaxial constant strain-rates. At low strain-rates, viscous flow is dominant with no signs of material damage, while at high strain-rates, the ice exhibits predominantly brittle behavior where microcracks are densely distributed and grow rapidly. At an intermediate range, both viscous flow and microcracking are important with significant strain-softening occurring at large strains. The brittle behavior of ice at high strain-rates and ductile behavior at low rates indicate that ice has a brittle-to-ductile transition point. The conditions associated with this transition were studied by Schulson [1979] and Schulson et al. [1984]. Temperature and grain size also influence the transition behavior greatly. In general ice becomes brittle as temperature decreases and grain size increases [Cole, 1985; Schulson and Cannon, 1984].

2.3.2 Constant Stress Deformation

Many investigators have observed the physical processes for deformation under constant stress of polycrystalline ice [Gold, 1960, 1970], and comprehensive data for constant stress creep of ice have recently become available [Mellor and Cole, 1982; Jacka, 1984]. They found that various phenomena are involved in the creep process. In

addition to elastic deformation and plastic deformation, grain boundary sliding, cavity formation at the grain boundary, and recrystallization were also observed.

In general, when plots of the creep deformation are carried to sufficiently large strains, they show: (i)an instantaneous elastic strain; (ii)a stage of decelerating creep (primary creep); (iii)a brief transition stage in which strain-rate becomes constant and minimum (secondary creep); and (iv)a stage of accelerating tertiary creep followed by a new stabilized steady state (Figure 2.3). The mechanisms for the damage processes leading to tertiary creep may include:

1) Nucleation and growth of microcavities; One of the interesting aspects observed in ice deformation is crack formation. During creep, damage accumulates in the form of internal microcavities. When the applied stress exceeds a certain level, microcavities form on the grain boundaries. They usually involve one or two grains. Once formed they do not appear to grow significantly with continued deformation, rather a different kind of cracking develops. Gold [1960] found that about two-thirds of the cracks that formed during creep were transcrystalline. These cracks tend to propagate across the grains. Although the rate of microcracking is slowing by the time tertiary creep develops, cavitation has been invoked as one possible cause of tertiary creep of polycrystalline materials [Hooke et al., 1980; Dyson et al., 1981; Levy, 1985].

2) Recrystallization accompanied by the development of favored orientation of microstructures; Strain-induced recrystallization process seems to dominate the tertiary creep behavior at higher strains when the applied stresses are too low to nucleate microcracks. The shape and the size of grains are altered during deformation and new crystals are formed with extensive grain boundary migration [Duval, 1981; Jacka and Maccagnan, 1984; Cole, 1986].

The limiting steady-state at larger strains may be achieved by balancing microstructural processes associated with microcracking and recrystallization.

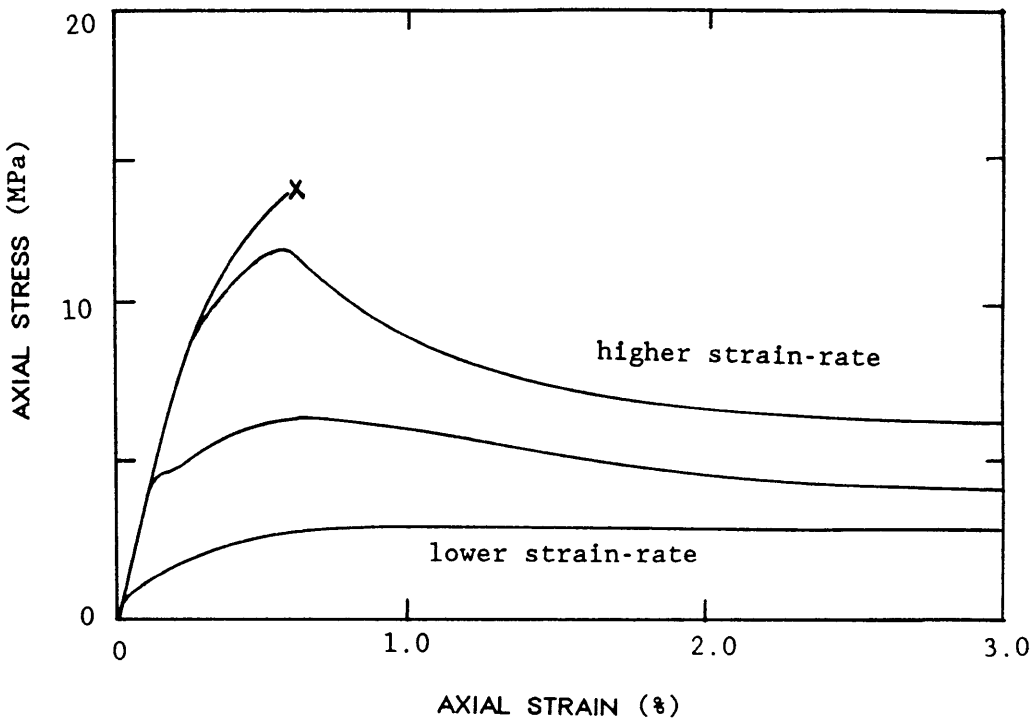

Figure 2.2 Typical Stress-strain Curves for Ice under Simple Compression.

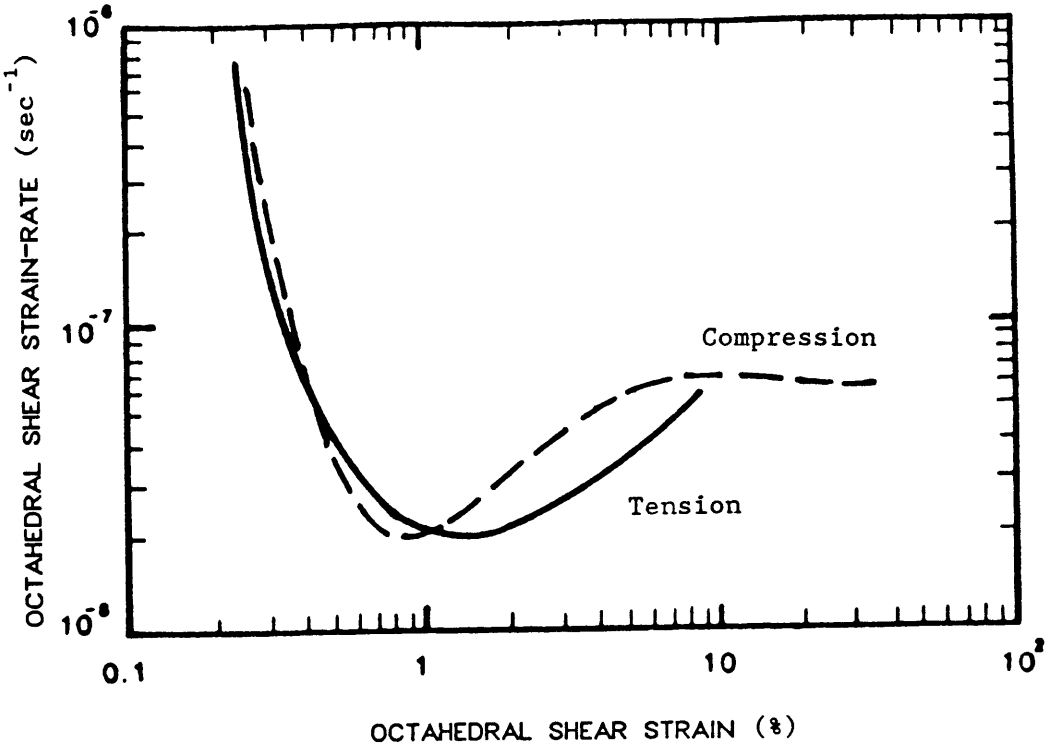

Figure 2.3 Typical Creep curves in Log-scale [Jacka and Maccagnan, 1984]. Octahedral shear strain-rate vs. octahedral shear strain plots are shown for uniaxial compression and tension.

CHAPTER 3

LITERATURE SURVEY

3.1 A REVIEW OF CONTINUUM DAMAGE MODELS

The mechanical properties of some crystalline materials, such as concrete, rocks, ceramics and even ice, are often characterized by the gradual change of elastic modulus with the negative slope of the stress-strain curve in the post-failure regime. These irreversible microstructural changes reflect the nucleation and growth of the microdefects which can not be interpreted within conventional plasticity theory. The changes in the dominant mode of the microstructural mechanisms have decisive effect on the macroscopic response. In plasticity, the macroscopic response of a material is determined by irreversible energy dissipation through dislocation movements during deformation. While being a successful macroscopic theory in describing numerous kinds of ductile behavior, the use of plasticity methods may not be appropriate in describing totally different mechanism like microcracking. In order to be able to predict the behavior of brittle materials under a variety of different circumstances, a theory that can capture the microcracking process is needed.

This was first recognized by Kachanov [1958], in describing creep rupture in uniaxial stress. He introduced a separate scalar variable defining the degradation of the material locally measured by means of void density in a cross section. In general the continuum damage

mechanics (CDM) was developed on the advantage of a state variable theory. Within the theory, it is assumed that the response of a material depends only on the current state of microstructural arrangement which is approximated by a set of internal state variables, the variables reflecting the macroscopic effects of the microdefects. However the exact description of the each individual microcrack evolution would be meaningless in view of the fact that the detail of the cracking pattern differs from one crack to the other. The useful "averaging" concept is applied for description of the macroscopic behavior of the material. Hence, instead of trying to reproduce the fine details of the microdefect pattern, it appears to be natural to attempt to formulate a theory that will reflect the influence of these defects on a solid in an approximate manner. In this sense the damage mechanics can be regarded as a branch of the continuum mechanics rather than of fracture mechanics.

The crucial step in establishing a damage model lies in the determination of the mathematical nature of the damage variable. The practical utility of CDM theory depends on the degree of approximation with which the the damage variable can describe the macroscopic effect of the microdefects. In the development of CDM theory the damage variable is often selected on the basis of intuition and for convenience of mathematical manipulation rather than on physical grounds. This causes confusion to some extent on the definition of damage variable. Most of the early works were based on a scalar representation of the damage in describing uniaxial creep deformation for metals. The theory of damage mechanics was later expanded to

three dimensional cases using scalar, vectorial or tensorial damage variables. To understand the mathematical nature of damage variable a review would be necessary and the details will be discussed in the following. Supplementary reviews on the continuum damage models and its applications may be found in Krajcinovic [1984a] and Lemaitre [1986].

3.1.1 Scalar Damage Models

Kachanov's [1958] original one dimensional model has much intuitive appeal and the idea that damage in a cross-section can best be measured by the relative area of voids was useful as a guideline in most of these works. In a simplified expression, the stress-strain relation can be of the form

$$\epsilon = \frac{\sigma}{E(1-\omega)} \tag{3.1}$$

where ω was the damage parameter and E the modulus of elasticity.

The stress-strain relationship given in (3.1) will be fully defined if the evolution of the damage parameter ω can be expressed as a function of strain or stress.

Rabotnov [1963, 1969, and 1971], in his study on creep rupture problems, introduced creep constitutive equations in the form of simultaneous differential equations. The creep strain-rate at given instant was determined by stress σ, temperature T, and the current damage state of structure.

$$\begin{aligned} \dot{\epsilon} &= \phi(\sigma, T, \omega) \\ \dot{\omega} &= \psi(\sigma, T, \omega) \end{aligned} \tag{3.2}$$

One of the simplest assumptions for the functional forms of ϕ and ψ was considered by Rabotnov [1971],

$$\dot{\epsilon} = a \left(\frac{\sigma}{1-\omega}\right)^n$$

$$\dot{\omega} = b \left(\frac{\sigma}{1-\omega}\right)^k \tag{3.3}$$

where a, b, n, and k are material parameters.

It should be noted that the instantaneous elastic strain and primary creep strain were neglected in the formulation and then the creep equations (3.3) reduce to a power-law creep in uniaxial loading when there is no damage development, i.e., $\dot{\epsilon} = a\sigma^n$ when $\omega = 0$. Rabotnov used again the relative crack area ratio as the "measure of brittleness" and later he suggested a possible form of generalized creep equations by equivalent stress concept, i.e., the creep strain-rate could be defined by a certain combination of equivalent stresses in principal directions.

Although such an approach can be used for predicting uniaxial behavior, it has limited scope for application in multiaxial loading conditions. The generalization of the scalar damage model was attempted to the various kinds of damage and creep behaviors by Leckie and Hayhurst [1974] and many others. In describing multi-dimensional creep problems with combined tension and torsion, Leckie and Hayhurst [1974, 1977] used a generalized creep equations of the form,

$$\dot{\epsilon}_{ij} = \dot{\epsilon}_0 \frac{3}{2} (\bar{\sigma}/\sigma_0)^{n-1} \sigma'_{ij}/\sigma_0 (1-\omega)^n$$

$$\dot{\omega} = \dot{\omega}_0 (\bar{\sigma}/\sigma_0)^{\nu} \sigma'_{ij}/\sigma_0 (1-\omega)^k \tag{3.4}$$

where $\bar{\sigma}$ is von Mises equivalent stress and the components of the strain-rate $\dot{\epsilon}_{ij}$ are proportional to the deviatoric stress σ'_{ij} with n, k, and ν as material parameters to be determined. $\dot{\epsilon}_0$, $\dot{\omega}_0$ and σ_0 are the reference values to meet nondimensional units in the equations. Although Leckie and Hayhurst [1977] and Leckie [1978] did not give a precise physical definition of the damage variable ω, there has been an interpretation of the term, $1-\omega$, as the reduced cross-section area due to damage. They recognized the damage variable as a normalized form of the actual physical damage and they attempted to combine the engineering approach (phenomenological theory, i.e., CDM) and the material scientist approach (micromechanical observation) to relate the physical interpretation of damage and its mathematical formulation. Their attempts have continued until recent years [Leckie, 1986; Hayhurst and Felce, 1986] in need of general description of damage and they turned to thermodynamical formalism using vector and tensorial damage variables.

A somewhat different approach with scalar damage models was performed by a group of French researchers. Lemaitre and Chaboche [1978] studied damage phenomena in ductile materials as progressive deterioration leading to final rupture and they developed constitutive equations coupled with damage and strains by way of the thermodynamics of irreversible processes. Their damage model was applied to various kinds of damage behaviors like plastic damage, fatigue damage, creep damage and coupling of those mechanisms [Chaboche, 1982; Lemaitre, 1984]. They derived a method of damage measurement through the macroscopic response, i.e., $D = 1 - \frac{\tilde{E}}{E}$ where damage variable D was

indirectly determined by measuring elasticity modulus $\tilde{E}$ of the damaged specimen. The assumption of isotropic damage was employed. In other words, if cracks and cavities are equally distributed in all directions, the damage variable defined as an effective area density of cavities on a plane does not depend on directions of the plane and in this sense the isotropic damage variable is a scalar in nature. Lemaitre [1985, 1986] and Tai and Yang [1986] followed this concept. Their damage models enable to calculate the damage evolution with time in each point of material up to the initiation of a macrocrack. Damage evolutions were linear on the plastic strain in Lemaitre's model and exponent-dependent in Tai and Yang's.

The weakness of these damage models lies in an assumption that the principal directions of stresses of the specimen are not changed after the deformation. Beside the hypothesis of isotropy it was assumed that the mechanical effect of cavities and microcracks are the same both in tension and compression which is generally not true in reality, especially for brittle materials. As mentioned in Tai and Yang [1986], the indirect damage measure, $D = 1 - \frac{\tilde{E}}{E}$, is caused not only by the microcrack evolution but also by the loss of external section (necking).

Bodner and Partom [1975] derived constitutive equations for elastic-viscoplastic strain hardening materials. In expanding their earlier model, Bodner [1981, 1985] added a scalar damage parameter to the hardening terms, where they coexist independently. In fact his damage parameter was introduced as a counterpart of the hardening terms, i.e., softening term. He recognized that the damage was an

essential contributing factor in tertiary creep and the exponential type damage evolution law fit well with experimental data for creep deformation of superalloy metals. Later Bodner and Chan [1986] further expanded Bodner's isotropic damage model to include directional (anisotropic) damage characters. They used a scalar variable for isotropic damage and a scalar effective value for anisotropic damage even though a second order tensor was introduced to account its directional behavior originally.

Levy [1985] derived a constitutive equation for describing creep damaging behavior of metals. He employed a damage variable defined as the area fraction of cavitated grain boundaries and developed a damage evolution law with exponentially-decaying rate based on the mechanical dashpot model and statistical strength theory. He assumed that the cavity formation occurs continuously and can be described by a Poisson random process with strain as a parameter. An application of the statistical strength theory on the brittle-ductile material was proposed by Krajcinovic and Silva [1982].

Most of papers following in the wake of Kachanov's original work were devoted to various of aspects of the metal behavior especially of ductile creep rupture. The first studies of brittle materials were somewhat long in coming. After initial works of Hult [1974] and Broberg [1974] on the brittle creep rupture criterion, Janson and Hult [1977], Krajcinovic [1979], Loland [1980], and Mazars [1981] studied concrete structures using continuum damage mechanics, often with combination of fracture mechanics.

Loland [1980] in his semi-empirical damage model of concrete in

uniaxial tension, assumed damage evolution law to be of an exponential form until the strain reached the maximum capacity of strength and of linearly increasing form after that point. He suggested that the cracking was more dependent on strains than on stresses and to use damage mechanics for the compression state of stresses, the maximum tensile strain direction should be considered. Mazars [1981], Mazars and Lemaitre [1984], and Legendre and Mazars [1984] developed an isotropic damage model to describe the multiaxial behavior of concrete with aid of thermodynamics approach and damage surface concept. They suggested an exponentially-decaying type of damage evolution law. Recently Mazars [1986] used a combination of damage from tensile stress and compressive stress. He recognized the dissymmetry between tensile and compressive behaviors: In the first case microcracks are created directly by extensions which are in the same direction as stresses and in the second case extensions are transmitted by the Poisson effect and then are perpendicular to the direction of stresses. Hence the evolution laws are different and a combination of these two kinds of damage are suggested for multiaxial cases.

$$D = \alpha_t D_t + \alpha_c D_c \tag{3.5}$$

where α_t and α_c are constants associated with damage evolutions D_t and D_c respectively.

While these scalar representations of damage could be useful in case of very ductile materials even for multiaxial problems, it is appropriate only in describing a dilute concentration of spheroidal voids where the directional properties of the cracking pattern are less important. However the observation of the brittle materials

reveals that the cracks are flat, planar shapes and oriented perpendicular to the direction of the maximum tensile strain. Therefore microcracking develops in the favored direction and this causes damage-induced anisotropy. This can not be modelled by using scalar damage variables. Many researchers admit that the vectorial or tensorial representation of damage should be an alternative in describing the highly directional field of flat and planar microcracks which are frequently observed in concrete, rock, ice, and other brittle materials.

3.1.2 Vectorial Damage Models

A continuum damage theory for brittle thermoelastic materials where spall damage takes the form of planar cracks was developed by Davison and Stevens [1972, 1973]. They recognized that spalling was not a discrete phenomenon but rather a result of continuous and progressive fracture development in the material and introduced a vectorial damage variable as a continuum damage measure. The planar crack was defined by a vector normal to the plane of the crack and magnitude equal to the area of the crack. The constitutive equations were derived from the Helmholtz free energy function and the influence of the damage on the free energy function was introduced through coupled invariants of damage and strain. Hence the cracking served simply to alter the elastic properties of the body. This formulation yielded a damage-induced anisotropy which is characteristic of the behavior of damaging materials. Although its application was limited to materials in which only brittle spall damage occurs, they suggested

a possible extension of the continuum damage theory to include plastic flow and ductile phenomena.

The constitutive theory developed by Davison and Stevens was further refined and applied to various brittle solids by Krajcinovic and his colleagues. Krajcinovic and Fonseka [1981], in their general formulation of continuum damage theory of brittle materials, developed a vectorial representation of damage variable consistent with the physical interpretation of the damage and described microcrack growth kinematics in relation with the damage characteristics. They defined a flat and planar microcrack by a vector, $\underline{\omega} = \omega_0 \underline{N}$, with ω_0 being the void area density in the cross-section with normal $\underline{N}$. As will be discussed later, the sense of an axial vector $\underline{N}$ was not uniquely defined. They recognized the change in the microcrack geometry as a combination of two basic modes: dilation and slip. To describe this change in the void geometry they introduced a second order tensor relating with the damage measure, $\underline{\omega}$. Through thermodynamical formalism, the damage surface, similar to the Mohr-Coulomb yield criterion, was defined in strain space and the normality rule was employed to calculate the increments of damage. With their formulation, it was able to predict most of the observed features for concrete in uniaxial tension and compression [Krajcinovic and Selvaraj, 1983].

It is encouraging that their vectorial damage formulation, with a relatively small number of material parameters for concrete, can predict and correlate with the experimental data for these kinds of material. Many researchers follow this vectorial damage model

approach because of its relatively simple physical interpretation. The representation of flat and planar microcracks by a vector with direction normal to the plane of crack and magnitude equal to the area of the crack, appears to be at least geometrically reasonable.

A more general formulation based on the theory of internal variables was developed by Krajcinovic [1983a, 1983b] and Krajcinovic and Ilankamban [1985] where both brittle and ductile materials were considered. To describe the gradual degradation of general materials they introduced several (usually two) sets of internal variables representing the plastic deformation and microcrack evolution and the strain tensor was decomposed into elastic and plastic components. The damage law was derived from the dissipation potential in the space of the conjugate thermodynamic forces. They derived quite a general constitutive equations valid for the materials ranging from perfectly brittle to very ductile solids but no numerical examples were given.

In conjunction with damage measures characterizing microstructural changes, Krajcinovic [1984b, 1985] suggested a concept of "averaging" procedure introducing a characteristic length and an appropriate weighting function. The distinction between the physical microcrack distribution and the damage measure may be the most important feature of Krajcinovic's continuum damage model, i.e., the continuum damage variable $\underline{D}$ is defined as a sum of the projections on each plane of all active microcrack vectors $\underline{\omega} = \omega_0 \underline{N}$, by the relation,

$$D_{KL} = \sum \omega_0 N_K N_L \qquad (3.6)$$

The product $N_K N_L$ is taken as positive on physical grounds and this

defines the orientation of the axial vector in a certain range. In fact a vector defined on an oriented surface is a second order tensor.

Most of the damage models described above deal with the quasi-static behavior of the material or its creep response. A theory capable of describing dynamic behavior of concrete was introduced by Suaris [1983] and Suaris and Shah [1984]. In their formulation, the damage was derived from Krajcinovic's vectorial model and the growth of damage variable was governed by second order differential equations by introducing an inertia term into the damage evolution equation. The concept of crack inertia was successfully employed for the analysis of strain-rate sensitive behavior of concrete, however, its applications were limited to uniaxial problems and multiaxial applications were not attempted.

3.1.3 Tensorial Damage Models

Damage representation in the form of a tensor was first formulated by Vakulenko and Kachanov [1971]. They described a fracture geometry by a pair of vectors (the unit normal to the crack surface and the displacement jump vector) and therefore a dyadic product of these vectors. They introduced the crack density tensor as a parameter that characterizes the effect of microcracking on the elastic properties of the solid through the state function which was quadratic in the twelve invariants of the strain and damage tensors. The crack density tensor ω_{ij} was defined as the mean value of the dyadic product over the representative volume element, V_r,

$$\omega_{ij} = \frac{1}{V_r} \sum_{k=1}^{N} \int n_i^{(k)} b_j^{(k)} \, dS_{(k)} \tag{3.7}$$

where $n_i^{(k)}$ denotes the unit normal vector to the crack surface $S_{(k)}$ and $b_j^{(k)}$ denotes the relative displacement (cleavage or slip modes) of the two points separated by the crack surface. The spherical part of the tensor ω_{ij} represents the macroscopic volume change under applied stresses.

Damage representation with tensorial damage variables was further developed by Dragon and Mroz [1979] to model the behavior of rock and concrete and by Murakami and Ohno [1981] for the creep damage behavior of metals at the elevated temperature.

Dragon and Mroz [1979] introduced a fracture surface concept in stress space separating purely elastic states from the states of progressive fracturing similar to yield surface in plasticity theory. They assumed the existence of a strain energy function which was defined in terms of the stress invariants and the damage tensor. This model was able to reproduce the observed behavior in uniaxial and also in biaxial states of stress. Later Dragon [1980] used the same tensor representation to model brittle creep behavior in rock-like solids and Mroz and Angelillo [1982] refined it for strain-rate dependent degradation of such materials. The fracture surface concept used by Dragon and Mroz was very similar to the one by Dougill [1975] which was defined in strain space. Dougill [1975] and Dougill et al. [1976], though it was not damage mechanics approach, used such fracture surface and introduced a softening term as an additional component to hardening term for extension of plasticity theory.

Murakami and Ohno [1981] and Murakami [1983] derived an anisotropic creep damage theory using a second order damage tensor. They noticed that the anisotropic feature of damaged state could not be described by the macroscopic parameter, i.e., cavity density alone, rather they described the damage effect on the deformation by using effective area reduction, which connects the real stress with net (effective) stress tensor. Their creep damage theory provided a mathematical generality in view of the general tensor formulation based on modern continuum mechanics. Later a coupled effect of time-independent plastic damage and creep damage were analyzed by Murakami and Sanomura [1985, 1986] using the same damage model. A similar theory for anisotropic creep damage has been developed by Betten [1980, 1981]. He derived a creep constitutive equation of anisotropic materials in terms of a second order damage tensor on the basis of creep potential and tensor function theory.

Leckie and Onat [1981] and Onat [1982, 1986] also developed a tensorial theory for the representation of anisotropic creep damage by introducing two sets of internal state variables, characterizing the grain boundary cavity growth and dislocation movement respectively. They noticed that these parameters should measure not only the magnitude of quantities of interest but also their directions. Considering material symmetry they suggested that the use of even rank irreducible tensors as state variable could lead to a convenient measure of the void distribution and the strength of anisotropy.

A formal mathematical generalization of scalar damage model by Kachanov [1958] and Rabotnov [1969], was developed by Chaboche [1978]

who introduced an eighth order tensor damage characteristics and later by Chaboche [1979, 1984] of fourth order tensor representation. He generalized the effective stress concept through the fourth order non-symmetric damage tensor to describe the anisotropic creep damage.

$$\tilde{\underline{\sigma}} = (\underline{I} - \underline{D})^{-1} : \underline{\sigma} \qquad (3.8)$$

To describe the plastic strain components he used a flow potential and normality rule to give an expression of generalized power law creep equation. He recognized that because of the anisotropic damage the plastic flow was no longer a constant volume deformation.

The simplest possibility for an anisotropic damage variable is a second order tensor. Although this choice has some limitations it has been widely used. Cordebois and Sidoroff [1979] and Sidoroff [1981] used a second order tensor as a damage parameter with an energetic identification of the constitutive relations instead of using direct strain equivalence of damaged and undamaged materials for derivation of constitutive relations. It was easy to manipulate the damage tensor in principal directions but some limitations were applied on this way since the strain tensor and the damage tensor had the same eigendirections which may not be true in general.

Recently Chow and Wang [1987] developed a comprehensive anisotropic damage theory for ductile deformation based on the work of Cordebois and Sidoroff [1979]. They employed two parameters representing elasticity stiffness degradation and plasticity stiffness degradation respectively. They formulated two very similar evolution laws for each parameter. They tried to verify the damage model by

experimental determination of the parameters. Their model was quite general and complicated in the stream of works by French researchers like Lemaitre, Chaboche, so on. One of the drawbacks of their model was on the fact that damage threshold and damage evolution were the same for compression and tension in magnitude hence the model could be applied to such ductile materials only.

Although some of the physical simplicity is lost, a tensorial damage model can store more information than a vectorial model. Main advantage of the tensorial state variable is that they contain information on the symmetry of a deformed element in description of anisotropic characteristics of a damaged material.

3.2 A REVIEW OF CONTINUUM DAMAGE THEORY IN ICE MODELLING

So far, few attempts were made to apply the continuum damage model to ice deformation response. In recent years, damage mechanics approaches have been introduced for describing constitutive equations of ice. A one dimensional model with scalar damage parameters was used by Karr [1984, 1985], for describing brittle-ductile behavior of polycrystalline ice in uniaxial compression. The damage law for ice was established based on the statistical strength theory. In his study microfracture and yielding were treated as mutually exclusive events and a joint probability density function was introduced. He related the development of internal fractures with the test result of acoustic emissions and formulated the accumulated damage directly from the total acoustic emission activity.

Ting and Shyam Sunder [1985] also used a scalar damage parameter which accounts for the strain-softening or tertiary creep behavior. In their formulation, a nonlinear spring-dashpot Maxwell model was used and a damage parameter was defined as a somewhat mathematically complicated, exponential function of strain and strain-rate for the description of rate-sensitive behavior of sea ice.

In analysis of the progressively microcracking on the global response of an ice sheet, Tomin et al. [1986] used a scalar damage model to simulate the degradation of ice sheet under edge indentation. In the modelling the shear modulus G was affected by the damage parameter D, i.e., $G = G_0(1-D)$, and the model was generalized to be used in existing finite element routine by introducing an equivalent strain and material stiffness. Most of the developed models for ice use scalar damage variables and they are developed to fit uniaxial test data so their generalization to three dimensional cases may be difficult.

Szyszkowski et al. [1985] developed a four-elements nonlinear spring-dashpot model to describe the primary and secondary creep stages of ice and later Szyszkowski and Glockner [1987] derived a generalized multiaxial form for the strain components and added damage effect of tertiary creep by introducing a scalar damage function which was assumed to be tensile stress dependent. They assumed that the microcracking affects only the permanent portion of the viscous strain.

For using non-scalar damage measure, Wu [1987] used a tensorial damage representation originally developed by Murakami and Ohno

[1981]. Combining with a rate-dependent constitutive model by Ting and Shyam Sunder [1985], Wu tested the tensorial damage model under a triaxial loading to model pressure sensitivity of sea ice deformation.

Following Krajcinovic's approach [1984b], Sjölind [1987] recently developed a rate-dependent, vectorial damage model with application to model ice deformation, especially to take account of the difference in tension and compression tests of columnar S2 ice. His model was quite general in view of the thermodynamical formalism with introducing free energy function and dissipation potential as a starting point in deriving constitutive equations which was designed to deal with anisotropic materials. However there was an inconsistency in using an elastic strain from free energy function which was based on the isotropic formulation while anisotropic formulation was used for viscous strain components. Moreover a large number of material parameters made his model difficult in identifying them without some intuitive handling. Kachanov [1984] mentioned that the actual number of the undetermined coefficients contained in the model might be quite large instead of two or three as in Krajcinovic's, because there was no reason to assume that the coefficients had to be the same for the invariants involving different microcrack fields. However in practical reason, the number of unknowns should be reduced to minimum with appropriate approximation.

CHAPTER 4

MODELLING OF ICE DEFORMATION

As reviewed in the preceding chapter, the continuum damage theory presents a suitable framework for the modelling of various materials with microcracking as an important deformation process. In this chapter constitutive equations of ice are derived on the basis of the thermodynamical formalism where the damage is treated as an internal state variable. In the following sections, a brief introduction of a conventional constitutive model without description of damage is presented. The definition of material damage will be followed in view of the physical aspects of microcracking processes. The methodology employed in this study is to incorporate damage with a conventional viscoelastic model through an effective stress concept in the multiaxial stress state.

4.1 ICE MODELLING WITHOUT DAMAGE DESCRIPTION

One of the interesting modes of deformation observed on ice is crack formation. Several observers have noted microcracking during deformation. However this microcrack formation was often neglected in the formulation of constitutive equations and therefore the constitutive models could describe the material behavior only up to the onset of failure beyond which the conventional viscoelastic models could not capture its post-failure behavior.

One of the simple viscoelastic constitutive models was developed by Sinha [1978b] for describing constant stress creep behavior of ice under uniaxial compression. Total strain was assumed as the sum of an instantaneous elastic strain part and a time-dependent viscous strain part. The latter was further decomposed into a recoverable part so-called delayed elastic strain and an irrecoverable part as permanent viscous strain. This approach involves expressing the total strain of the material as the sum of elastic, ϵ^e, delayed elastic, ϵ^d, and irrecoverable viscous strain, ϵ^v.

$$\epsilon = \epsilon^e + \epsilon^d + \epsilon^v \tag{4.1}$$

The elastic strain is related to the applied stress, σ, using Hooke's law, $\epsilon^e = \sigma/E$, where E is Young's modulus. Sinha described the time-dependent recoverable strain of ice at various temperatures,

$$\epsilon^d = \frac{c_1 d_1}{d} \left(\frac{\sigma}{E}\right)^s \left[1 - \exp\{-(a_T t)^b\}\right] \tag{4.2}$$

where E, c_1, d_1, s, and b are material constants and a_T is a temperature-dependent creep parameter.

Creep deformation models without damage often involve describing the irrecoverable viscous strain using the Norton-Bailey power-law [Glen, 1955],

$$\dot{\epsilon}^v = K_n \sigma^n \tag{4.3}$$

where K_n and n are material parameters to be determined.

This creep model well fits the experimental data, however the model is limited to show primary and secondary parts of creep

responses. Moreover the model has difficulty in application of the nonsteady stress history, especially in multiaxial problems (for multiaxial formulation see Szyszkowski and Glockner [1987]).

4.2 MATERIAL DAMAGE

4.2.1 Basic Concepts

There are two types of crack formation in ice. Cracks that pass through grains are called transgranular cracks and cracks that form along the grain boundaries are called intergranular cracks. Transgranular crack is a cleavage-type fracture caused by tensile forces acting across a well-defined plane, that usually develops when stress is sufficiently high [Dieter, 1961]. The accumulation of stress concentration around the grain boundaries results in the grain boundary sliding and further nucleation of microcracks along the boundary and also at the triple points. At low stresses diffusion processes overcome the initiation of microcracks while at higher stresses grain boundary cracking plays a dominant role [Sinha, 1982b].

Sinha [1979] found that the grain boundary cracking was closely related to the grain boundary sliding and delayed elastic strain. He observed that the initiation of grain boundary cracking in S2 ice (columnar grained ice with grain size 4.5 mm) occured when the amount of grain boundary sliding, i.e., delayed elastic strain, reached a critical value which was independent of applied stress (Figure 4.1).

Gold [1972] studied the influence of crack formation on the creep behavior of S2 ice (grain size 3 mm) at various temperatures. Under

constant load, strains and the occurrence of cracks were recorded. He observed that cracks began to form during creep when the constant compressive stress exceeded a threshold value, about 6 Kg/cm^2 ($\cong$ 0.59 MPa). For stresses less than about 10 Kg/cm^2, the cracking activity was confined mainly to the primary creep stage. When the stress was greater than about 12Kg/cm^2, crack formation brought on the failure condition before the constant creep stage could be established. Before the onset of failure, the cracking activity was essentially random and continuous event and it was appeared to be an contributing factor to the tertiary creep (Figure 4.2). The cracks formed in the region of grain boundaries running generally parallel to the applied stress. The presence of cracks during compressive creep indicates that local tensile stresses are developed during compressive creep.

He speculated that two independent cracking processes are involved. The strain dependence of the crack density involves two Weibull-type distributions, one associated with cracks nucleated by dislocation pile-ups or similar types of stress concentrations and the second with grain boundary cracks. With increasing strain the tendency for new cracks to nucleate decreases, that is, the sites available for crack initiation decrease with strain so that the cracking rate tends to zero. For sufficiently large stresses there is probably a continuous generation of new crack sites once structural instability has been established.

St. Lawrence and Cole [1982] in their work on polycrystalline ice (grain size 1.2 mm at -5°C) reported that the acoustic emission may be directly related to the occurrence of the internal microfractures.

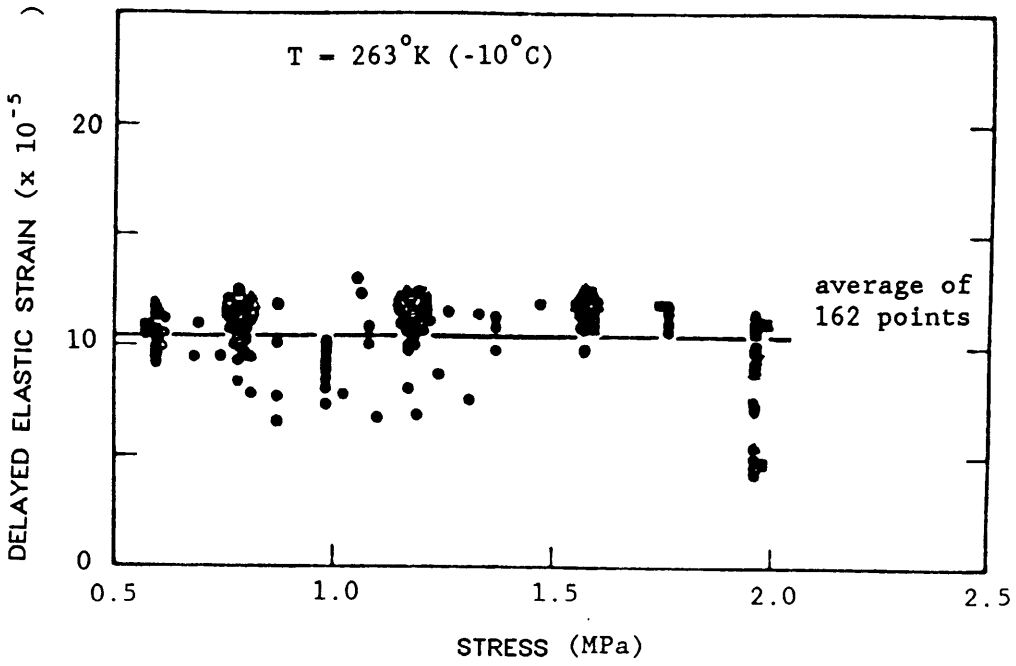

Figure 4.1 Delayed Elastic Strain for Formation of First Visible Cracks in S2 Ice at -10°C [redrawn from Sinha, 1982b].

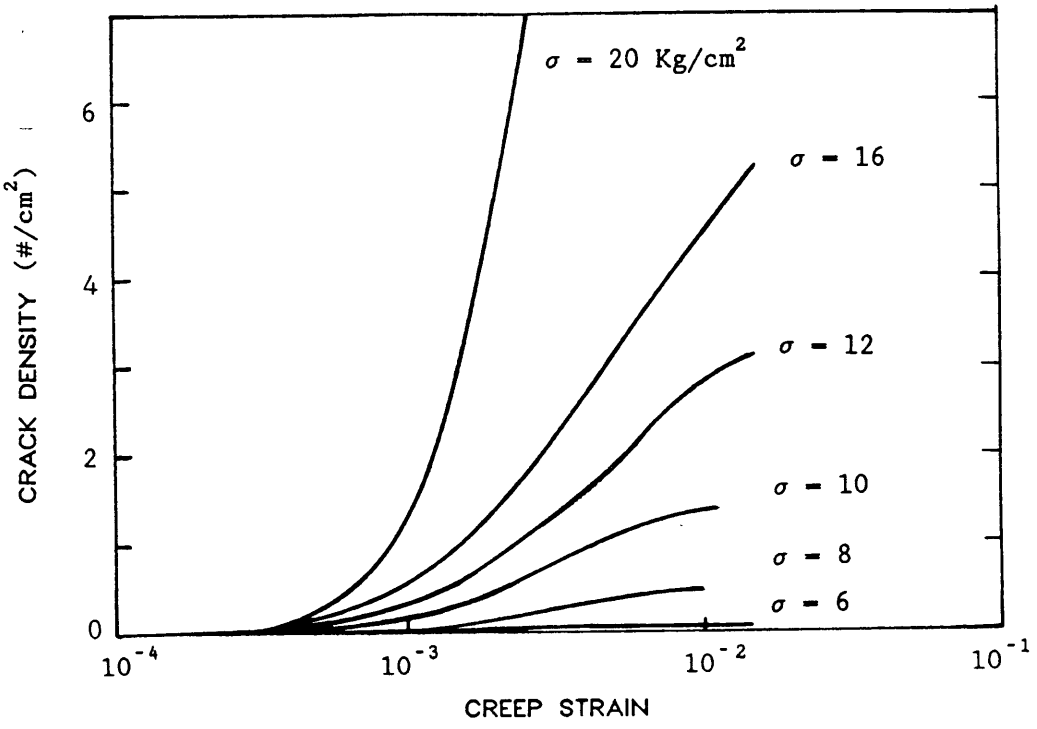

Figure 4.2 Strain Dependence of Crack Density in S2 Ice for Compressive Stress at -9.5°C [redrawn from Gold, 1972].

They observed a correspondence between acoustic emission activity and the microfractures in ice and this appears to be reasonable, especially when the stress levels are such that the visible cracks are produced. However they did not preclude other sources of sound, such as growth and coalescence of pre-existing cracks and voids. Although the source mechanisms of the acoustic emission activity are not clearly identified, the major source of the sound generation is the small fractures that take place at the grain boundaries and possibly from the inside of ice grains.

It is clear from the observations that brittle crack formation in ice has a significant effect on its deformation behavior even when it is ductile and it can be pointed out that cavity formation is one of the efficient mechanisms of relieving elastic strain energy through the irreversible processes.

4.2.2 Microcrack Systems

The recent development of continuum damage mechanics offers a rational method for the prediction of the nonlinear deformation of brittle solids caused by accumulating microcracks. The lack of a physically acceptable definition of damage causes some confusion. Consequently, it appears reasonable to consider the physically consistent representation of material damage .

Microcrack distribution affects the material by reduction of load-bearing cross-sectional area. The influence of microcrack distribution on the state of the solid were often defined by a scalar function of crack density, i.e., ratio of microcrack area to the

intact cross-section or volume average of voids, but this definition of damage, as mentioned in the previous chapter, can not describe the anisotropic behavior of damaged materials caused by flat, planar microcracks aligned in preferred direction. In the following, Krajcinovic's [1985] definition of damage is employed in the derivation of the present damage model.

With a proper definition of positive orientation, a single microcrack can be identified by its area and orientation normal to plane of the crack and the internal state of the material weakened by these microcracks is fully defined by vectors,

$$\underline{\xi}^{(i)} = \xi^{(i)}\underline{N} \qquad (i = 1,2, \ldots, n) \qquad (4.4)$$

In general the number of microcracks, n, is very large, so the details of microcracks distribution can never be known. In fact the exact shape and distribution of each individual microcrack is relatively unimportant since they vary to a significant degree from one specimen to the other. The shape of microcracks is assumed to have little or no effect on the material behavior. As a consequence, it is desirable to introduce an averaging variable, $\tilde{\xi}$, instead of using each individual microcrack field, $\xi^{(i)}$, as an appropriate measure of microcrack distribution in a smoothed manner over the volume.

Consider a solid with a large (but finite) number of flat and parallel microcracks. All microcracks have the same orientations in a parallel plane (see Figure 4.3). We call it a microcrack system. The physical meaning of the averaging variable should be. Among several possible averaging processes, it is reasonable to select a ratio of

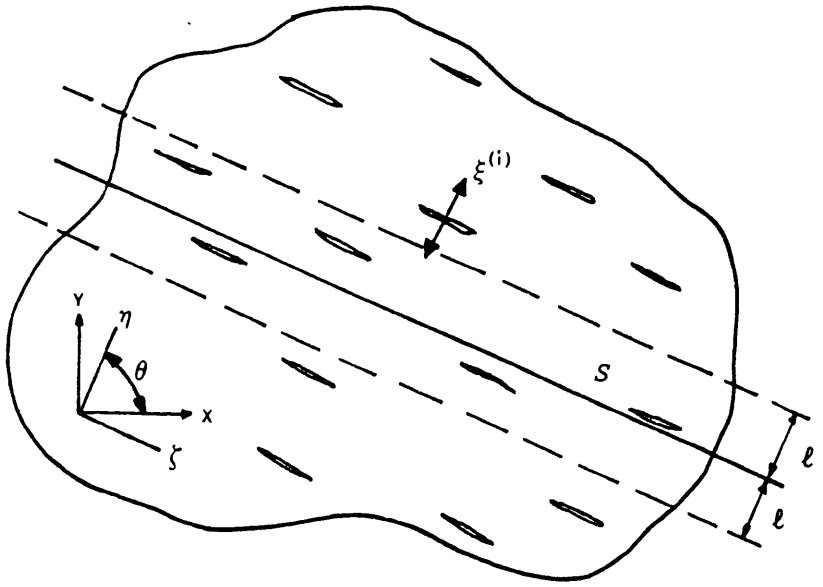

Figure 4.3 A System of Parallel Microcrack Field [redrawn from Krajcinovic, 1985].

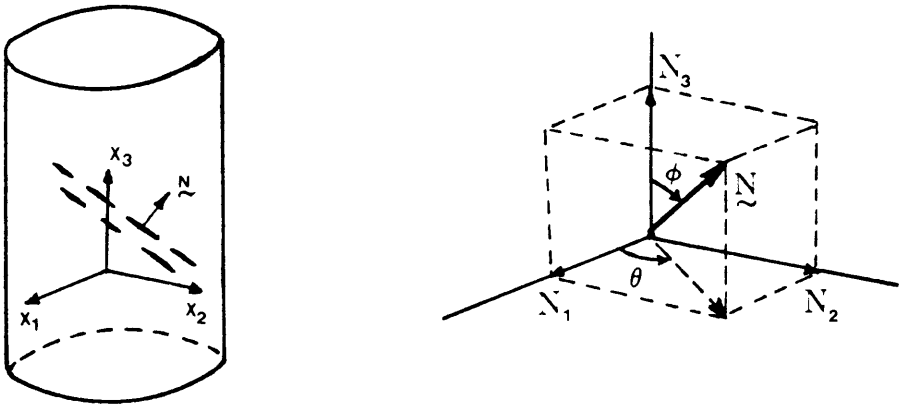

Figure 4.4 Definition of Axial Vectors in a Rectangular Coordinate.

the void area to the virgin area of a cross-section. Assuming that the influence of microcracks on the amount of load-bearing area in a cross-section is related to their neighboring section within the band ($-\ell < \eta < \ell$), then the reduced area which is not available for the transmission of stresses is,

$$\tilde{\xi} = \sum_i w^{(i)} \xi^{(i)} \tag{4.5}$$

where the weighting function $w^{(i)}$ reflects the distance separating the microcrack from the cross-section S. In general the weighting function can be selected to give the continuous change of microcrack distribution and to reflect microcrack interaction.

For a large enough area A of the plane S (Figure 4.3) containing a multitude of microcracks, a system of parallel microcracks can be defined by a vector,

$$\underline{\omega} = \frac{\tilde{\xi}}{A} \underline{N} = \omega \underline{N} \tag{4.6}$$

where $\underline{N}$ is the unit normal to the microcrack field. Expression (4.6) averages a large number of independent microcracks into a single vectorial function and enables us to use continuum concept in the crack-filled solids.

It is important to note that the vectors $\underline{\omega}$ do not represent the damage in the plane with normal $\underline{N}$. As will be discussed in the next section, the damage in a cross-section $\hat{\underline{N}}$ is obtained simply as a projection of the microcrack system $\underline{\omega}$ on the plane of the cross-section, that is, $\underline{\omega} \cdot \hat{\underline{N}} = \omega \cdot \cos\theta$, where θ is an angle between the microcrack system and the plane of a cross-section as in Figure 4.3.

Since the sense of microcrack orientation is not uniquely defined, we need a restriction on the positive orientation of microcrack. On purely physical grounds, the orientation θ of the axial vectors is defined on half space only.

Consider the general case when the normals of all cracks are embedded in a parallel plane with orientations ($0 \leq \theta \leq \pi$) as in Figure 4.3. Next assign orientation $\theta^{(\alpha)} = (\alpha - \frac{1}{2})\Delta\theta$, (where $\alpha = 1,2, \ldots, m$ and $m = \pi/\Delta\theta$) to all microcrack systems with orientations within a given range ($\theta^{(\alpha)} - \frac{\Delta\theta}{2}$, $\theta^{(\alpha)} + \frac{\Delta\theta}{2}$). To each system of parallel microcracks with orientation $\theta^{(\alpha)}$ corresponds an axial vector $\underline{\omega}^{(\alpha)}$ in the sense of Equation (4.6). Thus a general microcrack field is discretized into m systems of parallel microcrack systems which are represented by m vectors. The degree of approximation depends on the magnitude of $\Delta\theta$. In the limit as $\Delta\theta \to 0$ or $m \to \infty$, $\underline{\omega}^{(\alpha)}$ can represent infinite microcrack systems exactly. In the continuum model to be presented here, $\underline{\omega}^{(\alpha)}$, ($\alpha = 1,2, \ldots, m \ll n$) will thus represent the resultant of the microcrack vectors $\underline{\xi}^{(i)}$, ($i = 1,2, \ldots, n$) averaged in the neighborhood of a generic point [Krajcinovic, 1985].

4.2.3 Measure of Damage

To define the damage it is necessary to distinguish between active and passive microcrack systems. A microcrack system will be called active if the local stress or strain field allows discontinuity across the face of the crack.

Highly anisotropic characterization of damage requires a higher order tensor field to describe the changes in crack orientation. We

restrict ourselves to small deformation responses and a second order tensor may be used. The damage tensor D_{KL} is defined as a sum of projections (on the plane with normal N_L) of all active vectors $\underline{\omega}^{(\alpha)}$ (α = 1,2, ..., m) with normal N_K as in Figure 4.4.

$$D_{KL} = \sum_{\alpha} \omega^{(\alpha)} N_K^{(\alpha)} N_L^{(\alpha)} \tag{4.7}$$

In the limit as the number of microcrack fields m tends to infinity the damage can be rewritten as,

$$D_{KL} = \int_{\theta 1}^{\theta 2} \int_{\phi 1}^{\phi 2} \omega(\theta,\phi)\, N_{KL}(\theta,\phi) d\theta d\phi \tag{4.8}$$

with components,

$$N_{KL} = \begin{bmatrix} \cos^2\theta \sin^2\phi & \cos\theta \sin\theta \sin^2\phi & \cos\theta \sin\phi \cos\phi \\ & \sin^2\theta \sin^2\phi & \sin\theta \sin\phi \cos\phi \\ \text{sym.} & & \cos^2\phi \end{bmatrix}$$

where N_{KL} is the dyadic product of axial vectors N_K and N_L. The spherical coordinates θ and ϕ define the orientations of all active microcrack fields. $\omega(\theta, \phi)$ is the microcrack distribution. Here the direct coupling between microcrack systems is neglected.

The second order tensor D_{KL} provides the measure of damage. The diagonal terms represent the relative increase in damage associated with crack area in the plane perpendicular to its normal (cleavage mode). In a similar manner one can lead to the definition of the off-diagonal components representing the change of the damage associated with the rotation of the cracks (slip mode). The proposed

model in the limit becomes equivalent to some of the constitutive models based on the tensorial damage variable (see for example Vakulenko and Kachanov [1971] and Murakami and Ohno [1981]).

4.3 CONTINUUM DAMAGE MECHANICS

The observation presented in the preceding section emphasizes the fact that failure of ice is accompanied by a gradual accumulation of microcracks. The strategy for formulation of the constitutive equations of ice is based on continuum damage mechanics. In the following section a thermodynamical formalism developed by Krajcinovic and Fonseka [1981] and Sjölind [1987] will be employed. The theory incorporates damage in the material responses as an internal state variable. This is well applicable for various types of damaging materials such as concrete, rocks, ceramics, and ice.

4.3.1 Theory of Internal Variables

The thermodynamic theory with internal variables developed originally by Coleman and Noll [1963], Coleman and Gurtin [1967], and later applied to damaging materials by Davison and Stevens [1973], provides a starting point for the establishment of the continuum damage theory. The fundamental assumption forming the base of the continuum damage theory is that the response of the material depends on the current state of the microstructural arrangement rather than on the entire history of the deformation process. We restrict our consideration on the material such that the basic response functions

depend on the current pattern of microstructural arrangement. Moreover, it is assumed that the current state of the microstructural arrangement can be described approximately by a finite set of state and internal variables which can be determined without information on the past history [Kestin and Bataille, 1977]. This approach has been used in the context of dislocations for plastic deformation [Kratochvil and Dillon, 1969].

Disregarding the electrical and chemical processes, the basic response functions are as follows:

The stress tensor σ_{IJ}

the heat flux vector q_I

the specific entropy S

and the Helmholtz free energy ψ.

The state variables defining response functions are:

the strain tensor ϵ_{IJ}

the temperature T

and the temperature gradient grad T.

In view of the irreversible microcracking processes, it requires the introduction of a set of internal variables, $\omega_I^{(\alpha)}$ ($\alpha = 1,2, \ldots, m$) which represent the microcracking processes.

In this research, it is assumed that the material damage is in the form of densely distributed flat, planar microcracks and that there are no isolated single cracks that dominate the development of damage. The microcracks may exist with many independent orientations and their magnitudes are defined with sum of the projections on the other independent planes, thus those overlying damage fields will be a

tensor.

4.3.2 Thermodynamic Restrictions

In addition to the description of response functions and state variables, the following balance equations must be considered. The deformations are considered to be small. For the balance of linear momentum, we have

$$\sigma_{IJ,I} + \rho b_J = \rho \ddot{x}_J \tag{4.10}$$

where b_J is a body force per unit mass. The balance law of angular momentum is expressed by the symmetry of the stress tensor,

$$\sigma_{IJ} = \sigma_{JI} \tag{4.11}$$

The condition for the energy balance (i.e., first law of thermodynamics) is,

$$\rho u - \sigma_{IJ} \dot{\epsilon}_{IJ} + q_{I,I} = \rho r \tag{4.12}$$

where u is the internal energy per unit mass, r the external heat supply and q_I the heat flux vector. The second law of thermodynamics requires that

$$\rho \dot{S} - \left(\frac{\rho r}{T}\right) + \left(\frac{q_I}{T}\right)_{,I} \geq 0 \tag{4.13}$$

where S is the entropy per unit mass and T the absolute temperature respectively.

Introducing the Helmholtz free energy function, $\psi = u - ST$, the

combined form of Equations (4.12) and (4.13) gives the so-called Clausius-Duhem inequality, which is defined as a non-negative rate of entropy production.

$$\sigma_{IJ}\dot{\epsilon}_{IJ} - \rho(\dot{\psi} + S\dot{T}) - \frac{1}{T} q_I T_{,I} \geq 0 \qquad (4.14)$$

Helmholtz free energy function ψ is a smooth function of state and internal variables for which every admissible process has to satisfy the equation,

$$\psi = \psi(\epsilon^e_{IJ},\ T,\ q_I,\ \omega^{(\alpha)}_I) \qquad (4.15)$$

$$\dot{\psi} = \frac{\partial \psi}{\partial \epsilon^e_{IJ}} \dot{\epsilon}^e_{IJ} + \frac{\partial \psi}{\partial T} \dot{T} + \frac{\partial \psi}{\partial q_I} \dot{q}_I + \frac{\partial \psi}{\partial \omega^{(\alpha)}_I} \dot{\omega}^{(\alpha)}_I \qquad (4.16)$$

We assume here that the scalar function ψ is dependent on elastic strains and other state variables only. For small strain, the total strain ϵ_{IJ} is decomposed into the instantaneous elastic component, time-dependent recoverable delayed elastic and irrecoverable viscous strain components.

$$\epsilon_{IJ} = \epsilon^e_{IJ} + \epsilon^d_{IJ} + \epsilon^v_{IJ} \qquad (4.17)$$

The time dependent strain components, ϵ^d_{IJ} and ϵ^v_{IJ}, appear in the damage mechanics formulation only through the relation (4.17) and damage effects on these strain components are included by way of an effective stress concept. Substituting Equations (4.16) and (4.17) into Clausius-Duhem inequality (4.14) leads to:

$$(\sigma_{IJ} - \rho\frac{\partial\psi}{\partial\epsilon^{e}_{IJ}})\dot{\epsilon}^{e}_{IJ} + \sigma_{IJ}\dot{\epsilon}^{p}_{IJ} - \rho(S + \frac{\partial\psi}{\partial T})\dot{T} - \frac{q_i}{T}T_{,I}$$

$$- \rho\frac{\partial\psi}{\partial q_I}\dot{q}_I - \rho\frac{\partial\psi}{\partial\omega^{(\alpha)}_I}\dot{\omega}^{(\alpha)}_I \geq 0 \qquad (4.18)$$

where $\dot{\epsilon}^{p}_{IJ}$ denotes a sum of the time-dependent strain-rate components, i.e., $\dot{\epsilon}^{p}_{IJ} = \dot{\epsilon}^{d}_{IJ} + \dot{\epsilon}^{v}_{IJ} = \dot{\epsilon}_{IJ} - \dot{\epsilon}^{e}_{IJ}$.

If it is required that Equation (4.18) to be satisfied for all $\dot{\epsilon}^{e}_{IJ}$, $\dot{T}$, $\dot{q}_I$, and $\dot{\omega}^{(\alpha)}_I$, ($\alpha$ = 1,2, ..., m), we obtain the following thermodynamic restrictions,

$$\sigma_{IJ} = \rho\frac{\partial\psi}{\partial\epsilon^{e}_{IJ}} \qquad (4.19a)$$

$$S = -\frac{\partial\psi}{\partial T} \qquad (4.19b)$$

$$\frac{\partial\psi}{\partial q_I} = 0 \qquad (4.19c)$$

$$\sigma_{IJ}\dot{\epsilon}^{p}_{IJ} - \frac{q_I}{T}T_{,I} - \rho\frac{\partial\psi}{\partial\omega^{(\alpha)}_I}\dot{\omega}^{(\alpha)}_I \geq 0 \qquad (4.19d)$$

For an isothermal process (T = const.),

$$\sigma_{IJ} = \rho\frac{\partial\psi}{\partial\epsilon^{e}_{IJ}} \qquad (4.20a)$$

$$\sigma_{IJ}\dot{\epsilon}^{p}_{IJ} - \rho\frac{\partial\psi}{\partial\omega^{(\alpha)}_I}\dot{\omega}^{(\alpha)}_I \geq 0 \qquad (4.20b)$$

where $\psi = \psi(\epsilon^{e}_{IJ}, \omega^{(\alpha)}_I)$. The inequality (4.20b) can be written as a scalar product of the flux vector $\underline{\dot{J}}$ and the vector of conjugate thermodynamic forces $\underline{X}$.

$$\underline{X} \cdot \dot{\underline{J}} \geq 0 \tag{4.21}$$

where $\dot{\underline{J}} = \{ \dot{\epsilon}^{p}_{IJ}, \dot{\omega}^{(\alpha)}_{I} \}^{T}$ and $\underline{X} = \{ \sigma_{IJ}, R^{(\alpha)}_{I} \}^{T}$.

The thermodynamic force $R^{(\alpha)}_{I}$ is defined by

$$R^{(\alpha)}_{I} = -\rho \frac{\partial \psi}{\partial \omega^{(\alpha)}_{I}} \tag{4.22}$$

The force $R^{(\alpha)}_{I}$ which is conjugate to the microcrack evolution $\dot{\omega}^{(\alpha)}_{I}$ can be interpreted as damage strain energy release rate similar to the energy release rate or the crack resistance force in the fracture mechanics.

4.3.3 Helmholtz Free Energy Function

The restrictions imposed by material symmetry properties on the response functions were investigated by many researchers [Pipkin and Rivlin, 1959]. They used classical invariant theory, according to which any scalar function of tensors, which is invariant under a given orthogonal group of coordinate transformation, can be expressed in a finite number of polynomial scalar invariants. Such a set of polynomial scalar invariants is called an irreducible integrity basis for the tensors under the given orthogonal group of coordinate transformations.

Following the general constitutive theory [Coleman and Gurtin 1967; Malvern, 1969], integrity basis for a scalar function ψ will contain the following invariants,

$$I_1 = \epsilon^{e}_{KK}, \quad I_2 = \frac{1}{2} (I_1^2 - \epsilon^{e}_{KL} \epsilon^{e}_{LK}), \quad I_3 = \det \epsilon_{KL}$$

$$I_4 = \omega_K^{(\alpha)} \omega_L^{(\beta)} \quad , \quad I_5 = \omega_K^{(\alpha)} \epsilon_{KL}^e \omega_L^{(\beta)} \quad , \quad I_6 = \omega_K^{(\alpha)} \epsilon_{KL}^e \epsilon_{LM}^e \omega_M^{(\beta)}$$

where α and β denote occurrence of two or more damage systems which cannot be added vectorially. We consider a special case in which only terms quadratic in strain are retained then this special form of ψ is

$$\rho\psi = 1/2\ (\lambda + 2\mu)\ \epsilon_{KK}^e \epsilon_{LL}^e - \mu\ (\epsilon_{KK}^e \epsilon_{LL}^e - \epsilon_{KL}^e \epsilon_{LK}^e)$$

$$+ \sum_{\alpha}\sum_{\beta} (\omega_P^{\alpha}\omega_P^{\beta})^{-1/2} (C_1 \epsilon_{KL}^e \epsilon_{MM}^e\ \omega_K^{\alpha}\omega_L^{\beta} + C_2 \epsilon_{KL}^e \epsilon_{LM}^e\ \omega_K^{\alpha}\omega_M^{\beta}) \quad (4.23)$$

where ρ is the material density and λ, μ are Lame's constants. C_i's are material parameters to be determined from experiments. If the direct coupling between individual microcrack systems is neglected, expression (4.23) can be reduced to a simple form.

In the limit as the number of microcrack systems, $m \to \infty$, we have

$$D_{KL} = \lim_{m\to\infty} \sum_{\alpha=1}^{m} \omega^{(\alpha)} N_K^{(\alpha)}\ N_L^{(\alpha)}$$

$$= \int_{\theta_1}^{\theta_2} \int_{\phi_1}^{\phi_2} \omega(\theta,\phi)\ N_{KL}(\theta,\phi) d\theta d\phi \quad (4.24)$$

As before, $\theta_1 \le \theta \le \theta_2$ and $\phi_1 \le \phi \le \phi_2$ define the orientations of the microcrack fields. Using expression (4.24) the Helmholtz free energy function can be written in the form,

$$\rho\psi = 1/2\ (\lambda + 2\mu)\ \epsilon_{KK}^e \epsilon_{LL}^e - \mu\ (\epsilon_{KK}^e \epsilon_{LL}^e - \epsilon_{KL}^e \epsilon_{LK}^e)$$

$$+ C_1 \epsilon_{KL}^e \epsilon_{MM}^e D_{KL} + C_2 \epsilon_{KM}^e \epsilon_{ML}^e D_{KM} \quad (4.25)$$

The stress-strain relationship is given by Equation (4.19a),

$$\sigma_{IJ} = \rho \frac{\partial \psi}{\partial \epsilon^{e}_{IJ}}$$

$$= K_{IJKL} \epsilon^{e}_{KL} \tag{4.26}$$

where the stiffness tensor is given by

$$K_{IJKL} = \lambda \delta_{IJ} \delta_{KL} + \mu(\delta_{IK}\delta_{JL} + \delta_{IL}\delta_{KJ})$$
$$+ C_1(\delta_{IJ} D_{KL} + \delta_{KL} D_{IJ})$$
$$+ C_2(\delta_{JK} D_{IL} + \delta_{IL} D_{JK}) \tag{4.27}$$

In engineering use, the components of strain and stress are often expressed in matrix form as

$$\{ \underline{\epsilon} \} = [\epsilon_{11} \ \epsilon_{22} \ \epsilon_{33} \ 2\epsilon_{12} \ 2\epsilon_{23} \ 2\epsilon_{13}]^T$$

$$\{ \underline{\sigma} \} = [\sigma_{11} \ \sigma_{22} \ \sigma_{33} \ \sigma_{12} \ \sigma_{23} \ \sigma_{13}]^T$$

Equation (4.26) can be written by

$$\{ \underline{\sigma} \} = [K] \{ \underline{\epsilon}^{e} \}$$

$$= ([K^e] + [K^d]) \{ \underline{\epsilon}^{e} \} \tag{4.28}$$

where the stiffness matrix [K] is divided into two matrices $[K^e]$ and $[K^d]$ which denote the stiffness matrix for the undamaged material and for the added influence of damage respectively. The full expression of these matrix components is presented in Table 4.1.

Table 4.1 Stiffness Matrices for Isotropic Materials

$$K^{e}_{IJKL} = \lambda\delta_{IJ}\delta_{KL} + \mu(\delta_{IK}\delta_{JL} + \delta_{IL}\delta_{KJ})$$

$$K^{d}_{IJKL} = C_1(\delta_{IJ}D_{KL} + \delta_{KL}D_{IJ}) + C_2(\delta_{JK}D_{IL} + \delta_{IL}D_{JK})$$

$[K^e] =$

$$\left[\begin{array}{ccc:ccc}
\lambda+2\mu & \lambda & \lambda & 0 & 0 & 0 \\
 & \lambda+2\mu & \lambda & 0 & 0 & 0 \\
 & & \lambda+2\mu & 0 & 0 & 0 \\
\hdashline
 & & & 2\mu & 0 & 0 \\
 & \text{symmetric} & & & 2\mu & 0 \\
 & & & & & 2\mu
\end{array}\right]$$

$[K^d] =$

$$\left[\begin{array}{ccc:ccc}
2(C_1+C_2)D_{11} & C_1(D_{11}+D_{22}) & C_1(D_{11}+D_{33}) & C_1D_{23} & (C_1+C_2)D_{31} & (C_1+C_2)D_{12} \\
 & 2(C_1+C_2)D_{22} & C_1(D_{22}+D_{33}) & (C_1+C_2)D_{23} & C_1D_{31} & (C_1+C_2)D_{12} \\
 & & 2(C_1+C_2)D_{33} & (C_1+C_2)D_{23} & (C_1+C_2)D_{31} & C_1D_{12} \\
\hdashline
 & & & C_2(D_{22}+D_{33}) & C_2D_{12} & C_2D_{31} \\
 & \text{symmetric} & & & C_2(D_{11}+D_{33}) & C_2D_{23} \\
 & & & & & C_2(D_{11}+D_{22})
\end{array}\right]$$

4.4 MULTIAXIAL DEFORMATION MODELLING

In this section multiaxial constitutive equations for nonlinear deformation behavior are derived based on the generalized viscoelastic formulation. An often crucial aspect of nonlinear deformation is the time dependent components of strain. We first consider an approach taken by Sinha [1979] for describing the deformation of ice.

$$\epsilon_{total} = \frac{\sigma}{E} + \frac{c_1 d_1}{d} \left(\frac{\sigma}{E}\right)^s \left[1 - \exp\{- (a_T t)^b\}\right] + K_n \sigma^n t \qquad (4.29)$$

4.4.1 Delayed Elastic Strain

The phenomenological creep model (4.29) well describes the primary and secondary creep behavior of ice. However its ability to describe multiaxial behavior and time-varying stress creep is very limited. In order to describe delayed elastic component of the total strain we consider a simple mechanical model shown in Figure 4.5. The model is similar to the Kelvin-Voigt solid model. We emphasize that the proposed mechanical model shown in Figure 4.5 is used for modelling only the delayed elastic component, e^d, of the total strain.

Denoting stress and strain in the linear elastic spring as σ_1, ϵ_1^d and denoting stress and strain in the dashpot as σ_2, ϵ_2^d, the equilibrium requires that total stress, σ, in the system be simply

$$\sigma = \sigma_1 + \sigma_2 \qquad (4.30)$$

Strain compatibility further requires:

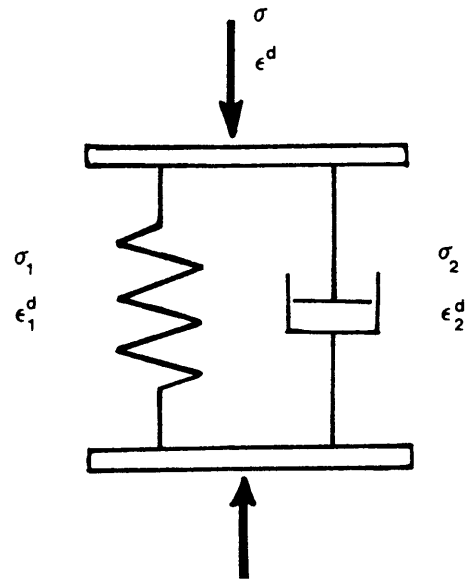

Figure 4.5 A Mechanical Spring-Dashpot Model for Delayed Elastic Strain.

$$\epsilon^d = \epsilon_1^d = \epsilon_2^d \tag{4.31}$$

The stress-strain relations for the spring and for the dashpot are:

$$\epsilon_1^d = K\sigma_1 \tag{4.32}$$

$$\dot{\epsilon}_2^d = \dot{\epsilon}_0 \sigma_2^m \tag{4.33}$$

where K, $\dot{\epsilon}_0$, m are material parameters. Combining Equations (4.30) through (4.33) yields the constitutive equation for the system,

$$\dot{\epsilon}^d = A(K\sigma - \epsilon^d)^m \tag{4.34}$$

This uniaxial relation can be generalized to multiaxial states of stress by associating the applied stress, σ, with the deviatoric stress, S_{IJ} [Ohno et al., 1985]. Equation (4.34) then takes the general form,

$$\dot{\epsilon}^{d}_{IJ} = A\left[\frac{3}{2} KS_{IJ} - \epsilon^{d}_{IJ} \right]^{m} \qquad (4.35)$$

Damage effects are incorporated in the formulation through the effective stresses $\tilde{S}_{IJ}$ by replacing S_{IJ} in Equation (4.35). This will be discussed in the next section. Equations (4.34) and (4.35) can be readily solved numerically for general loading conditions and closed form solutions exist for some simple cases.

Constant Applied Stress: For the particular loading condition in which a stress of $\sigma = \sigma_0$ is applied and maintained constant, the solution to Equation (4.34) yields

$$\epsilon^{d} = K\sigma_0 - [\ (m - 1)\ (At + C)\ ]^{\frac{1}{1-m}} \qquad (4.36)$$

for m greater than unity. Using the initial condition that at $t = 0$, $\epsilon^{d} = 0$, the constant in Equation (4.36) is found as

$$C = \frac{(K\sigma_0)^{1-m}}{m - 1}$$

If $m = 1$ in Equation (4.34) then, for the same initial condition,

$$\epsilon^{d} = K\sigma_0\ [1 - \exp\ (- At)] \qquad (4.37)$$

Equation (4.37) is similar to the expression proposed by Sinha [1979] for the delayed elastic strain for ice.

From Equation (4.34) the delayed elastic strain, resulting from a

constant applied stress asymptotically approaches a value of $K\sigma_0$. This component of strain is also recoverable and therefore the value for K can be determined by unloading a sample and measuring the recovered strain. Also the instantaneous strain-rate resulting from a sudden change in applied stress is

$$\dot{\epsilon}^d_{init} = A(K\sigma)^m \tag{4.38}$$

Equation (4.38) is very useful in establishing the constants, A and m, for a particular material.

Constant Stress Rate: For the particular case in which m = 1 in Equation (4.34), and under a constant stress-rate, $\dot{\sigma}_0$, the delayed elastic strain is given by

$$\epsilon^d = K\dot{\sigma}_0[t - \frac{1}{A}\{1 - \exp(-At)\}] \tag{4.39}$$

If m = 2, then the solution for a constant stress-rate is

$$\epsilon^d = K\dot{\sigma}_0[t - \frac{1}{\sqrt{AK\dot{\sigma}_0}} \tanh \sqrt{AK\dot{\sigma}_0}\, t] \tag{4.40}$$

Cyclic Stress: For the particular case, m = 1, under the cyclic stress $\sigma(t) = \frac{\sigma_0}{2}(1 - \cos \Omega t)$ where $\Omega = 2\pi f$ and f is a frequency of the cyclic loading, we have

$$\epsilon^d = B_1 \sin \Omega t + B_2 \cos \Omega t + B_3 \exp(-At) + B_4 \tag{4.41}$$

where

$$B_1 = -\frac{B\Omega}{\Omega^2+A^2}\ ,\ B_2 = -\frac{BA}{\Omega^2+A^2}$$

$$B_3 = -\frac{B}{A} + \frac{BA}{\Omega^2+A^2}\ ,\ B_4 = \frac{B}{A}$$

and

$$B = \frac{1}{2} AK\sigma_0.$$

At high frequencies the amplitude of oscillating term, $B/2\sqrt{\Omega^2+A^2}$ becomes smaller and at low frequencies, ϵ^d, approaches $K\sigma_0/2$. ϵ^d curve for a cyclic loading with $\sigma_{max} = \sigma_0$ is oscillating about the ϵ^d curve for constant applied stress $\sigma_0/2$.

4.4.2 Viscous Strain

Creep deformation models without damage often describe the irrecoverable viscous strain using the Norton-Bailey power-law, i.e., $\dot{\epsilon}^v = K_n \sigma^n$ where K_n and n are material parameters which may be dependent upon temperatures. Generalization of the power-law creep to three dimensional stress states gives,

$$\dot{\epsilon}^v_{IJ} = \frac{3}{2} K_n (3\bar{\sigma})^{n-1} S_{IJ}$$

$$= \frac{3}{2} K_n \left(\frac{3}{2} S_{KL}S_{KL}\right)^{\frac{n-1}{2}} S_{IJ} \qquad (4.42)$$

where $\bar{\sigma}$ denotes the von Mises equivalent stress and S_{IJ} denotes deviatoric stress tensor.

In a damaged material the anisotropic behavior can be originated from the material itself and also from the initiation and growth of microcrack fields during the deformation. Even though the undamaged material is isotropic, as damage proceeds the material behavior becomes anisotropic (damage-induced anisotropy).

Methods for analyzing creep deformation in anisotropic materials has been developed [Betten, 1979, 1980] using a mapping which relates the actual stress-state of the anisotropic material to the hypothetical stress-state in the isotropic manner. The idea of mapping for the anisotropic material was used by Sjölind [1987] to describe a damage-induced anisotropy for ice deformation with microcracks.

When the material contains damage in the form of microcracks their influence on the viscous strain-rate can be approximately taken into account by using the effective (deviatoric) stresses. We use an effective stress tensor for the delayed elastic strain and the viscous strain in the formulation to take account of damage effects on those strain components.

$$\{ \tilde{\underline{\sigma}} \} = \frac{1}{2} \{ [K^e][K]^{-1} + [K]^{-1}[K^e] \} \{ \underline{\sigma} \} \qquad (4.43)$$

Using the effective stress expression in Equation (4.43), the deviatoric stress tensor S_{IJ} in Equation (4.42) is replaced by $\tilde{S}_{IJ}$, then we have

$$\dot{\epsilon}^v_{IJ} = \frac{3}{2} K_n \left(\frac{3}{2} \tilde{S}_{KL} \tilde{S}_{KL}\right)^{\frac{n-1}{2}} \tilde{S}_{IJ} \qquad (4.44)$$

Special derivations will be given in detail in the next chapter.

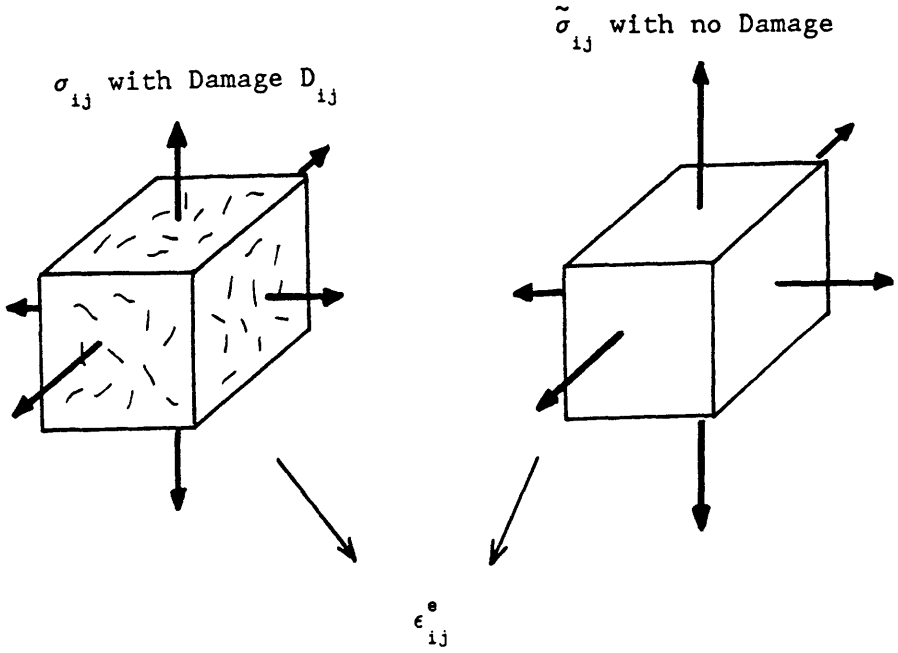

Figure 4.6 Concept of Effective Stress.

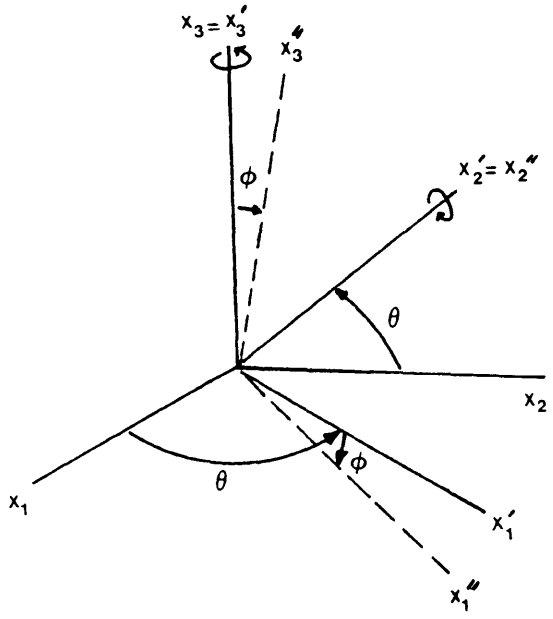

Figure 4.7 Orthogonal Coordinate Transformation with Successive Rotations of Axes.

4.5 DAMAGE EVOLUTION

An important step in deriving the constitutive laws by using continuum damage mechanics lies in the formulation of a damage evolution equation. The evolution law for damage growth is perhaps the most controversial part of the existing damage models. Damage growth in connection with phenomenological deformation model is in many cases on the basis of simple one dimensional approach. Most of these one dimensional damage models are insufficient to generalize while retaining their physical meanings. The purpose of deriving damage evolution law in this research is to develop a damage model compatible with physical interpretation of damage in multiaxial deformation of ice.

The step in establishing a damage evolution law consists of the determination of the relationship between the damage growth and the increments of stresses and strains. This can be achieved either by using concepts of the dissipation potential and the damage surface or by prescribing damage evolution law directly derived from simple physical modelling based upon observations. In view of the analogies with the conventional plasticity theory the idea of dissipation potential and damage surface seems to be so appealing that many researchers adopt this approach in their development of continuum damage mechanics.

The damage surface is simply an experimentally defined function enveloping all states of stress (in many cases damage surfaces have been defined in strain space rather than in stress space) which can be

reached without further increase in damage. In absence of the specific experimental data it is possible only to hypothesize the general shape of a dissipation potential and a damage surface on the basis of intuition and analogies with the conventional plasticity theory [Krajcinovic and Fonseka, 1981]. However the dissatisfactory correlation between the analytical and experimental results provides a limited application of damage surface concept.

In order to show its ability to duplicate the experimental data over a wide range of response modes, therefore it is necessary to select an approach, which is simple enough to generalize but mathematically rigorous. Damage evolution law based on the experimental observations and simple probabilistic approach may be an alternative to determine the strain increments and damage growth relation.

As explained in previous sections on the observation of microcracking activities of ice [Gold, 1972; Sinha, 1982a], we postulate two damage mechanisms in relation with damage growth: The first mechanism, intergranular cracking, is related with the grain boundary sliding of ice crystals and thus with the delayed elastic strains. The second one, transgranular cracking, is assumed to be related with total strains. Hence we use the relation,

$$D_{KL} = D_{KL}^{(1)} + D_{KL}^{(2)} \tag{4.45}$$

Each damage tensor is defined as before,

$$D_{KL}^{(1)} = \int_{\theta 1}^{\theta 2} \int_{\phi 1}^{\phi 2} \omega^{(1)} N_{KL} \, d\theta d\phi \tag{4.46a}$$

$$D_{KL}^{(2)} = \int_{\theta 1}^{\theta 2} \int_{\phi 1}^{\phi 2} \omega^{(2)} N_{KL} \, d\theta d\phi \qquad (4.46b)$$

Still undefined formulation in the definition of damage tensors (4.46a) and (4.46b), is the individual damage evolution laws $\omega^{(1)}$, $\omega^{(2)}$ for each mechanism. It is believed that the grain boundaries with normals in the direction of the tensile strain axes will be most susceptible to cracking. Here we define a damage criterion for microcrack initiation and growth as a function of resolved tensile strain.

Before deriving damage evolution laws it would be helpful to define a coordinate transformation. To find tensile strains in local coordinates, tensor transformation is applied (Figure 4.7).

$$\underline{\epsilon}'' = \underline{S} \; \underline{\epsilon} \; \underline{S}^T \qquad (4.47)$$

where $\underline{\epsilon}$ is the strain tensor in principal coordinates given by

$$\epsilon_{IJ} = \begin{bmatrix} \epsilon_I & 0 & 0 \\ 0 & \epsilon_{II} & 0 \\ 0 & 0 & \epsilon_{III} \end{bmatrix} \qquad (4.48)$$

and the transformation matrix by rotation of axes is:

$$\{ \underline{x}'' \} = [S] \{ \underline{x} \} \qquad (4.49)$$

rotation about x_3: θ $\qquad \{ \underline{x}' \} = [S_1] \{ \underline{x} \}$

rotation about x_2': ϕ $\qquad \{ \underline{x}'' \} = [S_2] \{ \underline{x}' \}$

where

$$[S_1] = \begin{bmatrix} \cos\theta & \sin\theta & 0 \\ -\sin\theta & \cos\theta & 0 \\ 0 & 0 & 1 \end{bmatrix}$$

$$[S_2] = \begin{bmatrix} \cos\phi & 0 & -\sin\phi \\ 0 & 1 & 0 \\ \sin\phi & 0 & \cos\phi \end{bmatrix}$$

and

$$[S] = [S_1][S_2]$$

$$= \begin{bmatrix} \cos\phi\cos\theta & \cos\phi\sin\theta & -\sin\phi \\ -\sin\theta & \cos\theta & 0 \\ \sin\phi\cos\theta & \sin\phi\sin\theta & \cos\phi \end{bmatrix} \qquad (4.50)$$

then the tensile strain normal to the microcrack system in local coordinates is given by

$$\epsilon''_{33} = \sin^2\phi \cos^2\theta \ \epsilon_I + \sin^2\phi \sin^2\theta \ \epsilon_{II} + \cos^2\phi \ \epsilon_{III} \qquad (4.51)$$

For uniaxial compression (with or without confining pressure), $\epsilon_I = \epsilon_{II}$ and then the local tensile strain is independent of angle θ.

$$\epsilon''_{33} = \epsilon_{nn} = \sin^2\phi \ \epsilon_I + \cos^2\phi \ \epsilon_{III} \qquad (4.52)$$

It is assumed here that the microcracks under tensile strains in local coordinate which is smaller than a certain critical value never experience a growth by microcrack opening. For simplicity we assume that the evolution of damage is dependent upon the resolved normal strain, strain-rate and stress. Since the tendency for new cracks to nucleate decreases as the cracks are accumulated, in other words, the rate of crack nucleation decreases until it reaches zero, thus the

damage growth should also be a function of existing damage. In view of the previous works on the scalar damage evolution law in power functions, we propose a rate-type equation for the first mechanism:

$$\frac{d\omega^{(1)}}{d\epsilon^{d}_{nn}} = f_1(\omega^{(1)}, \sigma_{nn}, \dot{\epsilon}^{d}_{nn})$$

$$= \beta_1(\alpha_1 - \omega^{(1)}) \qquad (4.53)$$

with initial condition,

$$\omega^{(1)} = 0 \quad \text{for } \epsilon^{d}_{nn} \leq \epsilon^{d}_{cr}$$

where α_1 represents a limiting amount of damage which is considered a function of the applied stress component and β_1 represents a damage growth rate factor which is considered a function of strain-rate.

In fact the responses under compressive and tensile stresses are significantly different for brittle materials. As Mazars [1986] mentioned, the tensile stress acting on the crack face tends to open the crack directly by extension which is in the same direction as stress. In the case of compressive stress the opening of the crack face is assumed to be forced by the extension transmitted by Poisson effect and is small compared to the extension by direct tensile stress. It should be noted here that this different assumption of microcrack development in tensile and compressive stresses is based on a macroscopic view of strain and stress components rather than on a microscale view. This causes some confusion when the controlling factor of microcrack development is concerned in the grain size level. In fact we can see local grain boundary wedging stresses on the grain

boundary facets in microscale systems even though there is not any applied tensile stresses on global systems. The strain and stress used in the formulation of damage evolutions should be regarded as macroscopic local strain and stress acting on the crack systems in continuum sense rather than as microscale strain and stress acting on the individual crack face. This is quite different from material scientists' view whose main consideration is a microscale level analysis.

Since the signs of stress and strain may be opposite this effect as well as the effect of strain-rate should be incorporated by some way in the formulation of damage evolution laws. As will be seen in later sections, uniaxial response is strongly dependent on strain-rate. With 10^{-5}sec^{-1} as an approximate threshold, the response may be regarded changing from ductile to brittle behavior. Upon this fact, we propose the simple functions:

$$\alpha_1 = \alpha_1(\sigma_{nn}) = \exp(\gamma_1 \sigma_{nn}) \qquad (4.54)$$

$$\text{or} \quad \alpha_1 = 1 \quad \text{for } \sigma_{nn} < 0$$

$$\beta_1 = \beta_1(\dot{\epsilon}^d_{nn}) = \xi_1 \log|\dot{\epsilon}^d_{nn}| + \eta_1 \qquad (4.55)$$

$$\text{or} \quad \beta_1 = -5\xi_1 + \eta_1 \quad \text{for } |\dot{\epsilon}^d_{nn}| < 10^{-5}$$

where γ_1, ξ_1, and η_1 are material constants to be determined from the experimental results. For uniaxial cases, the local stress σ_{nn} and local strain-rate $\dot{\epsilon}^d_{nn}$ are again calculated from the principal values,

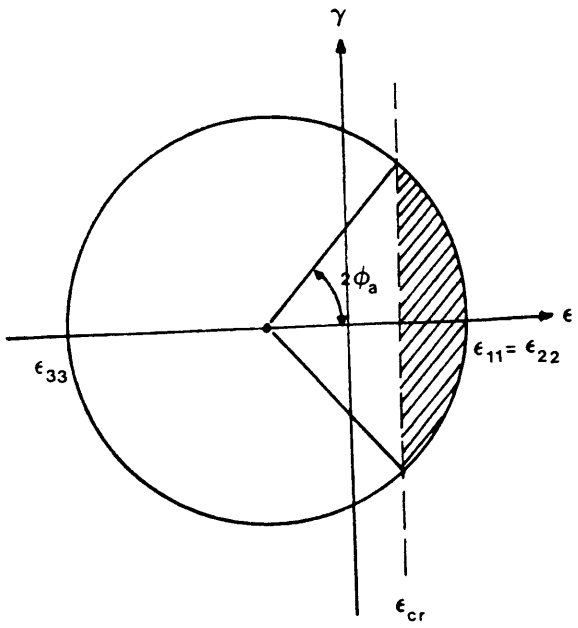

Figure 4.8 Mohr's Circle Representation of the Favored Microcrack Orientations for Uniaxial Loading.

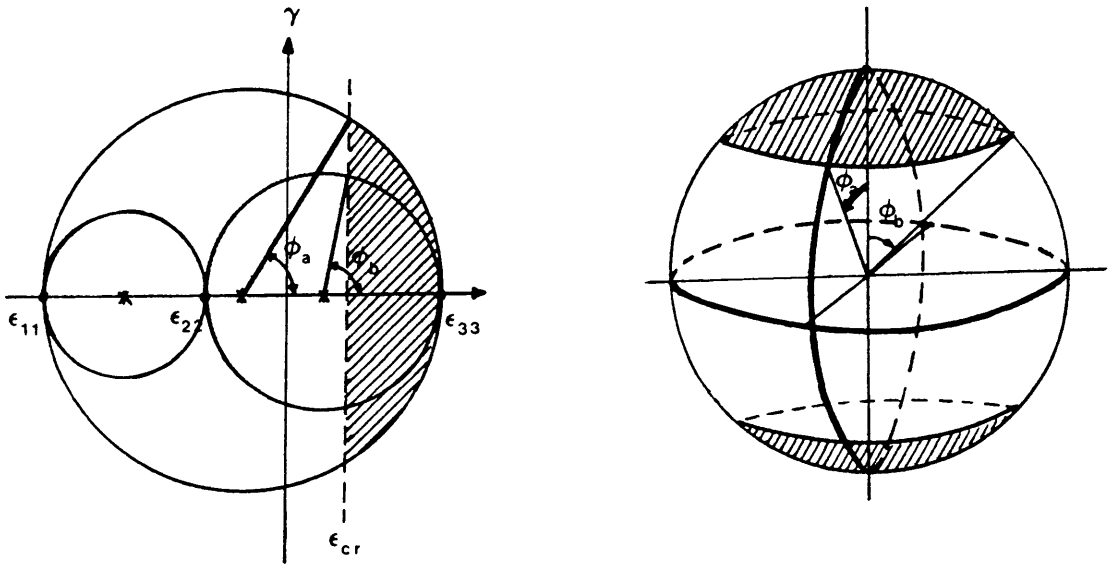

Figure 4.9 Mohr's Circle Representation of the Favored Microcrack Orientations for General Triaxial Loading.

$$\sigma_{nn} = \sin^2\phi\ \sigma_I + \cos^2\phi\ \sigma_{III} \tag{4.56}$$

$$\dot{\epsilon}^d_{nn} = \sin^2\phi\ \epsilon_I + \cos^2\phi\ \dot{\epsilon}^d_{III} \tag{4.57}$$

In a similar manner the damage evolution for the second mechanism is related to a total accumulated strain and the evolution for damage is expressed by

$$\frac{d\omega^{(2)}}{d\epsilon_{nn}} = f_2(\omega^{(2)},\ \sigma_{nn},\ \dot{\epsilon}_{nn})$$
$$= \beta_2(\alpha_2 - \omega^{(2)}) \tag{4.58}$$

with initial condition,

$$\omega^{(2)} = 0 \quad \text{for } \epsilon_{nn} \leq \epsilon_{cr}$$

where again α_2 and β_2 are parameters to take account stress and strain-rate dependency of the damage growth. We propose:

$$\alpha_2 = \alpha_2(\sigma_{nn}) = \exp(\gamma_2\sigma_{nn}) \tag{4.59}$$

$$\text{or} \quad \alpha_2 = 1 \quad \text{for } \sigma_{nn} < 0$$

$$\beta_2 = \beta_2(\dot{\epsilon}_{nn}) = \xi_2 \log|\dot{\epsilon}_{nn}| + \eta_2 \tag{4.60}$$

$$\text{or} \quad \beta_2 = -5\xi_2 + \eta_2 \quad \text{for } |\dot{\epsilon}_{nn}| < 10^{-5}$$

where γ_2, ξ_2, and η_2 are material constants to be determined from the experimental results. It should be noted here that ω actually is defined as a function of θ and ϕ implicitly through strains.

The limits of damage field must be established and we assume that

the region of active damage is limited to planes subject to strains which exceed the critical values, ϵ^{d}_{cr} and ϵ_{cr}. Thus, for given loading conditions the maximum and minimum principal strains ϵ_{I}, ϵ_{II} and ϵ_{III} can be determined and hence the orientations of the possible microcrack systems also can be determined from the Mohr's circle representation for simple loading condition (Figure 4.8). For general triaxial loading conditions a direct integration of Equation (4.46) is required (Figure 4.9).

4.6 SUMMARY OF THE FORMULATION

The total strain is considered as the sum of an instantaneous, a delayed elastic, and an irrecoverable viscous components. The constitutive equations are given by these three strain components each associated with damage variable as per Equation (4.28) for elastic strain where the stiffness matrix involves damage effect, the delayed elastic strain using Equation (4.35), and the power-law creep model (4.44) with the relations for the viscous strain. In both delayed elastic strain and viscous strain, the damage effect is included by way of the effective stresses.

$$\epsilon_{IJ} = \epsilon^{e}_{IJ} + \epsilon^{d}_{IJ} + \epsilon^{v}_{IJ} \tag{4.61}$$

$$\sigma_{IJ} = K_{IJKL}\epsilon^{e}_{KL} \tag{4.62}$$

$$\dot{\epsilon}^{d}_{IJ} = A\left[\frac{3}{2} K\tilde{S}_{IJ} - \epsilon^{d}_{IJ}\right]^{m} \tag{4.63}$$

$$\dot{\epsilon}^{v}_{IJ} = \frac{3}{2} K_n \left(\frac{3}{2} \tilde{S}_{KL}\tilde{S}_{KL}\right)^{\frac{n-1}{2}} \tilde{S}_{IJ} \tag{4.64}$$

where $\tilde{S}_{IJ}$ is effective deviatoric stress tensor. The damage evolution law is developed for two microcracking mechanisms.

$$D_{KL} = D^{(1)}_{KL} + D^{(2)}_{KL} \tag{4.65}$$

Each damage tensor is defined by,

$$D^{(1)}_{KL} = \int_{\theta 1}^{\theta 2} \int_{\phi 1}^{\phi 2} \omega^{(1)} N_{KL} \, d\theta d\phi \tag{4.66a}$$

$$D^{(2)}_{KL} = \int_{\theta 1}^{\theta 2} \int_{\phi 1}^{\phi 2} \omega^{(2)} N_{KL} \, d\theta d\phi \tag{4.66b}$$

and the evolution of individual microcrack system is assumed by

$$\frac{d\omega^{(1)}}{d\epsilon^{d}_{nn}} = f_1(\omega^{(1)}, \sigma_{nn}, \dot{\epsilon}^{d}_{nn})$$

$$= \beta_1(\alpha_1 - \omega^{(1)}) \tag{4.67a}$$

$$\frac{d\omega^{(2)}}{d\epsilon_{nn}} = f_2(\omega^{(2)}, \sigma_{nn}, \dot{\epsilon}_{nn})$$

$$= \beta_2(\alpha_2 - \omega^{(2)}) \tag{4.67b}$$

A schematic diagram that illustrates the combination of damage and the conventional viscoelastic model is given in Figure 4.10.

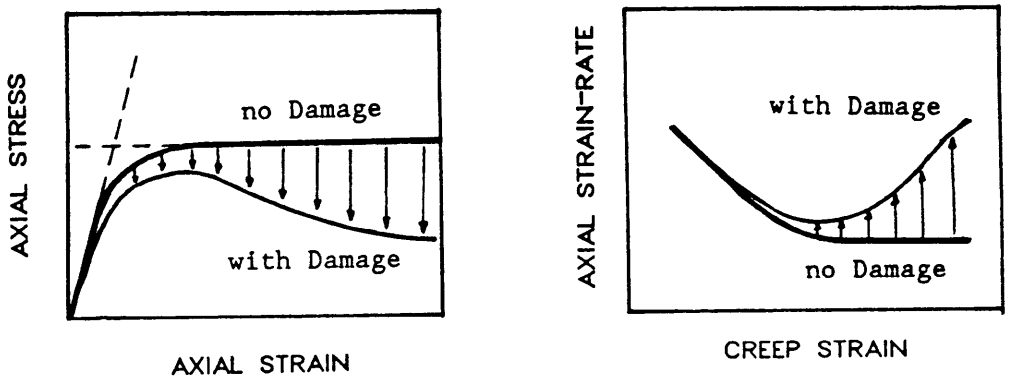

Figure 4.10 Combination of Damage with Conventional Viscoelastic Model.

CHAPTER 5

CONSTITUTIVE MODEL IN SIMPLE DEFORMATION MODES

The general three dimensional theory developed in Chapter 4 is specialized in this section for describing simple deformation modes. Two uniaxial loading conditions, i.e., constant strain-rate data and constant stress data for uniaxial compression test are used to identify the material parameters. Solution algorithms are also discussed.

5.1 FORMULATION OF SIMPLE DEFORMATION MODES

The damage model developed in this research is based on general three dimensional formulation. Consider first the case of uniaxial compressive loading (or tensile loading depending on the signs of applied stress) on a cylindrical specimen with confining hydrostatic pressure where the axial force is applied along the longitudinal axis (Figure 5.1), i.e., $\sigma_{11} = \sigma_{22}$ ($\neq \sigma_{33}$). In fact this is a special case of the general triaxial loading conditions and the uniaxial response can be easily obtained by letting confining hydrostatic pressure as zero, i.e., $\sigma_{11} = \sigma_{22} = 0$. In the general cases the microcracks are oriented upon the applied stresses and the damage variable will be a function of this orientation. Most of microcracks and ultimate fracture are developed in the planes perpendicular to the maximum tensile strain direction as the observation reveals.

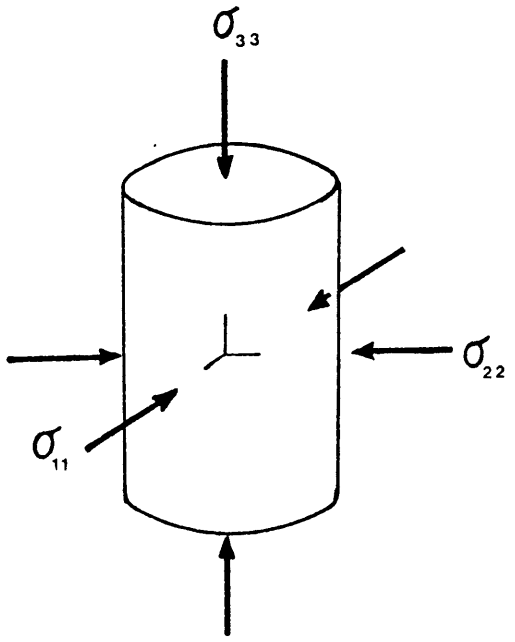

Figure 5.1 Uniaxial Compression with Confining Pressure.

Now consider the evolution of damage. As explained in the previous chapter we postulated two mechanisms in relation with damage growth. The first mechanism is associated with grain boundary cracking and is thought to be governed by delayed elastic strain. The second mechanism is related with crack nucleation governed by total accumulated strain. We note that two independent damage mechanisms are superimposed here and use the relationship,

$$D_{IJ} = D_{IJ}^{(1)} + D_{IJ}^{(2)} \tag{5.1}$$

The damage tensors $\underline{D}^{(i)}$, (i = 1,2) are defined again for general cases,

$$D_{KL}^{(i)} = \int_{\theta 1}^{\theta 2} \int_{\phi 1}^{\phi 2} \omega^{(i)} N_{KL}(\theta,\phi)\, d\theta d\phi \qquad (5.2)$$

where $\omega^{(i)}(\theta,\phi)$ is resultant of the microcrack distribution in a particular damage system and N_{KL} is the tensor product of the normal vectors N_K and N_L. The orientation of the microcrack system, θ and ϕ, defines the ranges of all active microcrack systems to be integrated over to yield the projections on the principal planes. Since it was assumed that the evolutions of two damage mechanisms are in the same manner, so the superscript, $^{(i)}$, will be omitted from now unless it is specified in order to distinguish two mechanisms in the formulation.

For uniaxial compression, using the integration limits, $-\frac{\pi}{2} \le \theta \le \frac{\pi}{2}$ and $\frac{\pi}{2} - \phi_a \le \phi \le \frac{\pi}{2} + \phi_a$, we can integrate to find the damage principal values while all other off-diagonal terms vanish since ω is independent of the angle θ in this uniaxial cases for both confined and unconfined cases (see Figure 5.2).

$$D_{12} = \int_{-\frac{\pi}{2}}^{\frac{\pi}{2}} \int_{\frac{\pi}{2}-\phi_a}^{\frac{\pi}{2}+\phi_a} \omega \cos\theta \sin\theta \sin^2\phi \, d\theta d\phi$$

$$= \int_{-\frac{\pi}{2}}^{\frac{\pi}{2}} \frac{1}{2} \sin 2\theta \, d\theta \int_{\frac{\pi}{2}-\phi_a}^{\frac{\pi}{2}+\phi_a} \omega \sin^2\phi \, d\phi$$

$$= \frac{1}{4} \left[-\cos 2\theta \right]_{-\frac{\pi}{2}}^{\frac{\pi}{2}} \int_{\frac{\pi}{2}-\phi_a}^{\frac{\pi}{2}+\phi_a} \omega \sin^2\phi \, d\phi = 0 \qquad (5.3)$$

Similarly $D_{23} = D_{13} = 0$, therefore

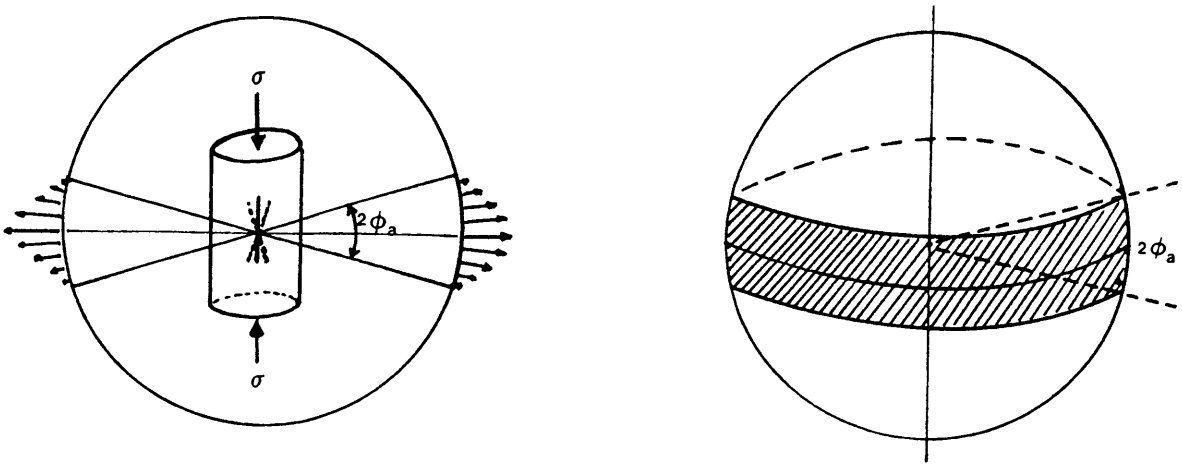

Figure 5.2 a) Damage Orientation under Uniaxial Compression.

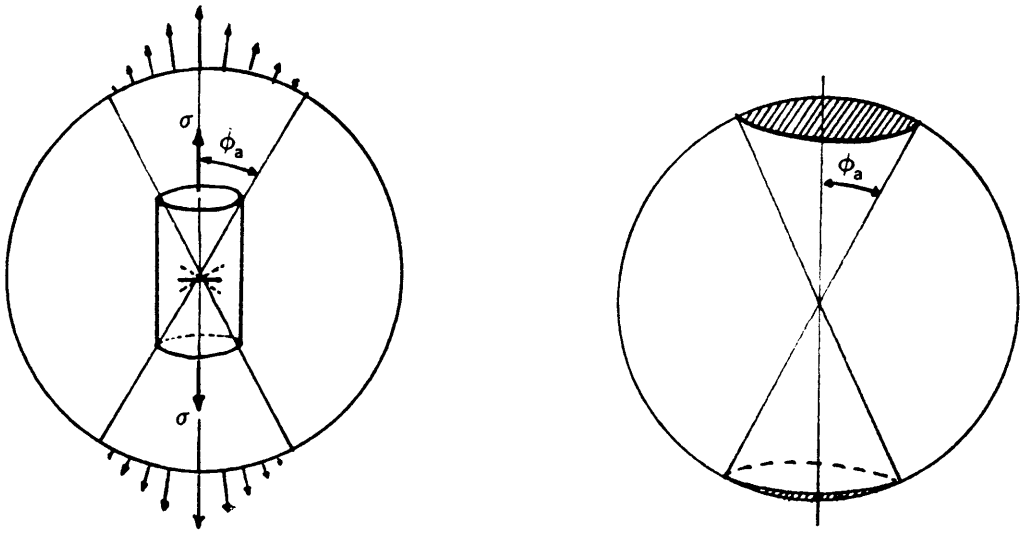

Figure 5.2 b) Damage Orientation under Uniaxial Tension.

$$D_{KL} = \begin{bmatrix} D_{11} & 0 & 0 \\ & D_{22} & 0 \\ \text{sym.} & & D_{33} \end{bmatrix} \tag{5.4}$$

with components

$$D_{11} = D_{22} = \frac{\pi}{2} \int_{\frac{\pi}{2}-\phi_a}^{\frac{\pi}{2}+\phi_a} \omega \sin^2\phi \, d\phi \tag{5.5}$$

$$D_{33} = \pi \int_{\frac{\pi}{2}-\phi_a}^{\frac{\pi}{2}+\phi_a} \omega \sin^2\phi \, d\phi \tag{5.6}$$

The angle ϕ_a in (5.3) is defined by (see Figure 5.2),

$$\phi_a = \frac{1}{2} \cos^{-1}\left[\frac{\epsilon_{cr} - \left(\frac{\epsilon_{11} + \epsilon_{33}}{2}\right)}{\left(\frac{\epsilon_{11} - \epsilon_{33}}{2}\right)} \right] \tag{5.7}$$

The damage component D_{33} represents the projection of the active microcrack field onto the plane perpendicular to the x_3 axis. This value is small compared to the effect of D_{11} (= D_{22}) and may be neglected in uniaxial compression case. However in uniaxial tension most of the microcracks develop in the x_1-x_2 plane or in the slightly tilted planes from it with orientation of $-\frac{\pi}{2} \le \theta \le \frac{\pi}{2}$ and $-\phi_a \le \phi \le \phi_a$, thus damage component D_{33} is much greater than the other two components.

Since there are no shear strains developed from applied uniaxial loading conditions the stress-strain (elastic) relationship can be expressed in terms of the normal strains.

$$\begin{Bmatrix}\sigma_{11}\\ \sigma_{22}\\ \sigma_{33}\end{Bmatrix} = \begin{bmatrix} \lambda+2\mu+2(C_1+C_2)D_{11}, & \lambda+C_1(D_{11}+D_{22}), & \lambda+C_1(D_{11}+D_{33}) \\ & \lambda+2\mu+2(C_1+C_2)D_{22}, & \lambda+C_1(D_{22}+D_{33}) \\ \text{sym.} & & \lambda+2\mu+2(C_1+C_2)D_{33} \end{bmatrix} \begin{Bmatrix}\epsilon^e_{11}\\ \epsilon^e_{22}\\ \epsilon^e_{33}\end{Bmatrix} \tag{5.8}$$

Rearranging the matrix equation (5.8) with notations introduced by Krajcinovic and Fonseka [1981],

$$\begin{Bmatrix}\sigma_{11}\\ \sigma_{11}\\ \sigma_{33}\end{Bmatrix} = E\cdot k \begin{bmatrix} 1+(K_1+K_2)D_{11}, & \bar{\nu}+K_1D_{11}, & \bar{\nu}+\frac{1}{2}K_1(D_{11}+D_{33}) \\ & 1+(K_1+K_2)D_{11}, & \bar{\nu}+\frac{1}{2}K_1(D_{11}+D_{33}) \\ \text{sym.} & & 1+(K_1+K_2)D_{33} \end{bmatrix} \begin{Bmatrix}\epsilon^e_{11}\\ \epsilon^e_{11}\\ \epsilon^e_{33}\end{Bmatrix} \tag{5.9}$$

or

$$\begin{Bmatrix}\sigma_{11}\\ \sigma_{33}\end{Bmatrix} = E\cdot k \begin{bmatrix} \frac{1}{2}(1+\bar{\nu})+(K_1+\frac{1}{2}K_2)D_{11}, & \bar{\nu}+\frac{1}{2}K_1(D_{11}+D_{33}) \\ \text{sym.} & 1+(K_1+K_2)D_{33} \end{bmatrix} \begin{Bmatrix}2\epsilon^e_{11}\\ \epsilon^e_{33}\end{Bmatrix} \tag{5.10}$$

where $\lambda = \dfrac{E\nu}{(1+\nu)(1-2\nu)}$, $\mu = \dfrac{E}{2(1+\nu)}$

$$\lambda + 2\mu = E\cdot k = \frac{E(1-\nu)}{(1+\nu)(1-2\nu)}$$

$$\bar{\nu} = \frac{\nu}{1-\nu}$$

and $K_i = \dfrac{2C_i}{E\cdot k}$, (i = 1,2)

The delayed elastic strain defined by Equation (4.63) can be calculated from the effective deviatoric stress tensor $\tilde{S}_{IJ}$.

$$\tilde{S}_{IJ} = \begin{bmatrix} -\frac{1}{3}(\tilde{\sigma}_{33} - \tilde{\sigma}_{11}), & 0, & 0 \\ & -\frac{1}{3}(\tilde{\sigma}_{33} - \tilde{\sigma}_{11}), & 0 \\ \text{sym.} & & \frac{2}{3}(\tilde{\sigma}_{33} - \tilde{\sigma}_{11}) \end{bmatrix} \tag{5.11}$$

and

$$\dot{\epsilon}^{d}_{IJ} = A\left[\frac{3}{2} K\tilde{S}_{IJ} - \epsilon^{d}_{IJ} \right]^{m} \tag{5.12}$$

then

$$\dot{\epsilon}^{d}_{11} = \dot{\epsilon}^{d}_{22} = A\left[\frac{1}{2} K(\tilde{\sigma}_{11} - \tilde{\sigma}_{33}) - \epsilon^{d}_{11} \right]^{m}$$

$$\dot{\epsilon}^{d}_{33} = A\left[K(\tilde{\sigma}_{33} - \tilde{\sigma}_{11}) - \epsilon^{d}_{33} \right]^{m} \tag{5.13}$$

and all other components vanish.

The effective stress tensor $\tilde{\underline{\sigma}}$ used in calculating the delayed elastic strain and viscous strain is given by

$$\{ \tilde{\underline{\sigma}} \} = \frac{1}{2} \{ [K^{e}][K]^{-1} + [K]^{-1}[K^{e}] \} \{ \underline{\sigma} \} \tag{5.14}$$

where

$$[K^{e}] = E \cdot k \begin{bmatrix} \frac{1}{2}(1+\bar{\nu}), & \bar{\nu} \\ \bar{\nu}, & 1 \end{bmatrix} \tag{5.15}$$

$$[K] = E \cdot k \begin{bmatrix} B_1, & B_2 \\ B_2, & B_4 \end{bmatrix} \tag{5.16}$$

$$= E \cdot k \begin{bmatrix} \frac{1}{2}(1+\bar{\nu}) + (K_1 + \frac{1}{2}K_2)D_{11}, & \bar{\nu} + \frac{1}{2}K_1(D_{11}+D_{33}) \\ \text{sym.} & 1 + (K_1 + K_2)D_{33} \end{bmatrix}$$

and

$$[K]^{-1} = \frac{1}{E \cdot k} \frac{1}{\Delta} \begin{bmatrix} B_4 , & -B_2 \\ -B_2 , & B_1 \end{bmatrix} \tag{5.17}$$

where $\Delta = B_1 B_4 - B_2 B_2$ is the determinant of the matrix [K]. Hence the effective stress components are calculated by

$$\begin{Bmatrix} \tilde{\sigma}_{11} \\ \tilde{\sigma}_{33} \end{Bmatrix} = \frac{1}{\Delta} \begin{bmatrix} G_1 , & G_2 \\ G_2 , & G_4 \end{bmatrix} \begin{Bmatrix} \sigma_{11} \\ \sigma_{33} \end{Bmatrix}$$

$$= \frac{1}{\Delta} \begin{bmatrix} \frac{1}{2}(1+\bar{\nu})B_4 - \bar{\nu}B_2 , & \frac{1}{2}[\bar{\nu}(B_1+B_4) - \frac{1}{3}(3+\bar{\nu})B_2] \\ \text{sym.} & -\bar{\nu}B_2 + B_1 \end{bmatrix} \begin{Bmatrix} \sigma_{11} \\ \sigma_{33} \end{Bmatrix} \tag{5.18}$$

The viscous strain-rate components given by Equation (4.64) are obtained by replacing deviatoric stresses S_{IJ} with effective deviatoric stresses $\tilde{S}_{IJ}$ to include damage effect on the viscous strains.

$$\dot{\epsilon}^v_{IJ} = \frac{3}{2} K_n \left(\frac{3}{2} \tilde{S}_{KL} \tilde{S}_{KL}\right)^{\frac{n-1}{2}} \tilde{S}_{IJ} \tag{5.19}$$

hence

$$\dot{\epsilon}^v_{11} = \dot{\epsilon}^v_{22} = -\frac{1}{2} K_n (\tilde{\sigma}_{33} - \tilde{\sigma}_{11})^n$$

$$\dot{\epsilon}^v_{33} = K_n (\tilde{\sigma}_{33} - \tilde{\sigma}_{11})^n \tag{5.20}$$

where $\tilde{\sigma}_{33} - \tilde{\sigma}_{11} = \frac{1}{\Delta} [(G_2 - G_1)\sigma_{11} + (G_4 - G_2)\sigma_{33}]$.

For the definition of individual damage evolution laws $\omega^{(1)}$, $\omega^{(2)}$ for each mechanism, we proposed similar differential equations for each mechanism. For the first mechanism,

$$\frac{d\omega^{(1)}}{d\epsilon^{d}_{nn}} = f_1(\omega^{(1)},\ \sigma_{nn},\ \dot{\epsilon}^{d}_{nn})$$

$$= \beta_1(\alpha_1 - \omega^{(1)}) \qquad (5.21)$$

with initial condition,

$$\omega^{(1)} = 0 \quad \text{for } \epsilon^{d}_{nn} \leq \epsilon^{d}_{cr}$$

and α_1, β_1 are parameters which take account of stress and strain-rate dependency of damage growth respectively. we proposed simple functions for these parameters:

$$\alpha_1 = \alpha_1(\sigma_{nn}) = \exp(\gamma_1 \sigma_{nn}) \qquad (5.22)$$

$$\text{or} \quad \alpha_1 = 1 \quad \text{for } \sigma_{nn} < 0$$

$$\beta_1 = \beta_1(\dot{\epsilon}^{d}_{nn}) = \xi_1 \log|\dot{\epsilon}^{d}_{nn}| + \eta_1 \qquad (5.23)$$

$$\text{or} \quad \beta_1 = -5\xi_1 + \eta_1 \quad \text{for } |\dot{\epsilon}^{d}_{nn}| < 10^{-5}$$

where γ_1, ξ_1, and η_1 are material constants to be determined from the experimental results. In a similar manner the damage evolution for the second mechanism is related to a total accumulated strain and the evolution for damage is expressed by

$$\frac{d\omega^{(2)}}{d\epsilon_{nn}} = f_2(\omega^{(2)},\ \sigma_{nn},\ \dot{\epsilon}_{nn})$$

$$= \beta_2(\alpha_2 - \omega^{(2)}) \qquad (5.24)$$

with initial condition,

$$\omega^{(2)} = 0 \quad \text{for } \epsilon_{nn} \leq \epsilon_{cr}$$

where again α_2 and β_2 are parameters to take account stress and

strain-rate dependency of the damage growth. Again we proposed

$$\alpha_2 = \alpha_2(\sigma_{nn}) = \exp(\gamma_2 \sigma_{nn}) \tag{5.25}$$

$$\text{or} \quad \alpha_2 = 1 \quad \text{for } \sigma_{nn} < 0$$

$$\beta_2 = \beta_2(\dot{\epsilon}_{nn}) = \xi_2 \log|\dot{\epsilon}_{nn}| + \eta_2 \tag{5.26}$$

$$\text{or} \quad \beta_2 = -5\xi_2 + \eta_2 \quad \text{for } |\dot{\epsilon}_{nn}| < 10^{-5}$$

where γ_2, ξ_2, and η_2 are material constants.

5.2 CALIBRATION OF MATERIAL PARAMETERS

The presented damage model is employed for uniaxial compression and tension of polycrystalline ice specimens to examine the experimental results presented by Mellor and Cole [1982] and Jacka [1984]. The material is assumed to be initially isotropic and no defects are assumed to exist prior to application of loads. The material parameters are determined by first considering constant strain-rate tests and also constant stress tests data.

The damage model contains a number of material parameters of which can be selected on a physical grounds. The remaining parameters are determined by using trial and error methods in connection with test data especially of uniaxial constant strain-rate and constant stress test results.

The parameters A, K, m in delayed elastic strain and K_n, n in viscous strain are selected from the log-stress vs. strain-rate data for low constant stress creep or low strain-rate tests since these

parameters should be determined based on the perfect ductile (elastic-perfectly plastic) material states where no microcracks are assumed to exist but in reality no such states exist. Hence the only possible material data to be used in selecting these five parameters are in low stress or low strain-rate test since it is widely known that below a certain critical value of stress or strain-rate the damage never develops no matter how long the load continues [Gold, 1972; Sinha, 1982b]. A least squares method is used in determination of viscous strain parameters K_n and n.

The threshold values ϵ^d_{cr} and ϵ_{cr} of the microcrack formation can be reasonably selected upon the microscopic observations of the cavity formation. Sinha [1984] suggested a criterion for the first appearance of cracks from the assumption that the cracking begins when the delayed elastic strain reaches a critical value. However this criterion was derived for columnar S2 ice and uniaxial compressive creep condition only. Moreover the critical delayed elastic strain was defined as global compressive strain of the specimen measured along the axis of applied load, so its physical meaning was not clear in the other stress states (e.g., tension). Unfortunately there are no such experimental criteria so far developed for the polycrystalline ice under constant strain-rate tests and even constant stress tests. Therefore these values are selected as arbitrarily small values but in a reasonable range.

Summary of the material parameters determined is listed in Table 5.1. The same parameters are used in all deformation tests in this research.

5.3 SOLUTION ALGORITHMS

The preferred numerical algorithm depends on whether the strain-rate or the stress is prescribed. An iterative solution algorithm is developed for constant strain-rate responses to solve the nonlinear constitutive equations and damage evolution equations. The computational method consists of determining at each time increment the stress consistent with the imposed strain-rate and the constitutive equations. Starting from the initial state a value for axial stress σ is assumed for the next time increment. The elastic strains, delayed elastic strains and thus viscous strain-rates are calculated from the constitutive equations and the assumed stress σ. The stress output from the calculated viscous strain-rate would be different from the assumed stress. If not, the value of σ is altered and the calculations are repeated in an iterative manner until an agreement is established under the given strain-rate condition. The procedure is then repeated for the next time increment.

The algorithm for constant stress is much simpler. For each time increment the damage configuration is held fixed and new strain components are calculated. The damage configuration is then updated using the evolution laws and new effective stresses are then determined for use in the succeeding time step.

Table 5.1 Damage Model Material Parameters

Elastic	Delayed	Viscous
$E = 9500$ MPa	$A = 1.5\text{x}10^{-3}\text{sec}^{-1}$	$K_n = 1.71\text{x}10^{-7}\text{MPa}^{-n}\text{sec}^{-1}$
$\nu = 0.35$	$K = 1.2\text{x}10^{-3}\text{MPa}^{-1}$	$n = 3.11$
	$m = 1$	
	Damage Parameters	
$K_1 = 0.18$	$\gamma_1 = 1\ \text{MPa}^{-1}$	$\gamma_2 = 1\ \text{MPa}^{-1}$
$K_2 = -0.45$	$\xi_1 = 100$	$\xi_2 = 160$
	$\eta_1 = 525$	$\eta_2 = 830$
	$\epsilon_{cr}^{d} = 1\text{x}10^{-6}$	$\epsilon_{cr} = 1\text{x}10^{-5}$

CHAPTER 6

APPLICATIONS

With material parameters given in Table 5.1, the constitutive equations (5.10), (5.13), (5.20) and the damage evolution equations (5.1), (5.2), (5.21), and (5.24) are solved numerically to obtain results in the following.

The applications are tested first on the uniaxial cases and the analysis of multiaxial deformation problems will follow. The uniaxial tests include constant strain-rate test, constant stress test, and cyclic stress test. The multiaxial tests include axial compression test with confining hydrostatic pressure and biaxial plane stress test performed at constant strain-rate.

6.1 UNIAXIAL DEFORMATION RESPONSES

6.1.1 Constant Strain-Rate Deformation

Strain-rates of $\dot{\epsilon} = 1.0\text{x}10^{-7}$, $1.15\text{x}10^{-6}$, $1.13\text{x}10^{-5}$, $1.03\text{x}10^{-4}$ and $1.14\text{x}10^{-3}$ sec^{-1} are examined first to compare with test results and the resulting stress-strain predictions are shown in Figure 6.1 for uniaxial compression. Some selected data points from the experimental results by Mellor and Cole [1982] are also shown in the same figure. At higher strain-rates the influence of damage is very important as evidenced by the strain softening of the material. The predicted stress-strain curves corresponding to lower strain-rates fit the

experimental results very well while the difference between the calculated responses and test data is relatively larger at higher strain-rates. Although the experimental results by Mellor and Cole [1982] show well-developed and smooth stress-strain curves, however there are many scattered test results reported by others [Hawkes and Mellor, 1972; Wang, 1981] especially for strain softening regimes due to inhomogeneity of ice samples and inaccuracy of test machine control.

Furthermore most of the experiments conducted under the constant strain-rates are actually constant deformation-rate tests or constant cross-head speed tests. Sinha [1981b] indicated that loading a compression test specimen under constant cross-head speed leads to an increasing effective strain-rate which will reach the nominal strain-rate at some finite time. Because of the machine stiffness in addition to specimen stiffness, the effective cross-head speed of the testing machine during the loading can not be regarded as constant. The actual cross-head speed has a minimum value at the beginning of the test and continues to increase as strain increases. In order to meet the constant strain-rate condition the cross-head speed of test machine should be adjusted continuously. As the stiffness of the testing machine decreases the specimen will have a ductile-like response [Hamza, 1985]. In constant deformation-rate tests, a similar situation arises. In experiments where the control of strain-rate is difficult, total deformation is normally measured. Since the length of the specimen changes continuously during the test, the strain-rate calculated based on deformation or displacement divided by its current

length is not the same as constant value. Instead of true constant strain-rate an average strain-rate is sometimes used. As a consequence of using average strain-rate which is smaller than true strain-rate, the strength obtained in the experiments is expected to be less than the actual constant strain-rate test results.

The stress-strain curves for uniaxial tension are shown in Figure 6.2 (a) for several strain-rates. A combined figure of compression and tension is shown in Figure 6.2 (b) in the same scale. Uniaxial compressive strength shows strong dependence on the strain-rate while tensile strength shows little dependence on strain-rate. When the strain-rate is less than $10^{-5}sec^{-1}$, the compressive response is ductile with stress reaching an asymptotic value. When the strain-rate is increased further the ice shows a strain softening characteristics. This strain softening behavior caused by damage accumulation becomes pronounced as strain-rate is increased. A comparison of tensile and compressive failure strength (maximum stress) of ice for variation of strain-rates is plotted in Figure 6.3. The proposed model follows the overall trend of the data very well (also see Hawkes and Mellor [1972]). For many years there has been a debate about the existence of ductile-to-brittle transition behaviors and about whether the strength at very high strain-rates drops or continues to increase. Our model shows a steadily increasing and flattened trend in compression while nearly constant trend for tensile loadings. As we observed in the different test data which is widely scattered, the trend about the strength at very high strain-rate is not yet clear. However it is somewhat obvious that the beginning of

transition strain-rate is around $10^{-5}sec^{-1}$ and the continuum damage model may not be appropriate for strain-rate greater than $10^{-2}sec^{-1}$, since a sudden macrofracture causes a total material rupture.

In Figure 6.4 the strains at failure are shown as functions of applied strain-rate and experimental results are shown in the same figure. Mellor and Cole [1982] concluded that the strain data for maximum stress occurs at approximately 1% strain for constant strain-rate tests and there is a corresponding relation for constant stress tests, too. The failure strain data scattered around 1% of strain shows a good agreement with the proposed damage model. However the deviation between failure strain data and 1% strain becomes greater at the relatively high strain-rates and the transition seems to occur at about $10^{-5}sec^{-1}$. Our model shows a similar trend, i.e., decreasing failure strains with increasing strain-rate. In fact, the damage parameters of the proposed model was determined based on this trend.

Typical damage evolution curves at constant strain-rate are shown in Figure 6.5 (a) for uniaxial compression. As expected in the previous sections, for uniaxial compression the accumulation of damage in the plane parallel to the direction of compressive stress is much larger than the damage in the other planes perpendicular to loading axis. The same results are obtained for uniaxial tension with larger damage in planes according to maximum tensile strain direction, which are readily verified by experimental observations. The accumulation of material damage is significant for high strain-rates while for lower strain-rates damage growth is slow and small. The strain

softening behavior at higher strain-rates can be explained by this fast damage growth. The growth of each damage component according to two different damage mechanisms is given in Figure 6.5 (b). This illustrates an example of the evolution of the damage components, for the constant strain-rate condition $\dot{\epsilon} = 1.0\text{x}10^{-3}\text{sec}^{-1}$, that are assumed to be a function of delayed elastic strain and total strain respectively. Note that the total damage is simply a sum of the two damage components $D_{11}^{(1)}$ and $D_{11}^{(2)}$. The ratio of these two damage evolutions varies with strain-rate and strain. As strain-rate or strain increase, the second damage mechanism which is a function of total strain plays an important role.

For uniaxial deformation results, two multiaxial aspects, i.e., apparent Poisson's ratio and volumetric strain, should be pointed out. The stress-strain behaviors in axial and lateral directions are examined. Poisson's ratio ν is defined as the ratio of lateral strain to axial strain. Dynamic values of Poisson's ratio in the range 0.31 ~ 0.38 for fresh water ice were known [Gold, 1958; Weeks and Assur, 1968] but ice at high homologous temperature may exhibit peculiar material behaviors beyond elastic response for static deformation processes. Since Poisson's ratio is an elastic parameter, the term "apparent Poisson's ratio" may not be appropriate for tests with inelasticity. Instead the term "strain ratio" is preferred here. Sinha [1987] stated that the contribution of grain boundary sliding, in addition to that of pure elastic and viscous strain, could influence the strain ratio. In discussing experimental results by Murat and Lainey [1982], he showed a strain-rate dependence of strain

ratio in isotropic ice, where the ratio was near 0.5 for low strain-rates and decreasing to a dynamic value with increasing strain-rate. Similar results are obtained here.

In Figures 6.6 (a) and (b), the strain ratios ($-\frac{\epsilon_{11}}{\epsilon_{33}}$) for compression and tension are shown. The strain ratio in uniaxial compression approaches 0.5 as strain increases. For ductile deformation where strain-rates are sufficiently slow, the strain ratio increases fast with strains while for brittle deformation it approaches 0.5 slowly compared to ductile cases. In tension the strain ratio reaches 0.5 again with the same trend as in compression. These results are somewhat different from those discussed in Sjölind [1987] where the strain ratios at high strain-rates drop to below its dynamic value for uniaxial tension and increase to above 0.5 for uniaxial compression tests. In view of his stress-strain results which showed sudden drops after the peak stress for higher strain-rates, very high values of strain ratio for compression and lower value than its dynamic value for tension could have been due to very high cracking activity where only elastic deformation displayed. That may be unrealistic and should be verified by proper experiments.

In Figures 6.7 (a) and (b) we see dilatancy effect of ice deformation as the volumetric strain increases and decreases to change its sign. The curves describing volumetric strain as a function of stress show the familiar behavior often seen in compression tests of brittle material, in general. These results confirm the observed experimental behaviors of concrete [Krajcinovic and Selvaraj, 1983].

6.1.2 Constant Stress Deformation

A way to check the validity of proposed model with regard to damage accumulation, is to compare creep strain and strain-rate prediction with the observed tertiary creep deformation data. The calculated creep response curves for the various applied stresses are shown in Figures 6.8 (a)-(d). Test data of Mellor and Cole [1982] under uniaxial constant stress condition are also shown in the figures to compare with the proposed model. The model prediction agrees well with the test results for moderate stress range. Compressive stresses σ = 1.0, 1.54, 2.0, 2.35 and 3.06 MPa are applied to samples and the resulting strains and strain-rates are recorded.

In Figure 6.9 an effort is made to compare microcrack damage measure with a measured value of crack density. In the figure (a), damage accumulation ω of a particular orientation ($\phi = 90^{\circ}$) is shown as function of elapsed time and in the figure (b), crack density recorded by Gold [1972] for various constant stress condition is shown. It is difficult to measure a current state of damage directly by inspecting microcrack distribution of a specimen. However it may be possible for ice to relate the experimental crack density with microcrack damage measure. Integrating ω over all active planes may lead to a qualitative connection with measured crack density of ice. Even though a quantitative agreement can not be expected here, such a comparison clearly demonstrates a plausible connection between physical cracking processes and model parameters.

In the conventional strain/time curves and the log-scale strain-rate/strain/time curves, the model shows classical stages of

primary creep and secondary creep (in fact it is just an inflection point rather than a long period) and rapidly increasing strains during tertiary creep stage. The agreement is satisfactory except for large strains (5 ~ 10 %) where the experiments tend to reach a steady-state tertiary plateau while the model behaves increasing strain-rate at large strains. This is believed that the discrepancy between the theory and the experiments (compression test) is primarily due to the lack of proper mechanism in the modelling of damage. As noted earlier the deformational recrystallization process plays an important role in the deformation of ice under compression at higher strains where tertiary plateau is attained. Actually the adopted damage evolution law would have to be modified to account for this mechanism in the future.

An interesting aspect of the results is the relations between minimum strain-rate and strength. For a constant strain-rate test, the strength is the maximum stress which the sample resists. Mellor and Cole [1982, 1983] have observed that the applied stress and minimum strain-rate for a creep test correspond respectively to the peak strength and constant applied strain-rate for a strength test. They discussed the correspondence between the characteristics of constant stress curves and constant strain-rate curves, considering some identifiable points on both curves. Shown in Figure 6.10 is the strain-rate versus strain prediction from the model for an applied stress of 2.35 MPa. The minimum strain-rate is found to be 3.46×10^{-6} sec^{-1}. Using this strain-rate in a strength test, the resulting stress-strain curve can then be obtained as shown in the same figure

with a maximum stress of 2.41 MPa. We note that the "strain to failure" is similar in both cases ($\epsilon_{33} = 9.5\text{x}10^{-3}$ for the strength test and $\epsilon_{33} = 9.18\text{x}10^{-3}$ for the creep test). Thus this model shows very close agreement with the observation of Mellor and Cole even though a definite one-to-one correspondence is not established.

Figure 6.4 contains the constant stress creep results as well as constant strain-rate results in the form of failure strain versus applied strain-rate. For constant stress condition, a strain-rate in the horizontal axis means the minimum strain-rate obtained during deformation. Most of creep data falls on low strain-rate region in the sense of constant strain-rate tests. Failure strain at the minimum strain-rate is around 1% again. In most cases of experiment it is not easy to maintain ideal creep condition which requires a sudden applied loading. In reality a finite time of a few seconds is unavoidable before it reaches an equilibrium of constant stress creep condition. The finite rise time does influence the initial part of the primary creep however its influence is negligible for long time period, especially in tertiary creep.

In examining experimental data by Jacka [1984] for creep of ice, Ashby and Duval [1985] suggested a uniaxial creep constitutive model formulated in dimensionless form, leading to a single set of master curves. Up to the onset of tertiary creep their model describes creep behaviors very well regardless of stress and temperature variations. Jacka's creep data and Ashby and Duval's dimensionless equations is shown in Figure 6.11. Even though there is some scattering, the single master curve well relates the dimensionless variables

throughout the primary creep.

The nondimensional time is defined by normalizing time with respect to the applied stress, Young's modulus, and the minimum strain-rate:

$$\bar{t} = \frac{t\dot{\epsilon}_{min}E}{\sigma} \tag{6.1}$$

The nondimensional strain-rate is defined by normalizing with respect to the minimum strain rate:

$$\bar{\dot{\epsilon}} = \frac{\dot{\epsilon}}{\dot{\epsilon}_{min}} \tag{6.2}$$

and for nondimensional strain:

$$\bar{\epsilon} = \frac{\epsilon E}{\sigma} \tag{6.3}$$

In Figure 6.11 the nondimensional relation suggested by Ashby and Duval was:

$$\bar{\epsilon} = 1 + A\,[1-\exp\{-(C\bar{t})^{\frac{1}{n}}\}] + \bar{t} \tag{6.4}$$

where A, C and n are constants. Values of A = 70, C = 0.016 and n = 3 were applied.

The same scheme is applied to Mellor and Cole's [1982] creep data to examine the validity of the master curves. The results are shown in Figures 6.12 (a)-(c). It should be noticed that the stress level used in Mellor and Cole's experiments was 0.80 to 3.70 MPa which was much higher values compared to Jacka's stress level 0.12 to 1.47 MPa. It is not surprising that the low stress (less than 1.0 MPa) data from Mellor and Cole fall nicely on the Jacka's data and Equation (6.4).

The deviation from Equation (6.4) is most significant at higher strains and increases for higher stresses. The master curves based on low stress creep data are valid only in the low stress criterion where no damage effects are expected. With significant damage accumulation at high stress and large strains, especially in tertiary regime, the master curves do not apply at all. The proposed damage model is capable of describing this behavior by incorporating the effects of microcracking. Figures 6.12 (a)-(c) depict Equation (6.4) in a plot of dimensionless variables with the result of proposed damage model. Results from the damage model are shown for stress levels of σ = 3.06 MPa and σ = 1.54 MPa.

6.1.3 Cyclic Stress Deformation

The main purpose of this test is to check a possible application of the damage model to changing stress history and to see any changes in the cumulative damage responses under cyclic stresses. The experimental data on cyclic loading or on fatigue tests are rare and Mellor and Cole's [1981] result is the only available test data for isotropic polycrystalline ice.

The model is applied to uniaxial compressive sinusoidal stress between zero and a prescribed maximum stress level, i.e., 2.0 and 3.0 MPa. In Figures 6.13 (a) and (b) typical cyclic stress history and strain variations are shown for maximum stress 2.0 MPa and frequency of 0.043 Hz. The stress-strain curves in Figures 6.14 (a) and (b) show hysteresis loops progressing along the strain axis. The damage evolution under cyclic loading shows in Figure 6.15 that damage

evolution is a cumulative process, in other words, a monotonically increasing function. The delayed elastic strain and its time delayed effect partly results in the hysteresis loops under cyclic loadings. As Mellor and Cole [1981] noticed in their experiments, the cyclic stress creep behavior is similar to the behavior in constant stress creep curves as in Figures 6.16 (a) and (b). Even though the comparison with the test results is somewhat disappointing the model clearly shows important features of response of cyclic loading. For high stress (σ_{max} = 3.0 MPa) the creep strain well fits data but low stress (σ_{max} = 2.0 MPa) shows significant difference. As expected the mean strain curve for maximum cyclic stress 2.0 MPa lies below the constant stress (σ = 2.0 MPa) creep curve. These results illustrate an apparent limitation to the proposed model in that high cycle predictions may be inaccurate, particularly for lower stress levels.

It is not quite obvious what causes the discrepancy at lower stress behavior, however one answer could be that the thermally activated process prevails at lower stress level [Dillon, 1976]. Our damage model does not include any processes related with that. There seems to be certain mechanisms, such as recrystallization, which must be considered to model cyclic behaviors. The cyclic stress or fatigue problem requires further study.

6.2 MULTIAXIAL DEFORMATION RESPONSES

6.2.1 Axial Deformation under Confining Pressure

From the previous discussion on the dilatancy effect of volumetric strain we can readily understand that the triaxial state of stresses has a great influence on the deformation of ice. Quantitative investigations of the role of confining hydrostatic pressure on the accumulation of damage during deformation of ice are somewhat limited. The majority of available data are reported on constant strain-rate tests in comparison with unconfined cases.

For a high compressive confinement the microcracks will be arrested and the resulting behavior will be more ductile than the unconfined cases. Main effect of the confining pressure on the mechanical properties of ice is to close the microcracks and to suppress the cracking activities. In general the degree of ductility increases with an increase in confinement pressure. Like the observation on concrete, the strength of ice in triaxial loading is expected to increase considerably with increasing confining hydrostatic pressure and this was verified by experiment by Jones [1978, 1982] for polycrystalline ice and by Richter-Menge [1987] for anisotropic sea ice.

In Figure 6.17 test results by Jones [1982] are given. His ice sample was of different temperature and different grain size (1.0 mm at -11.5°C) from those used for present damage model, however a qualitative trend may be compared to. Jordaan [1986] assumed that the creep was independent of hydrostatic pressure at high confinement pressure and described Jones' data points with smooth lines in Figure

6.17. However it is not obvious to conclude whether ice has a pressure insensitivity at high confinement pressure or not at the present time, in view of other experimental results by Richter-Menge [1987] where the deviatoric strength of ice were increased with an increase in confining pressure and then decreased at high confining pressure.

Predicted stress-strain curves and failure strength versus confining pressure are given in Figures 6.18 and 6.19. As observation reveals, the confined strengths are always greater than the unconfined case for high strain-rate tests but the two sets of results converge at low strain-rate. It is evident that damage growth is restricted for high triaxiality and thus the material shows more ductile behavior. Peak stresses increase with increasing confining pressures.

Confining pressure effects for constant stress creep tests are examined in Figure 6.20 where less damage growth makes each creep curve move downward in the figure. As reported by Domaschuk et al. [1987] for creep of a frozen sand, the failure strain at minimum strain-rate increases as confined pressure increases.

6.2.2 Biaxial Plane Stress Deformation

Unfortunately the research on biaxially loaded ice has only concerned constitutive behavior in monotonic loading. Very little is known about biaxial softening behavior and rate dependence. Qualitatively the mechanical behavior of ice in biaxial states of loading is similar to that of concrete. But still there is an uncertainty in experimental data which makes the mathematical

formulation of failure criterion difficult. In Figure 6.21 model predictions are shown in the biaxial planes and similar failure envelopes by Timco and Frederking [1984] are also shown in Figure 6.22 for comparison.

Biaxial failure envelopes in Figure 6.21 show rate-dependent behavior in strength of ice where the failure strength in biaxial compression and biaxial tension tends to follow a von Mises yield criterion at low strain-rates. At high strain-rates tensile strength slightly decreases with increase of strain-rate however the difference is very small so basically tensile strength reaches a maximum value regardless of strain-rate. Compressive strength at high strain-rates shows a different behavior: the failure curve looks like a bell shape rather than an oval shape usually seen in brittle materials. The strength ratio of compression to tension is smaller than the values of 8 to 10 in Griffith type brittle materials.

Failure criteria are often expressed as a function of the stress invariants. In Figure 6.23, for constant strain-rates, $\dot{\epsilon} = 1.0\text{x}10^{-3}$ and $1.0\text{x}10^{-5}$ sec^{-1}, the model predictions are represented in the form of I_1 versus $\sqrt{J_2}$ plot, where I_1 is a first invariant of the stress tensor, i.e., σ_{ii} hydrostatic pressure and J_2 is a second invariant of the deviatoric stress tensor, i.e., $\frac{1}{2} S_{ij} S_{ij}$. Model predictions are obtained from uniaxial compression and tension, biaxial compression and tension, confined compression loadings. It is noted that I_1 vs. $\sqrt{J_2}$ plots are highly nonlinear unlike a von Mises yield criterion or a Mohr-Coulomb criterion which are straight lines in the I_1 versus $\sqrt{J_2}$ plot.

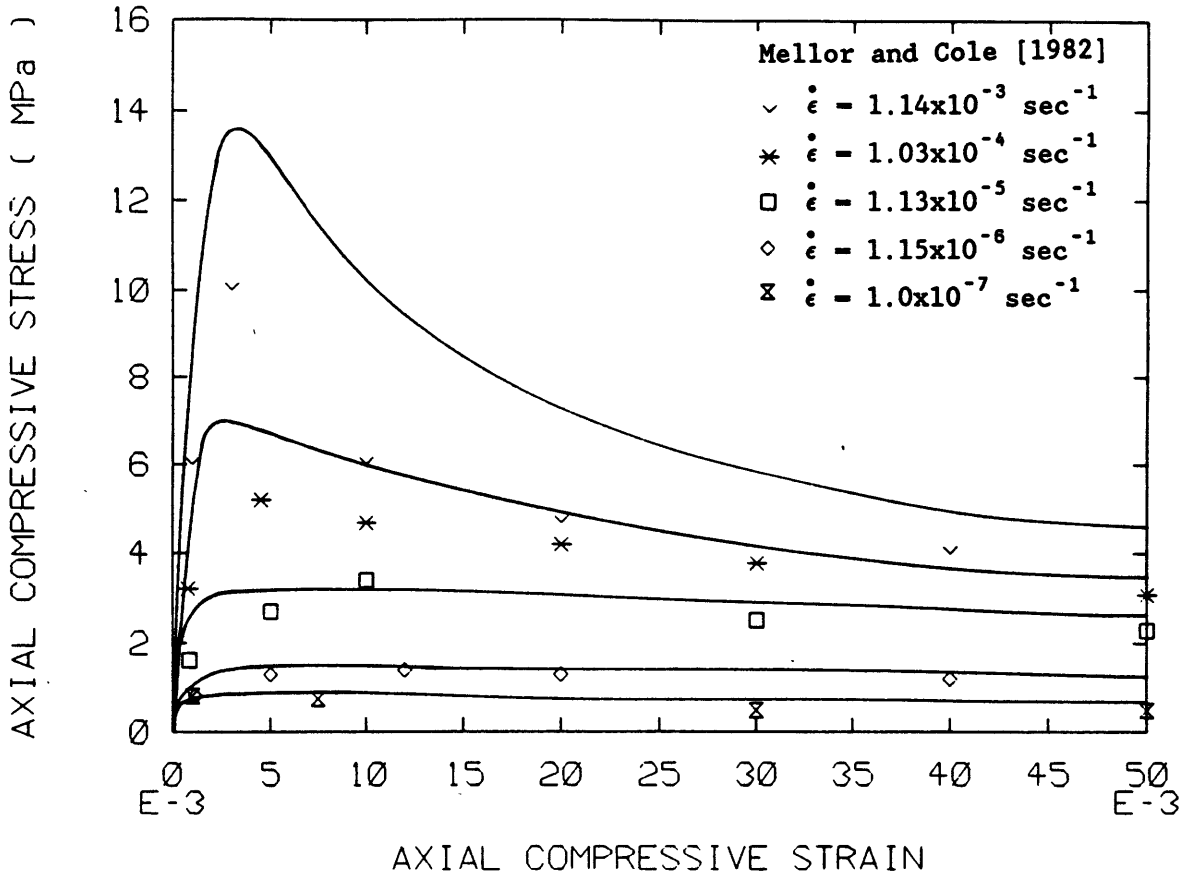

Figure 6.1 Predictions of Stress-strain Plots under Uniaxial Compression. Data points are selected from the test results of Mellor and Cole [1982].

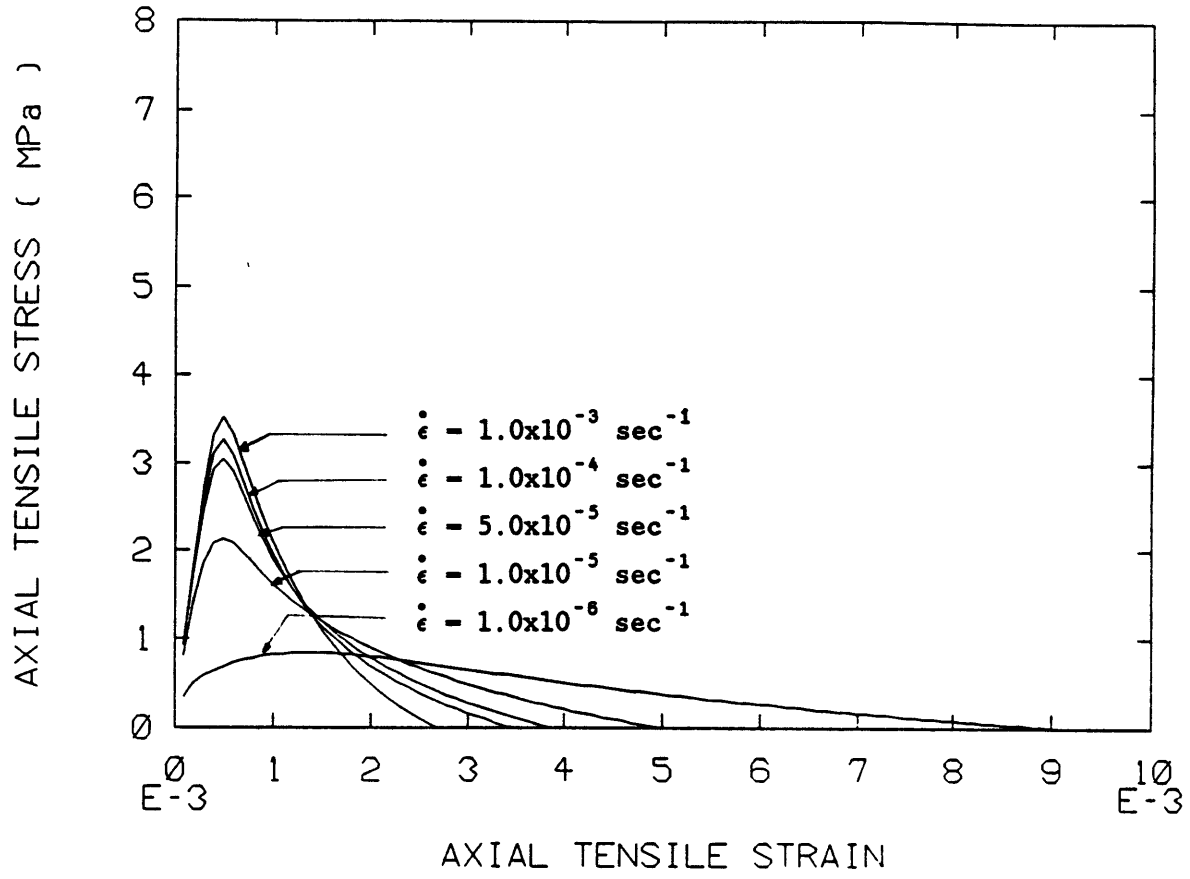

Figure 6.2 a) Stress-strain Plots for Uniaxial Tension.

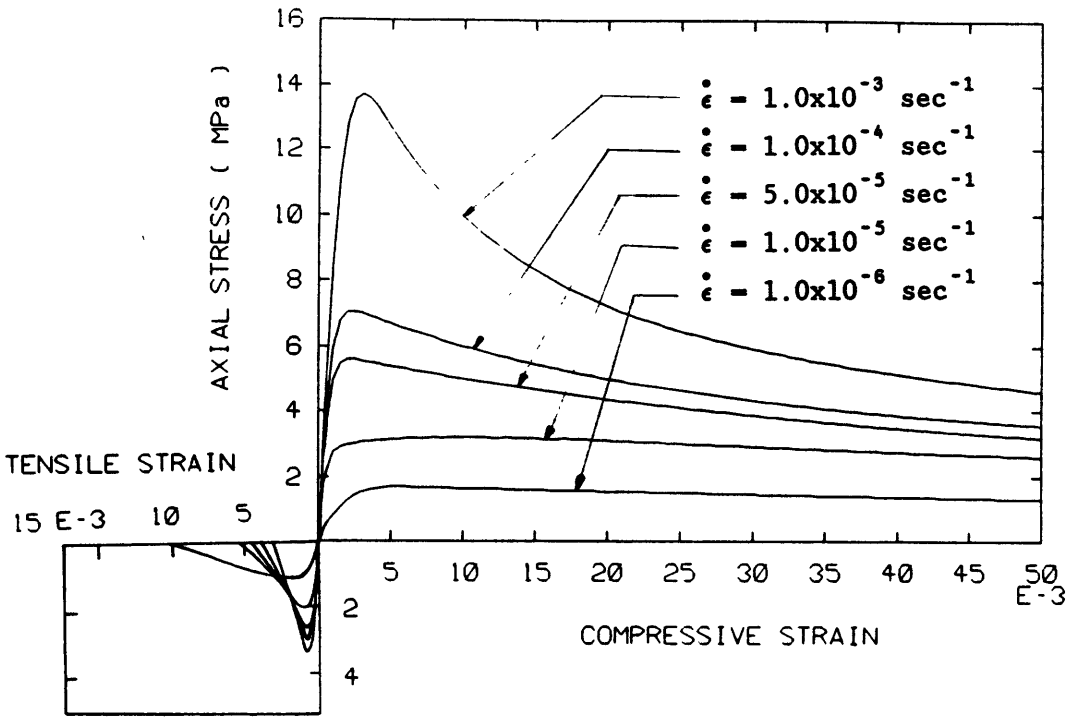

Figure 6.2 (b) Stress-strain Plots for Uniaxial Compression and Uniaxial Tension at Constant Strain-rate. The same scales are used in compression and tension.

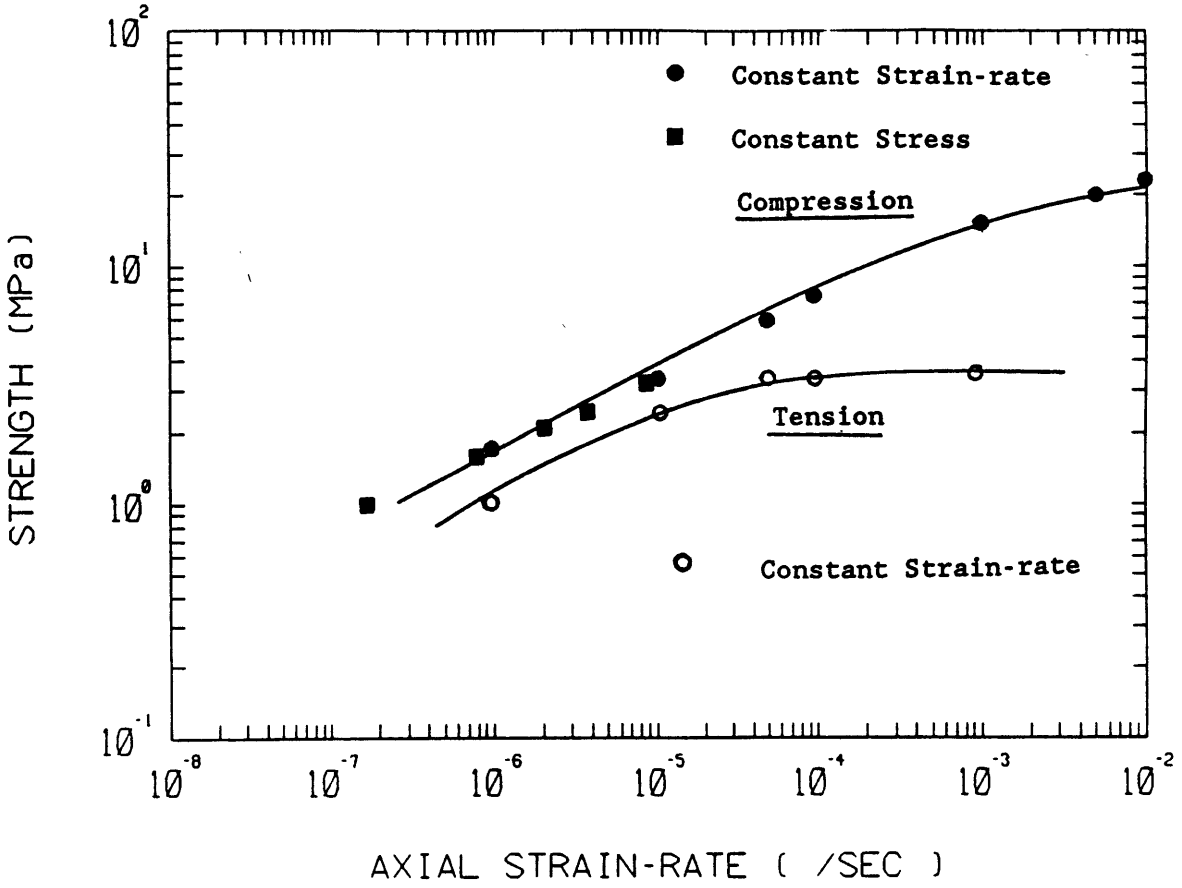

Figure 6.3 Strength of Ice in Strain-rate Variations.

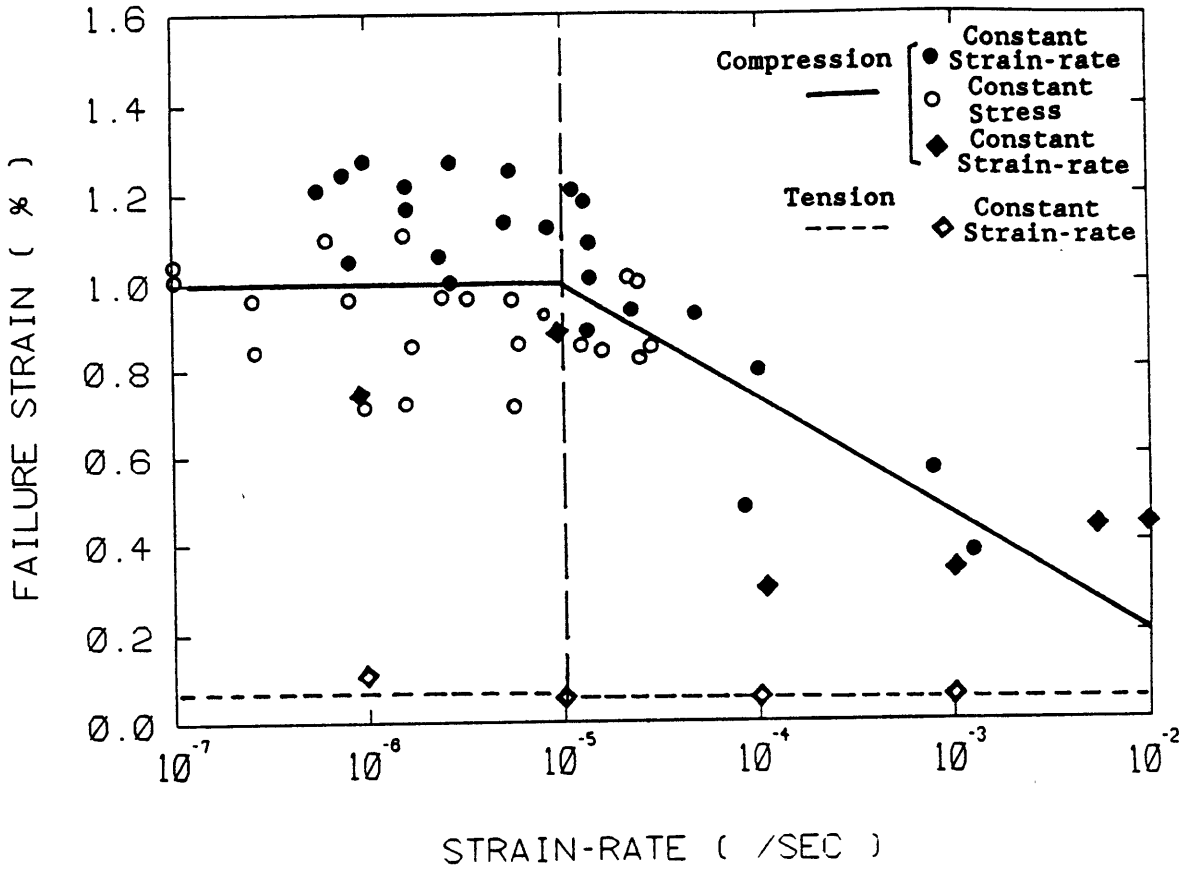

Figure 6.4 Failure Strains against Strain-rate. Data points (circle) are from Mellor and Cole [1982]. Squares are the model predictions. The trend of low strain-rate test data is different from that of high strain-rate data with strain-rate $10^{-5}sec^{-1}$ as an approximate border.

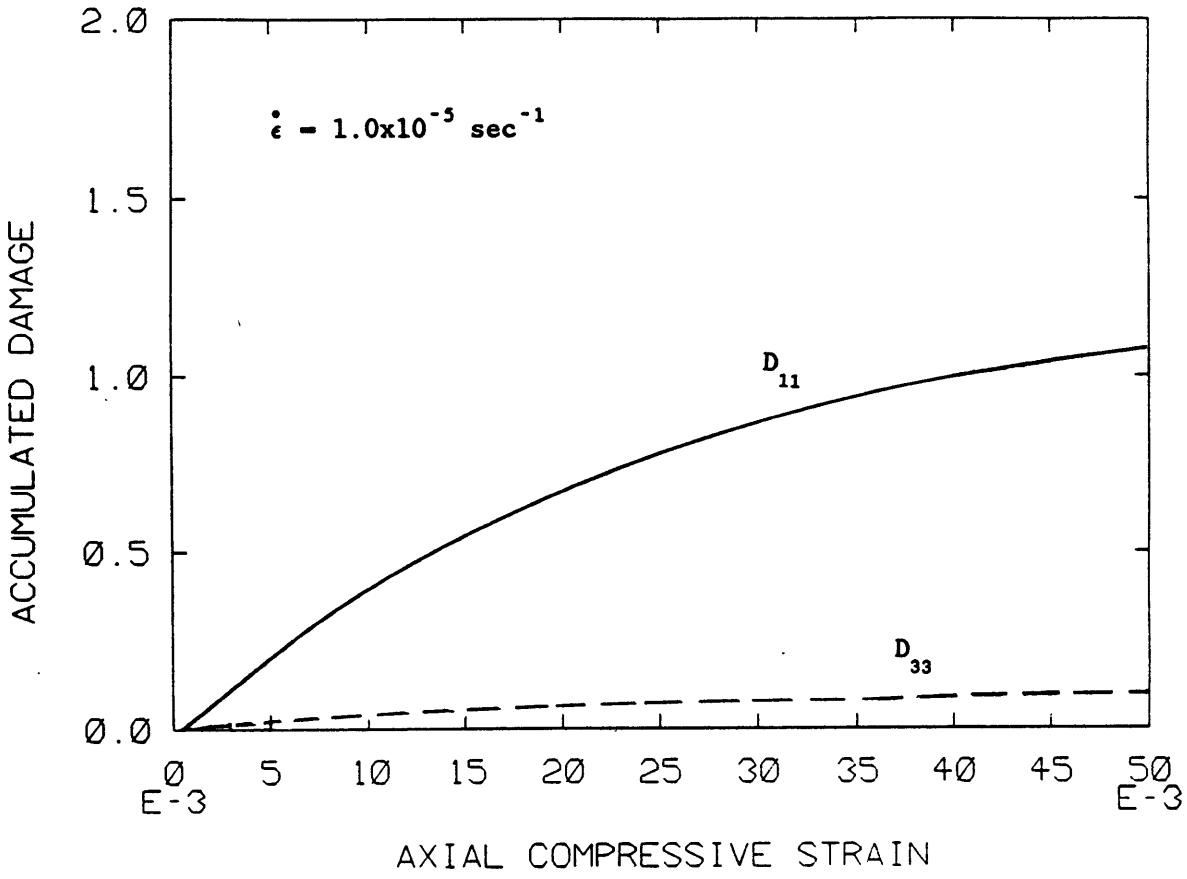

Figure 6.5 a) Damage Evolution Curves for Uniaxial Compression.

Solid line represents D_{11} and dashed line D_{33}.

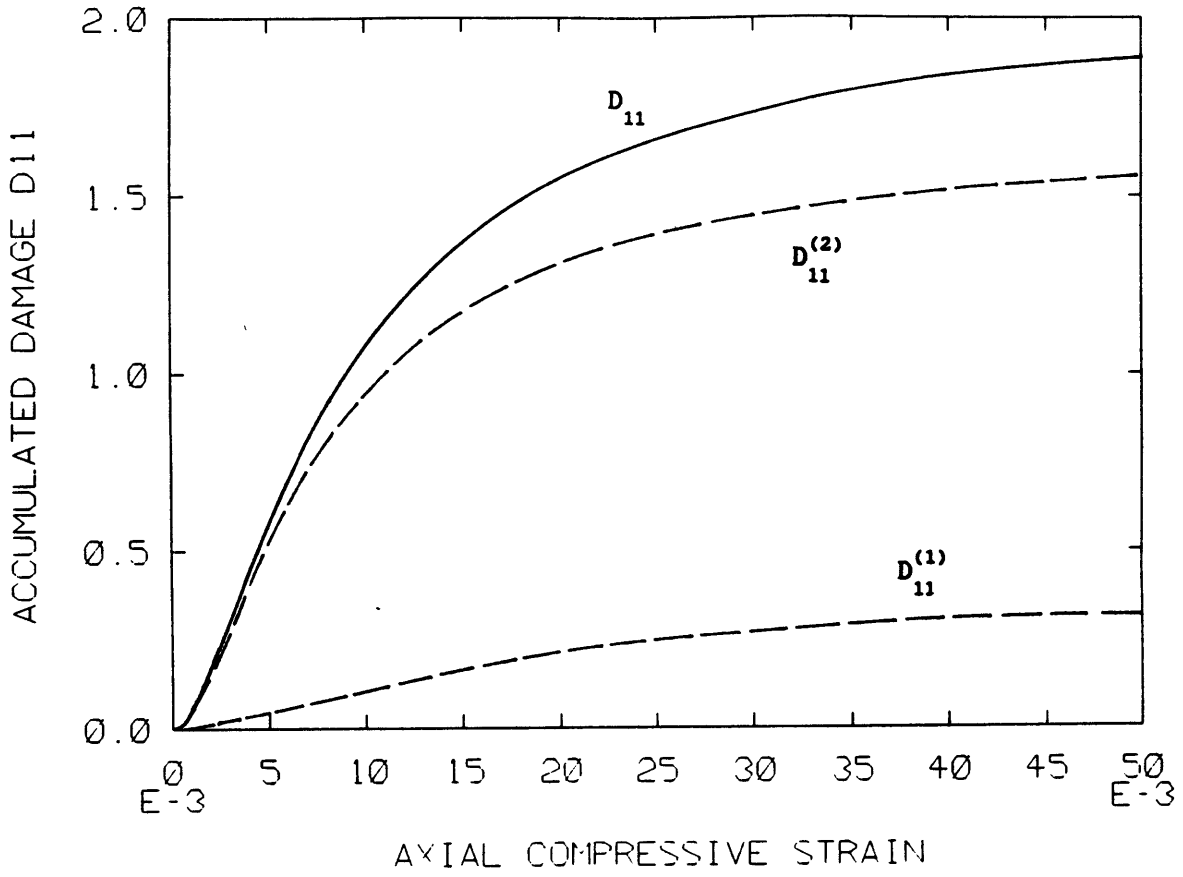

Figure 6.5 b) Damage Evolution Curves for Each Damage Mechanism in Uniaxial Compression at $\dot{\epsilon} = 1.0 \times 10^{-3} sec^{-1}$.

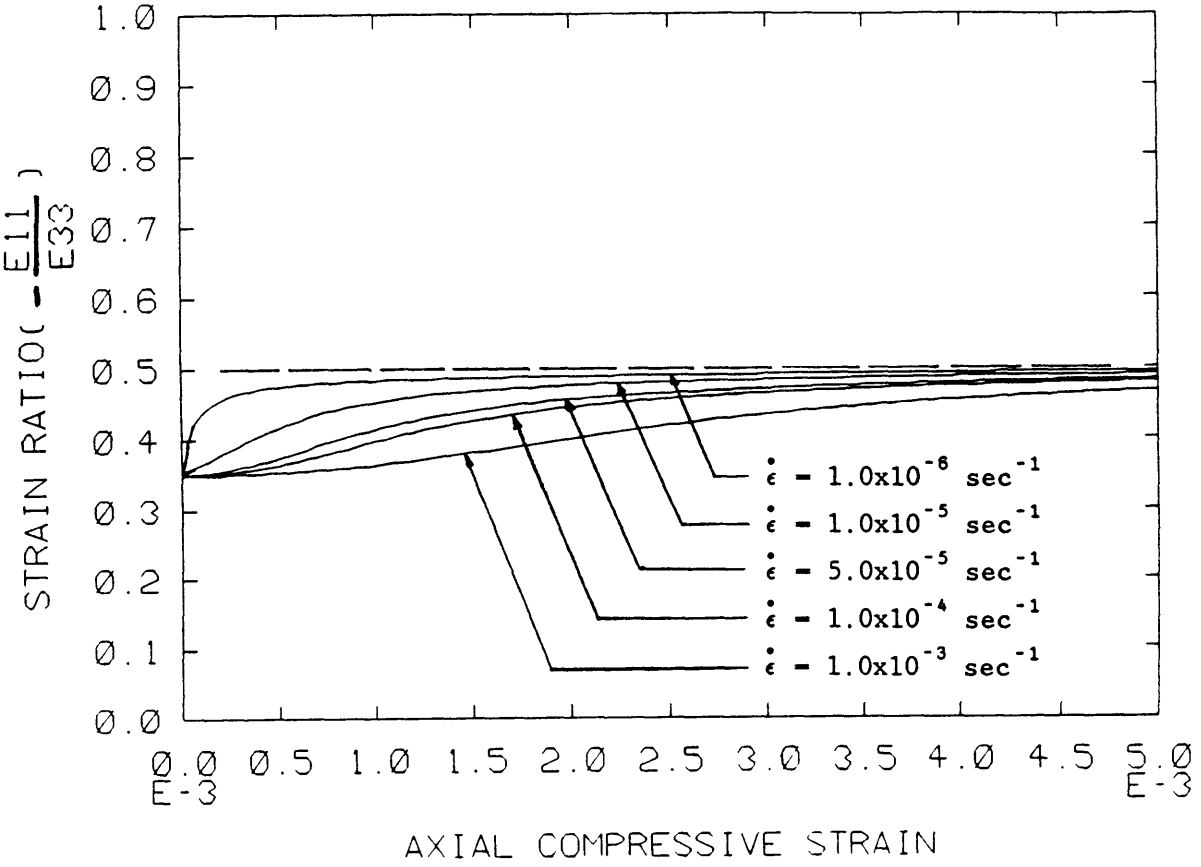

Figure 6.6 a) Strain Ratio Variation for Uniaxial Compression.

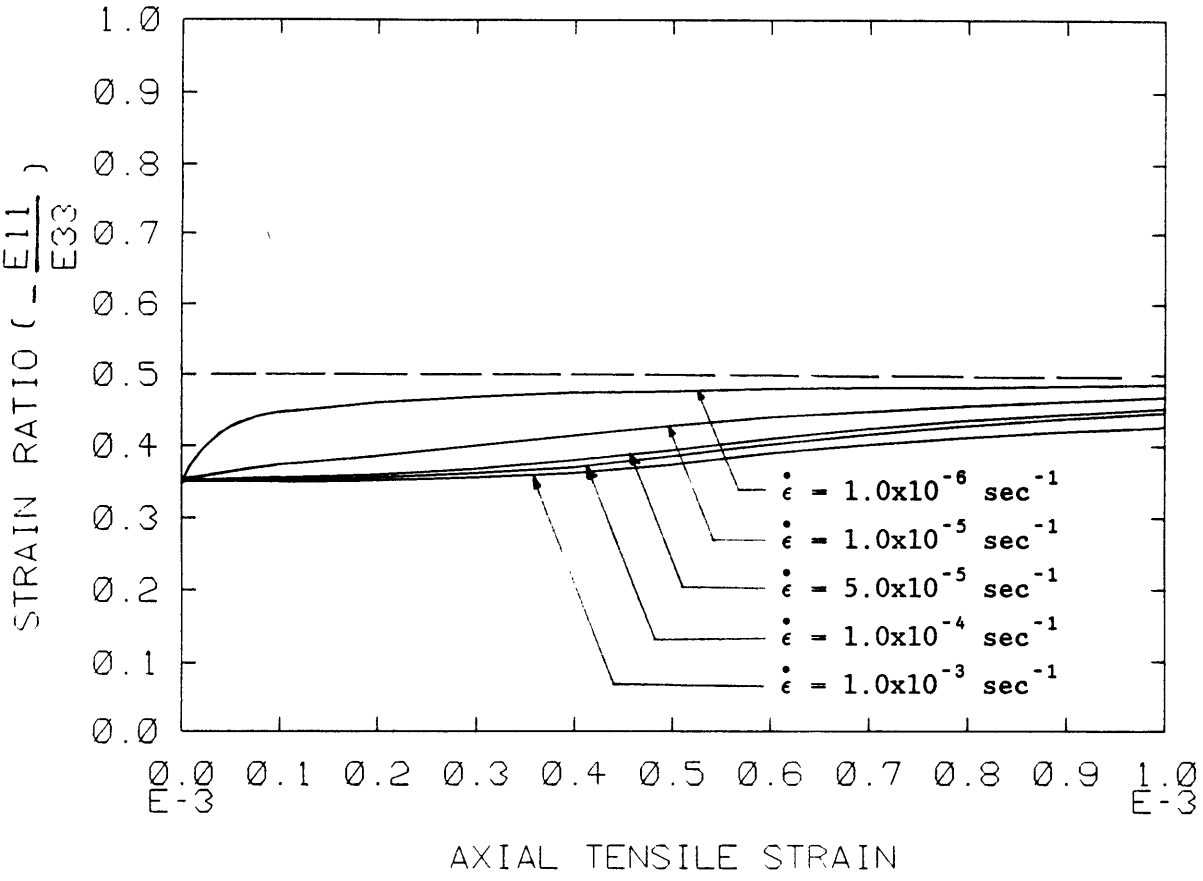

Figure 6.6 b) Strain Ratio Variation for Uniaxial Tension.

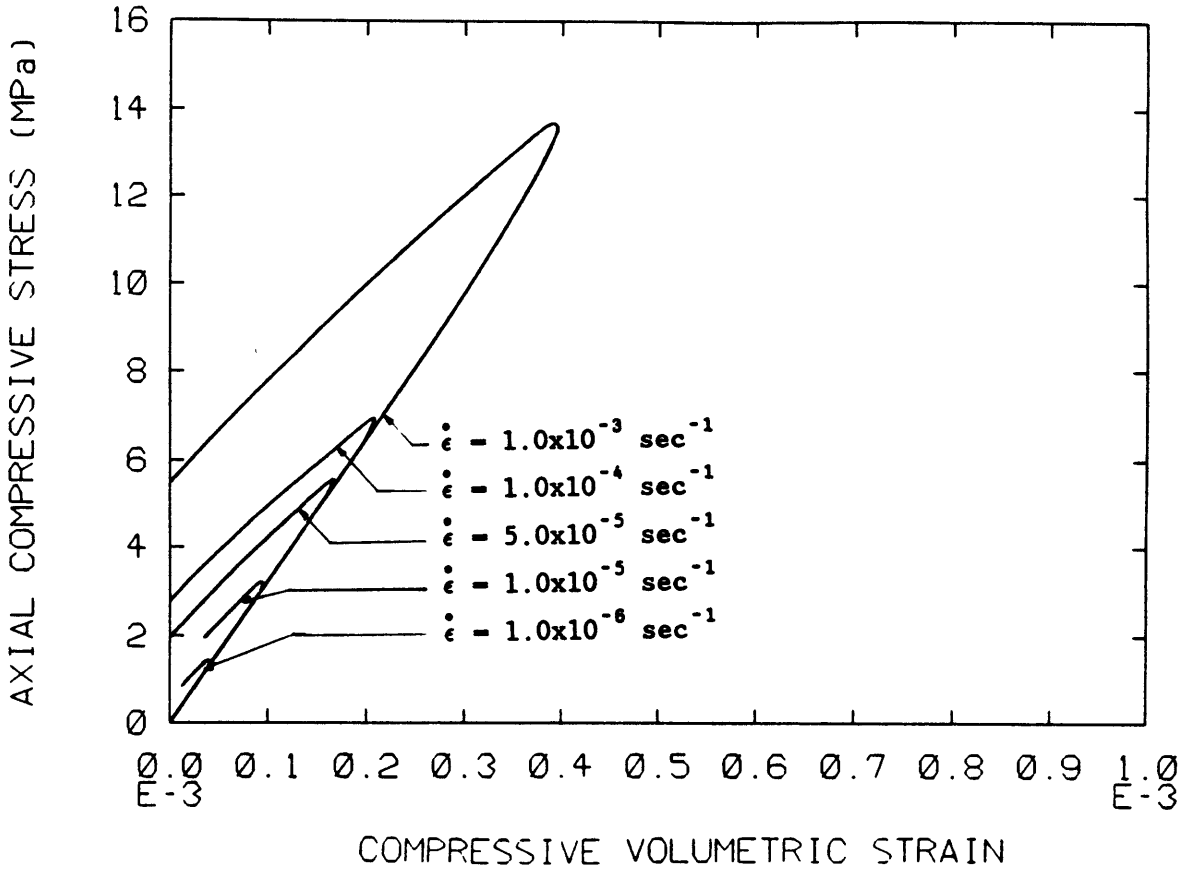

Figure 6.7 a) Stress versus Volumetric Strain Plots for Uniaxial Compression.

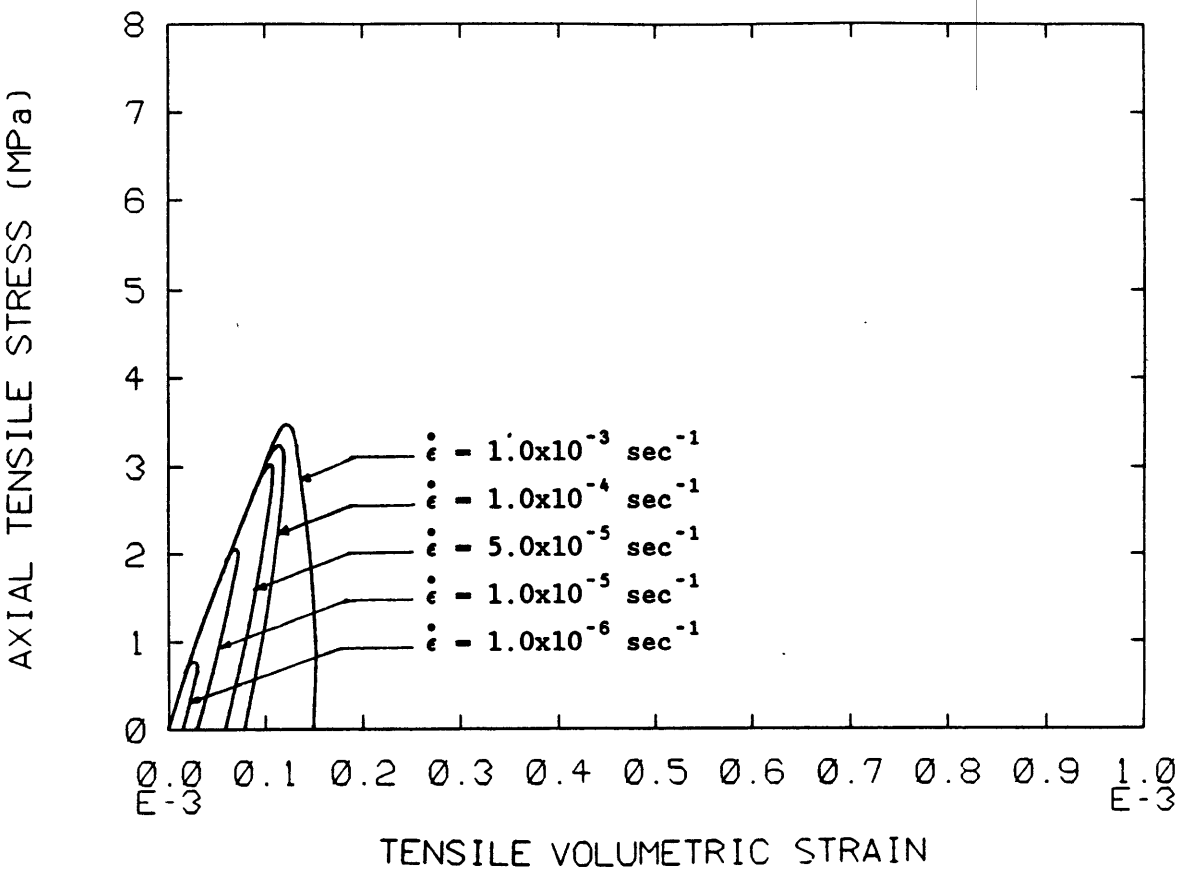

Figure 6.7 b) Stress versus Volumetric Strain Plots for Uniaxial Tension.

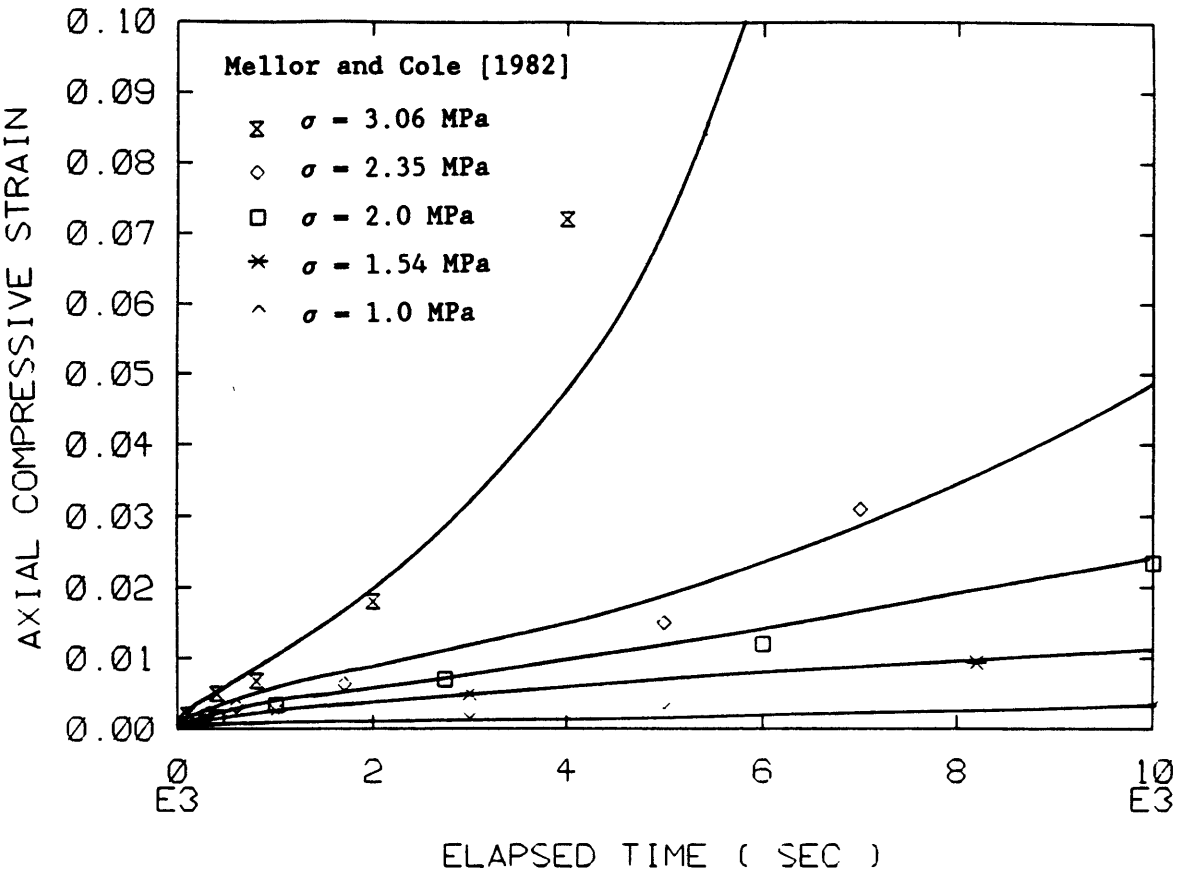

Figure 6.8 a) Conventional Linear Scale Plots for Creep Strain versus Elapsed Time. Data points are selected from Mellor and Cole's [1982] results.

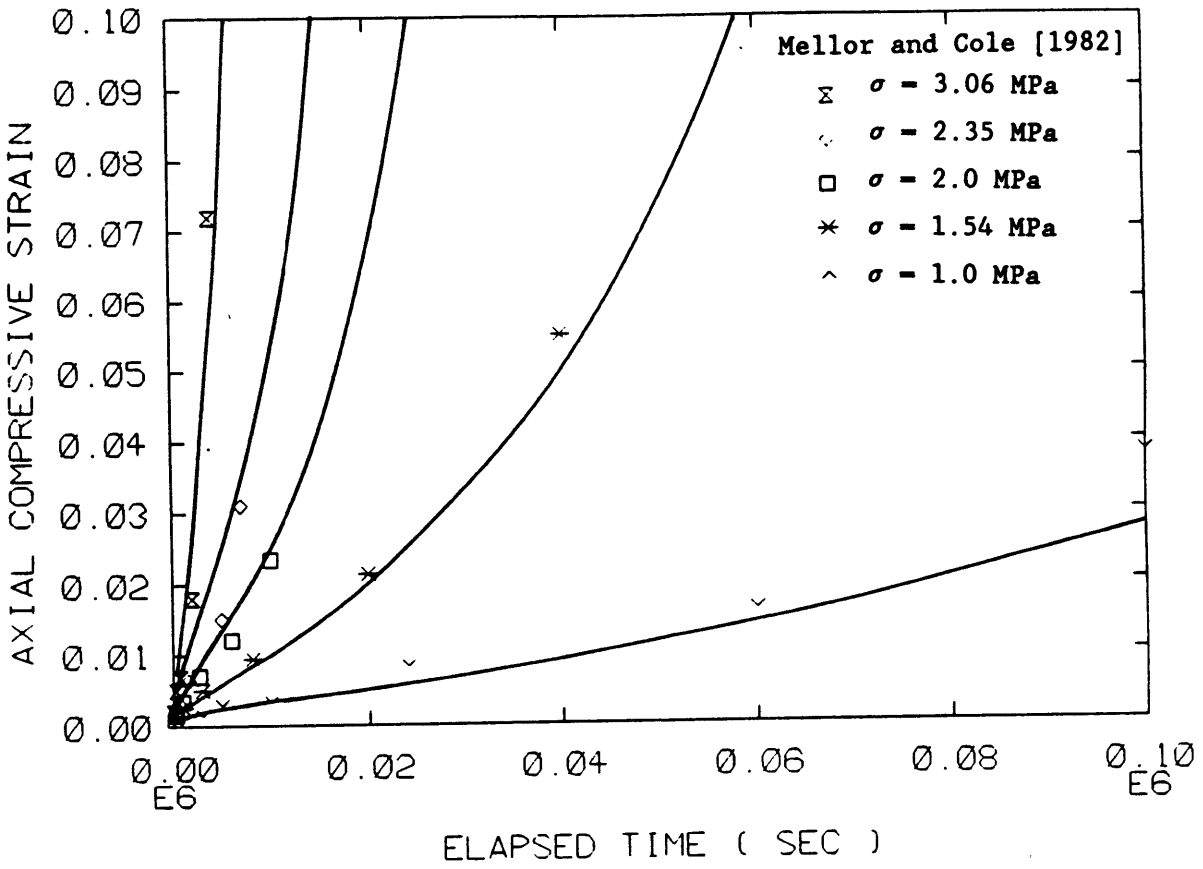

Figure 6.8 b) Conventional Linear Scale Plots for Creep Strain versus Elapsed Time. (continued)

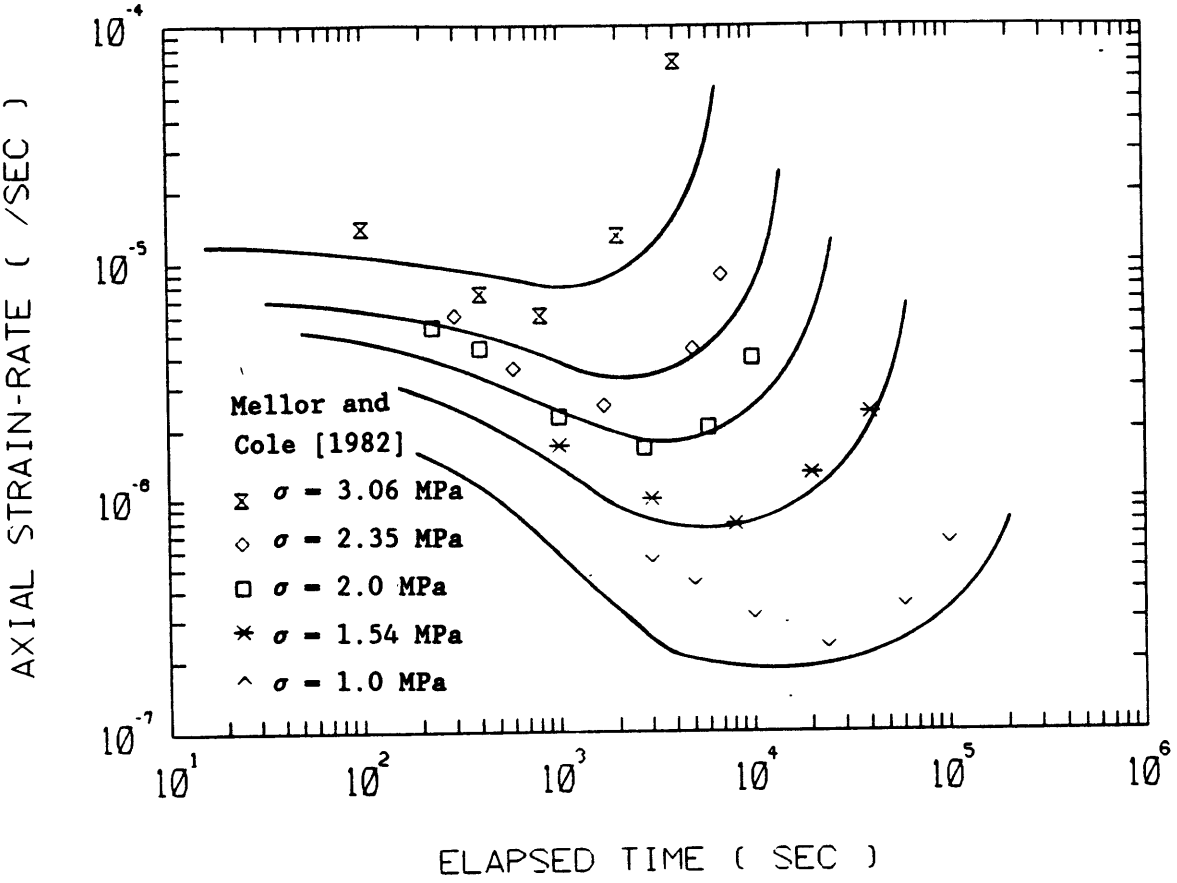

Figure 6.8 c) Log-Scale Plots for Creep Strain-rate vs. Elapsed Time. Data points are selected from Mellor and Cole's [1982] results.

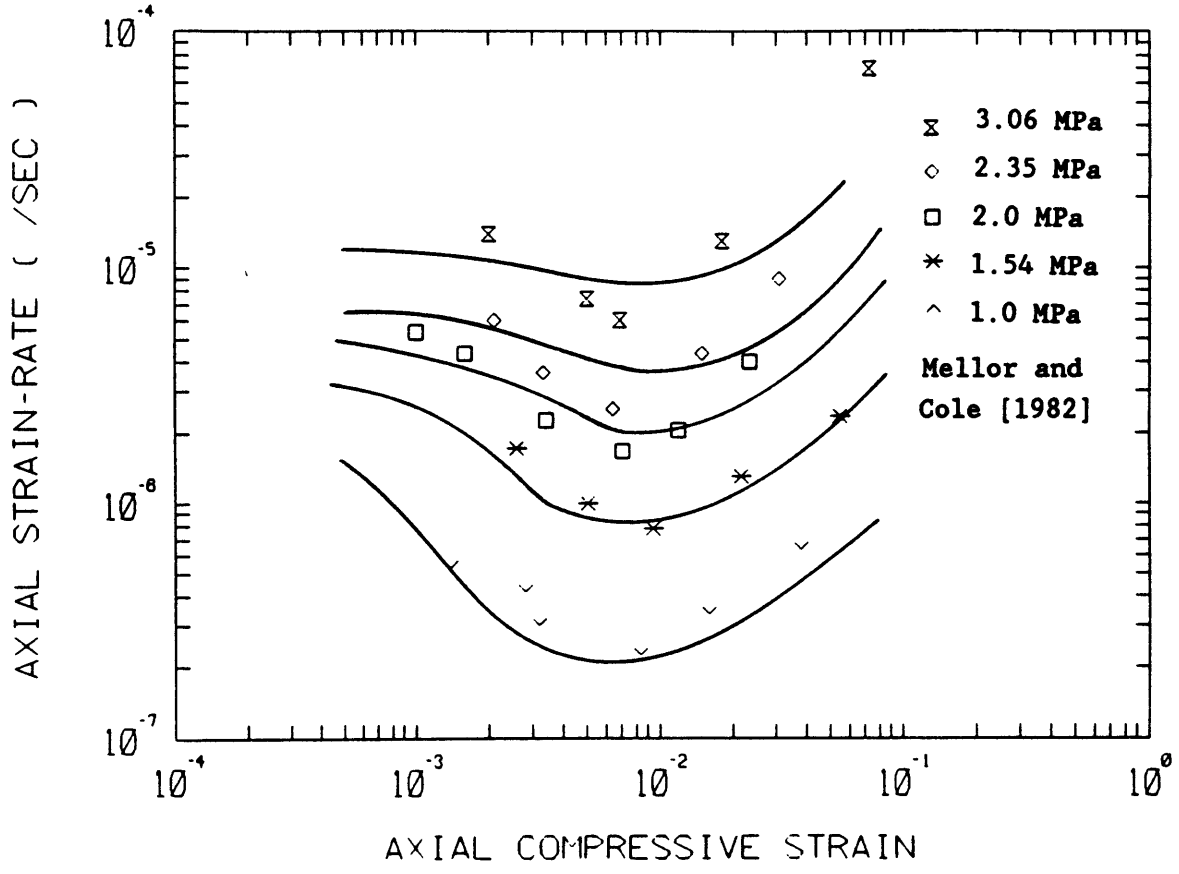

Figure 6.8 d) Log-Scale Plots for Creep Strain-rate vs. Strain.

(a)

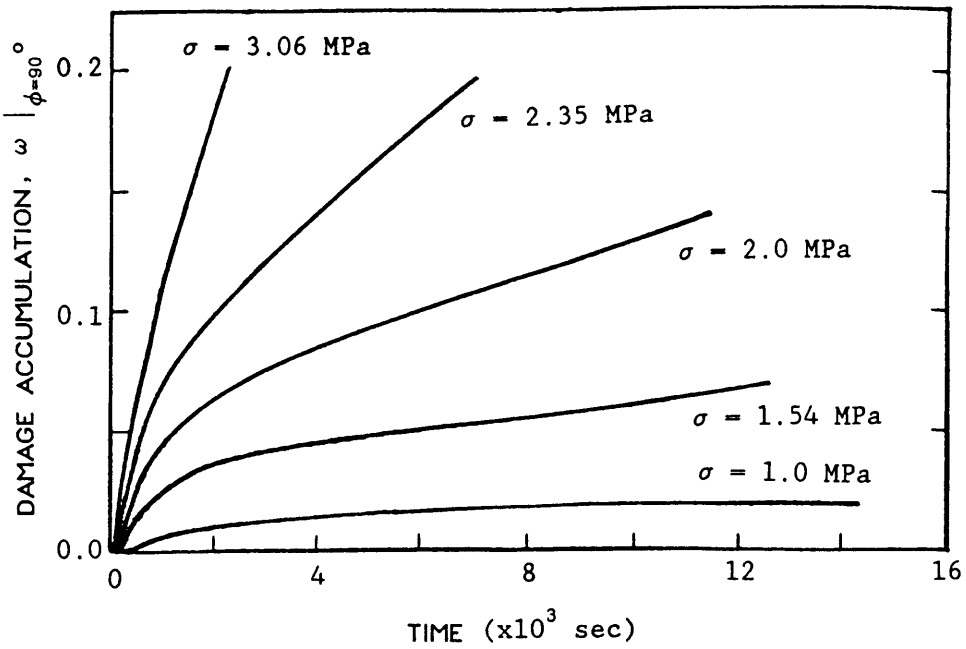

(b)

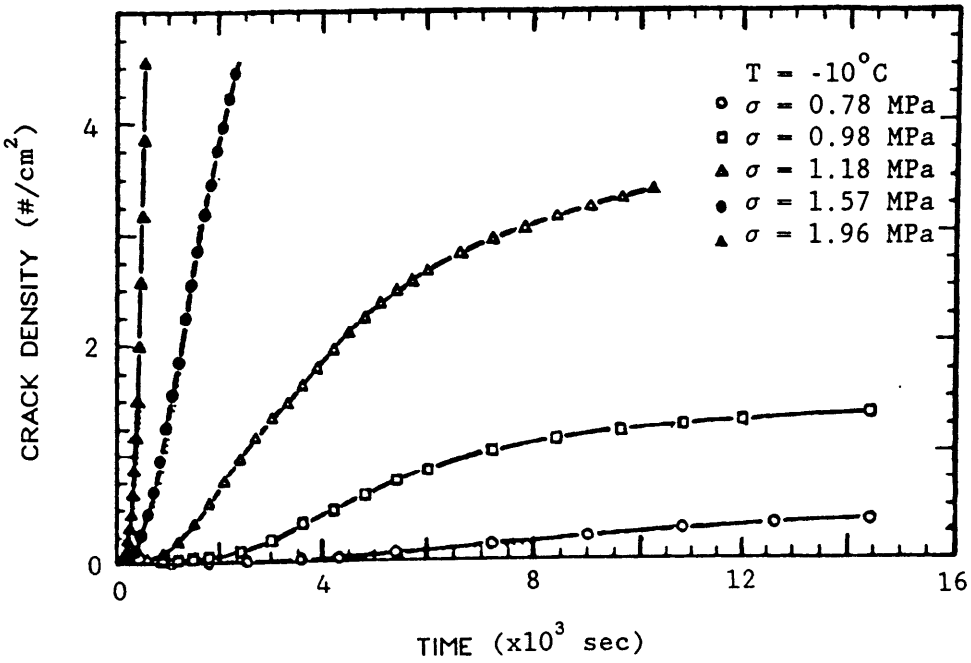

Figure 6.9 Comparison of Damage Accumulation with Macroscopic Damage Measure (Crack Density) at Constant Stresses.

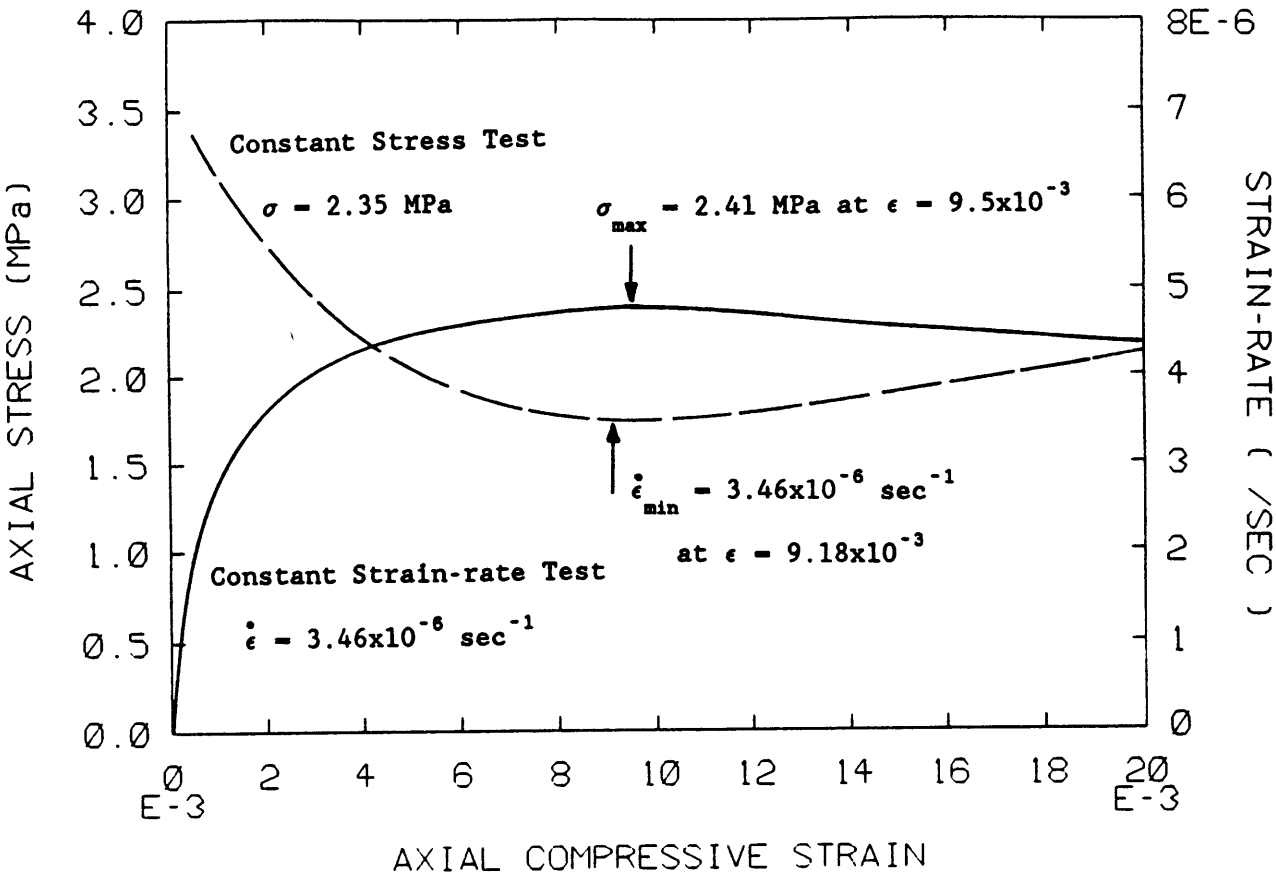

Figure 6.10 Correspondence of Constant Stress curve and Constant Strain-rate curve.

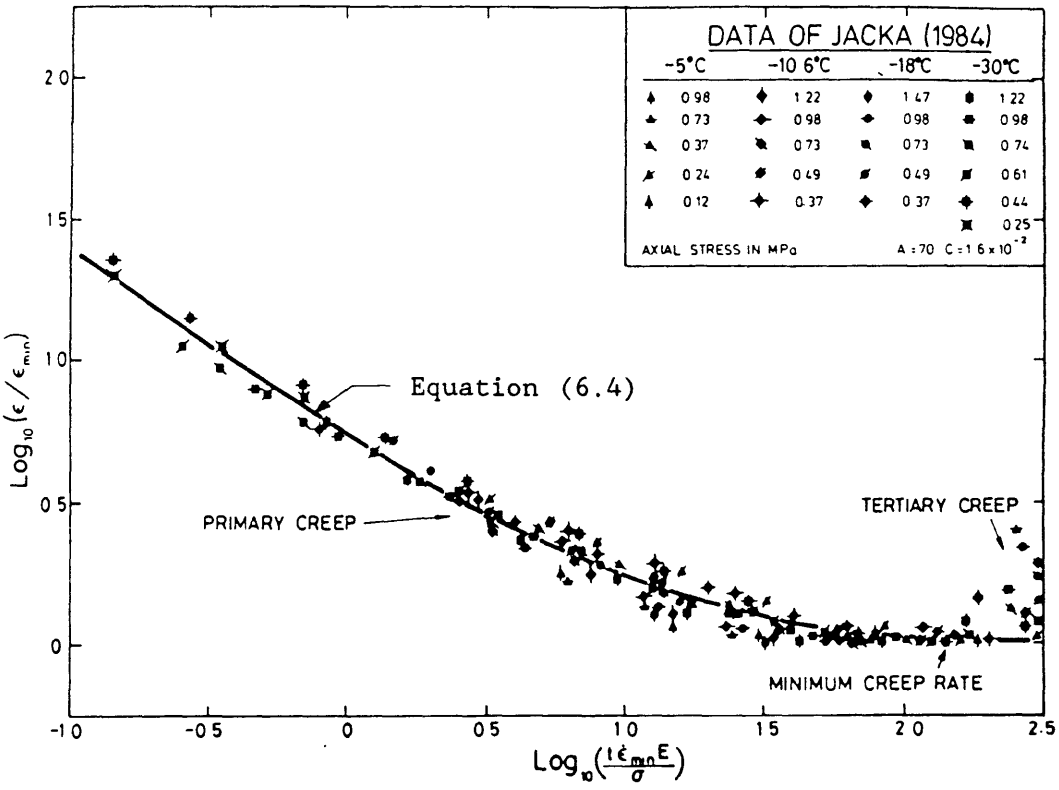

Figure 6.11 Strain-rate plotted against Time using Dimensionless Variables [Ashby and Duval, 1985].

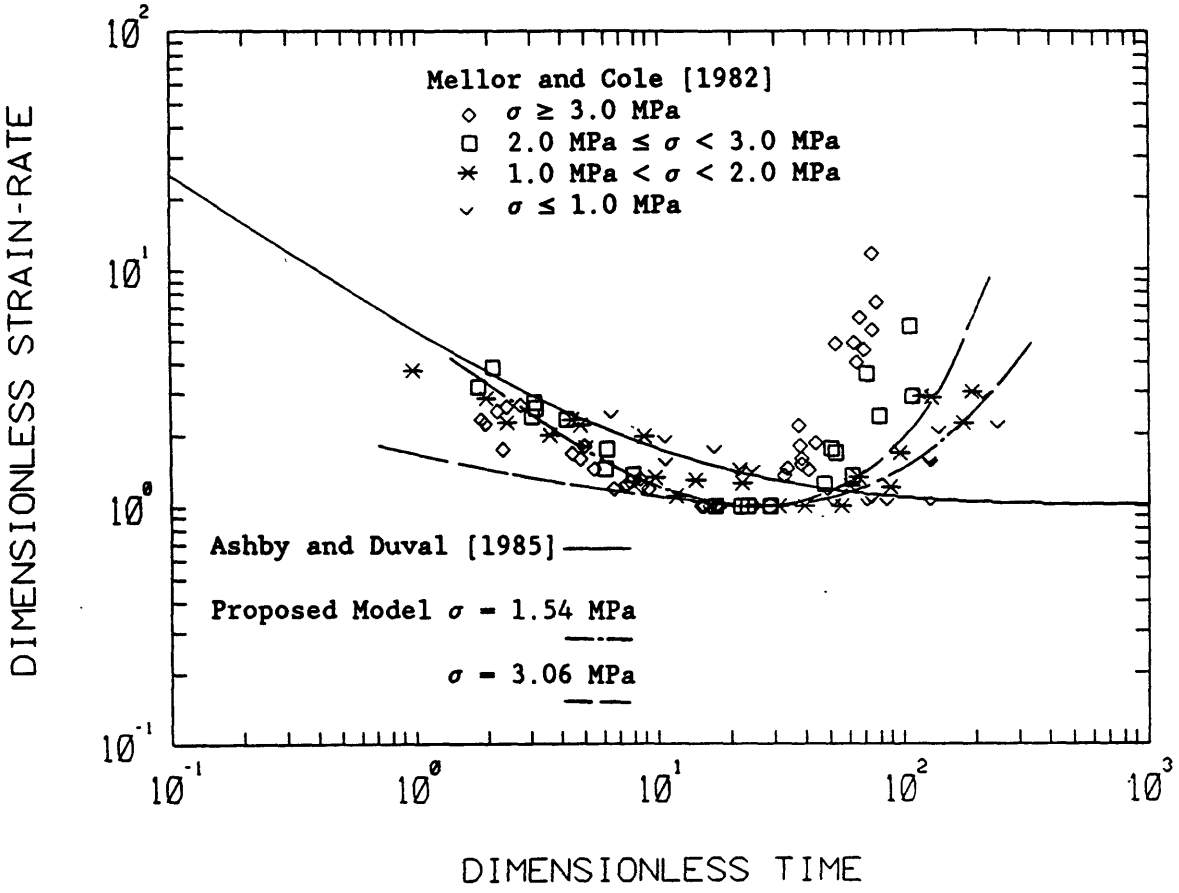

Figure 6.12 a) Strain-rate plotted against Time using Dimensionless Variables to Mellor and Cole [1982]'s data.

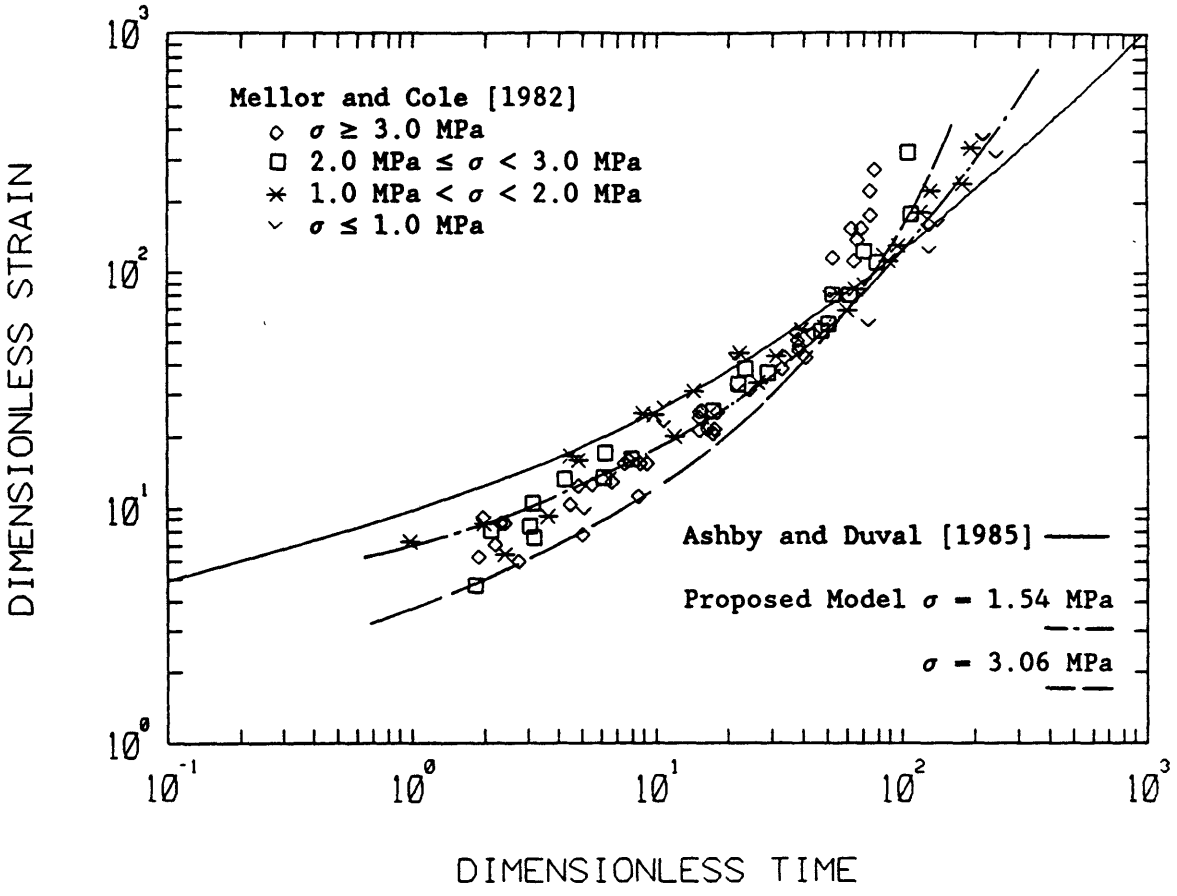

Figure 6.12 b) Strain plotted against Time using Dimensionless Variables to Mellor and Cole [1982]'s data.

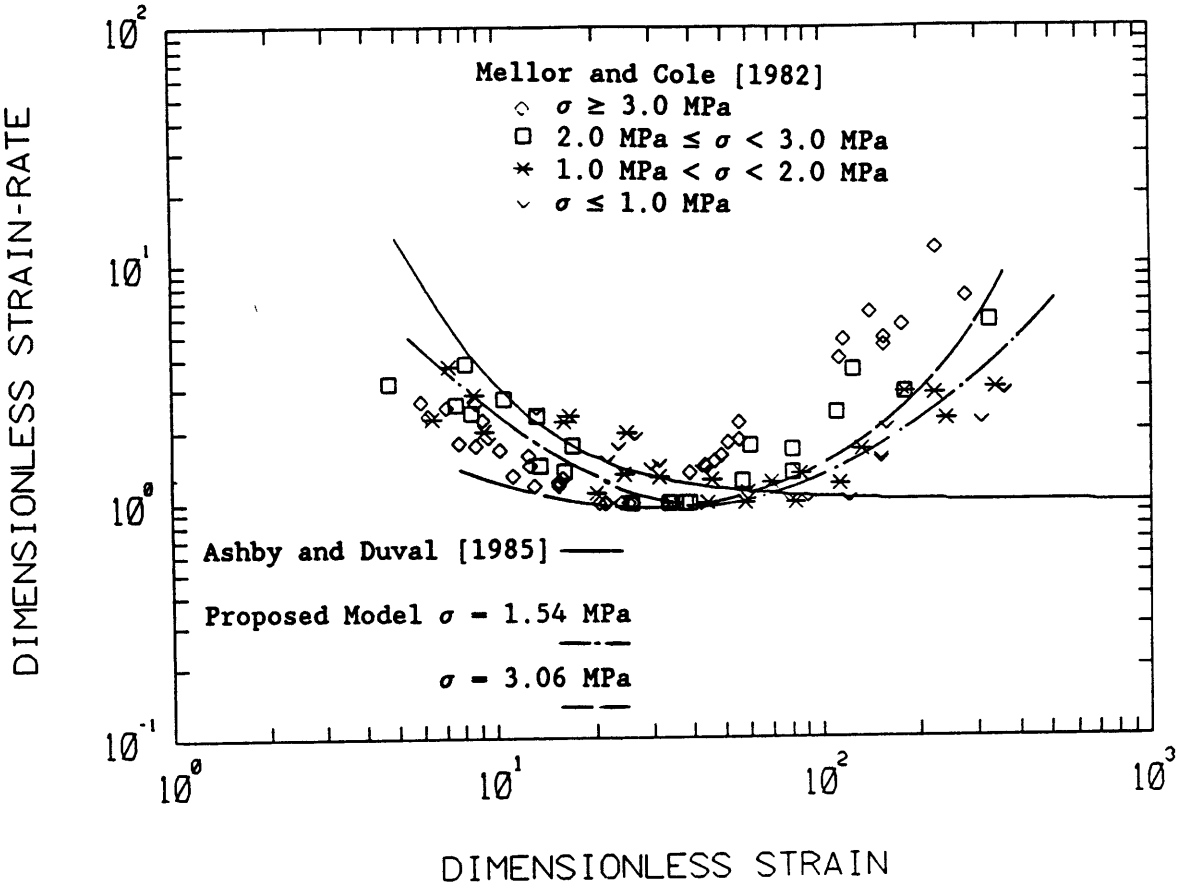

Figure 6.12 c) Strain-rate plotted against Strain using Dimensionless Variables to Mellor and Cole [1982]'s data.

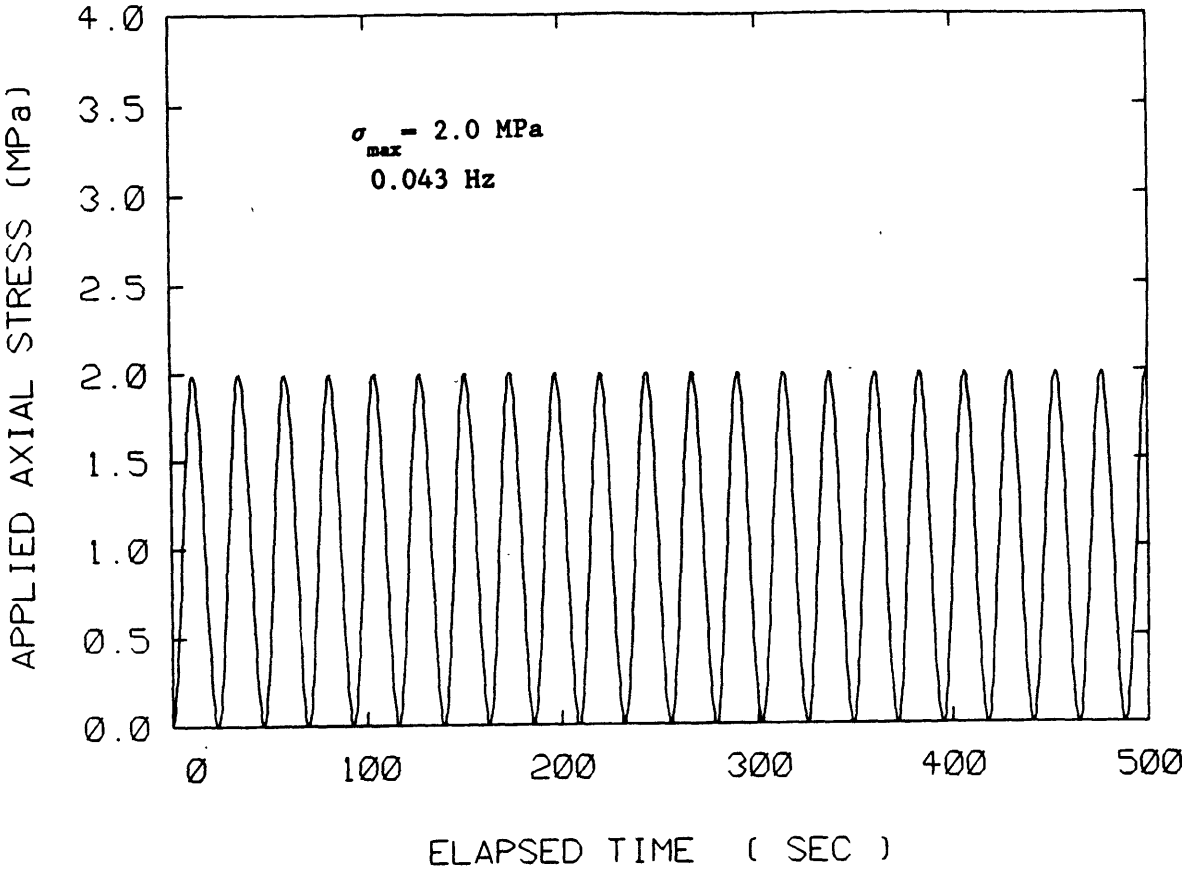

Figure 6.13 a) Cyclic Stress History for Maximum Stress 2.0 MPa.

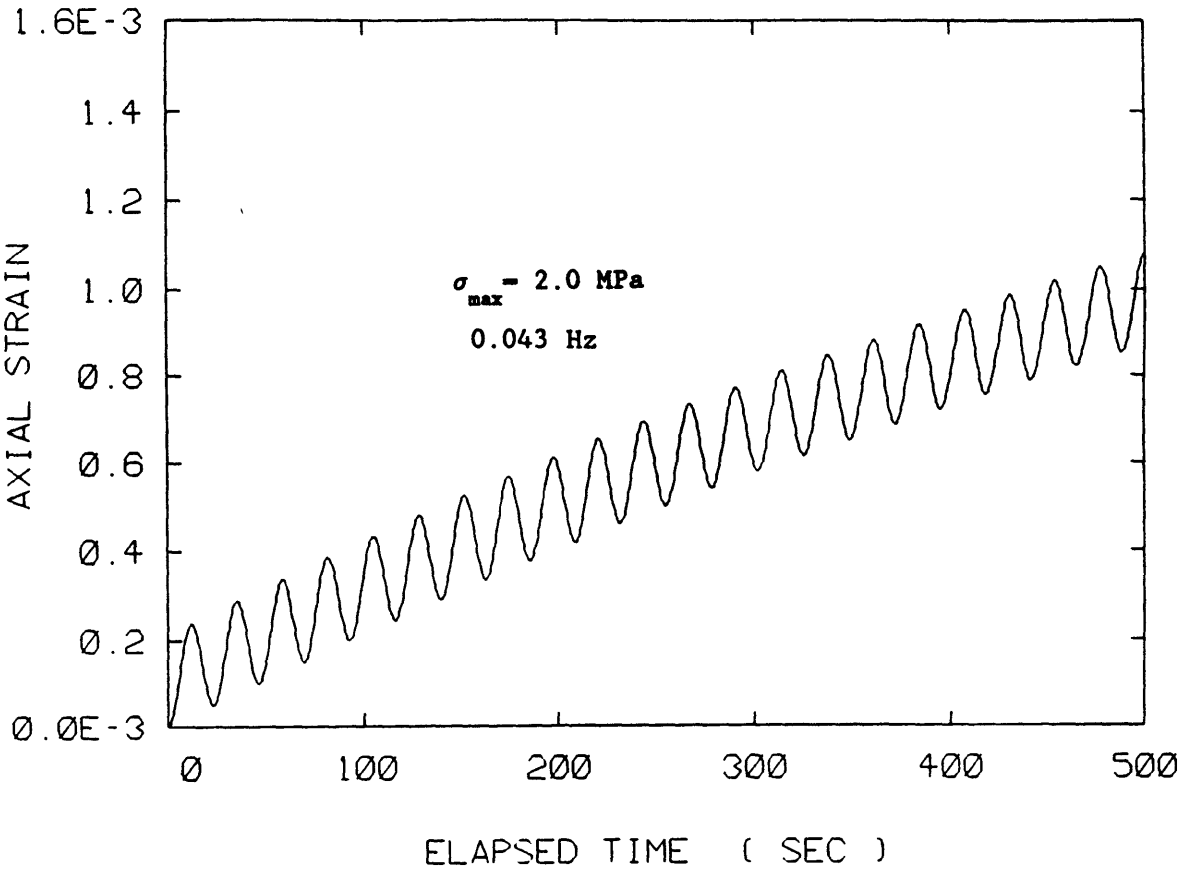

Figure 6.13 b) Creep Strain plotted against Time under Cyclic Stress.

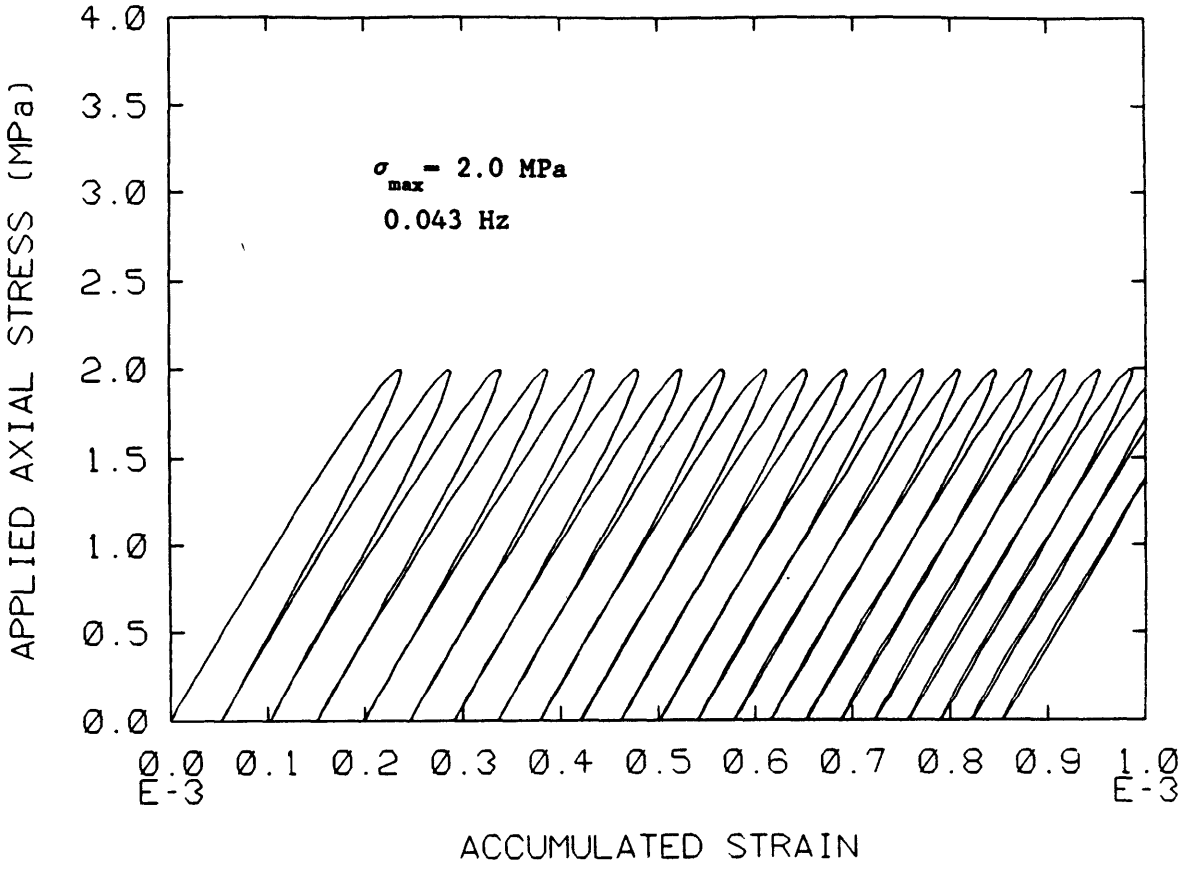

Figure 6.14 a) Stress-strain Plot at Initial Stage for Maximum Cyclic Stress 2.0 MPa.

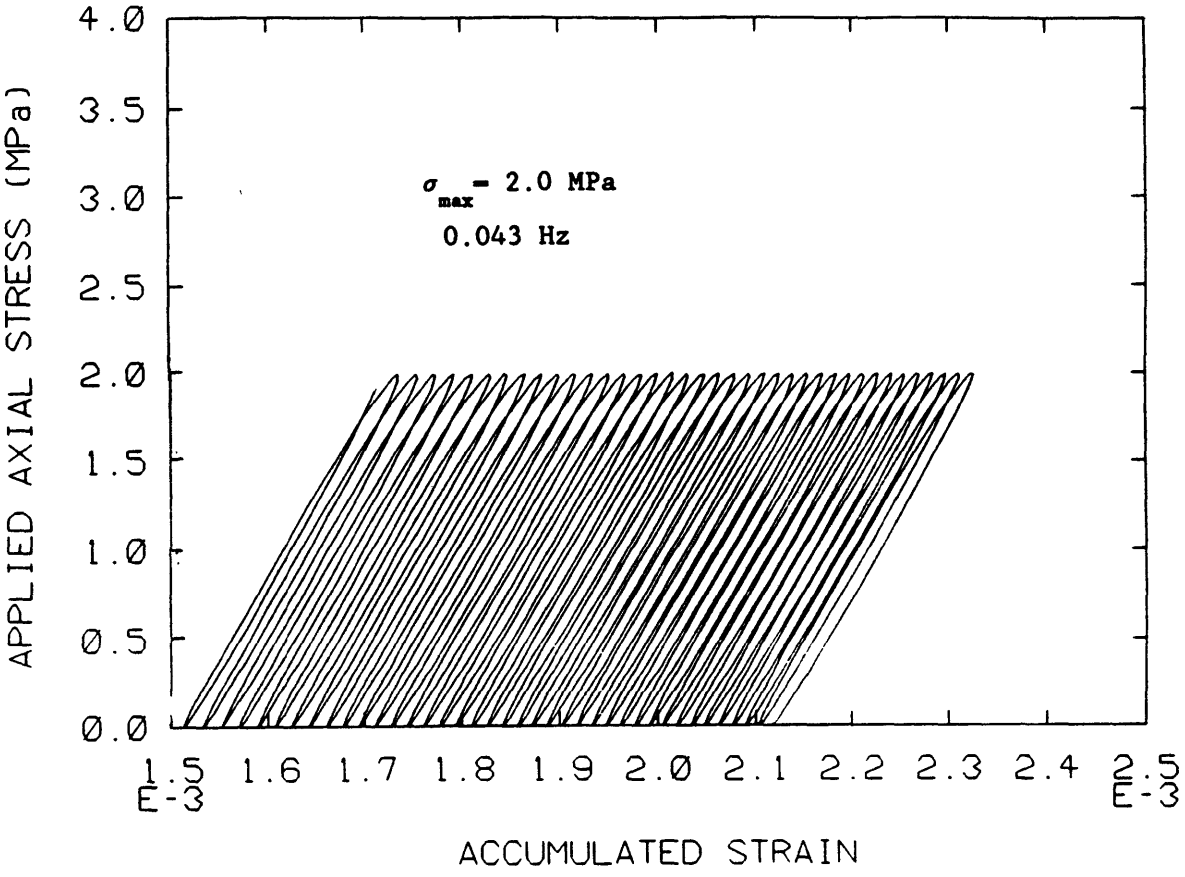

Figure 6.14 b) Stress-strain Plot at Intermediate Stage.

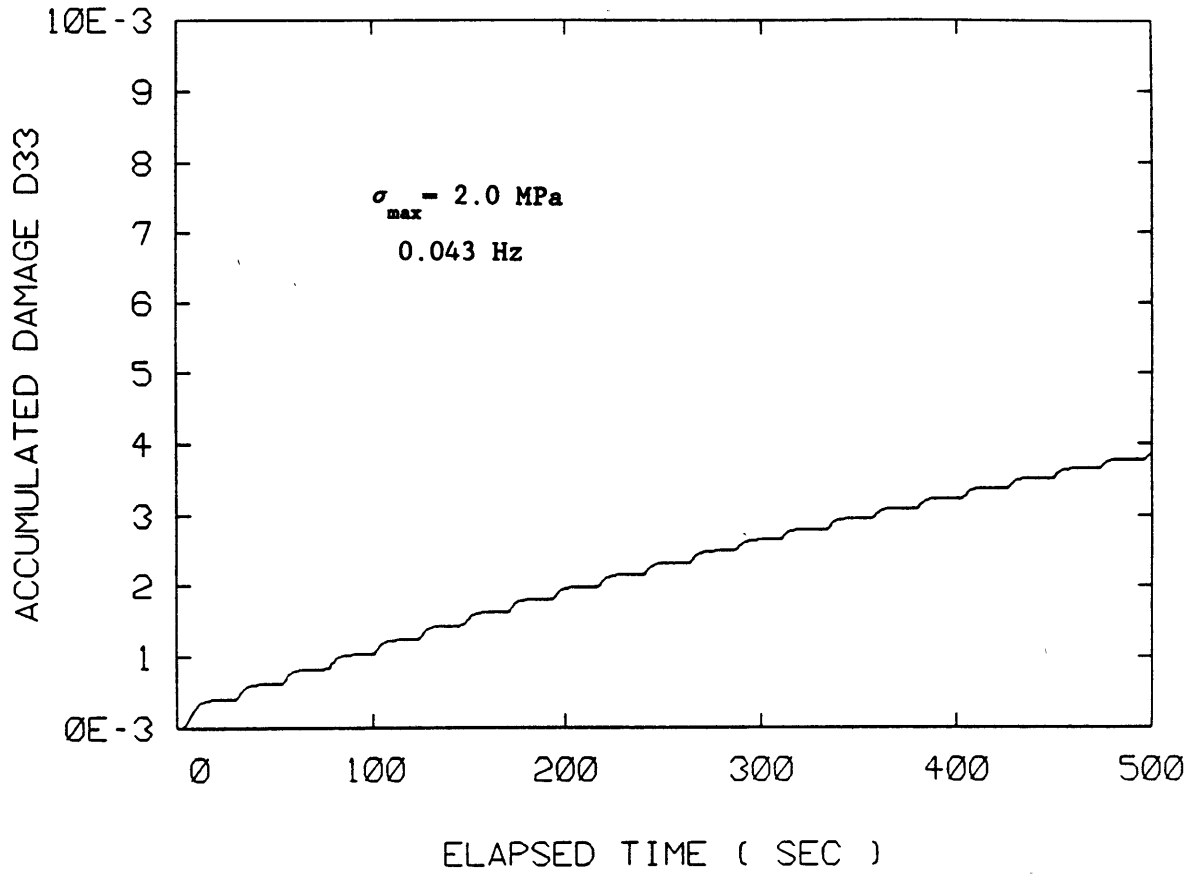

Figure 6.15 Damage Evolution Curve for Cyclic Stress Creep.

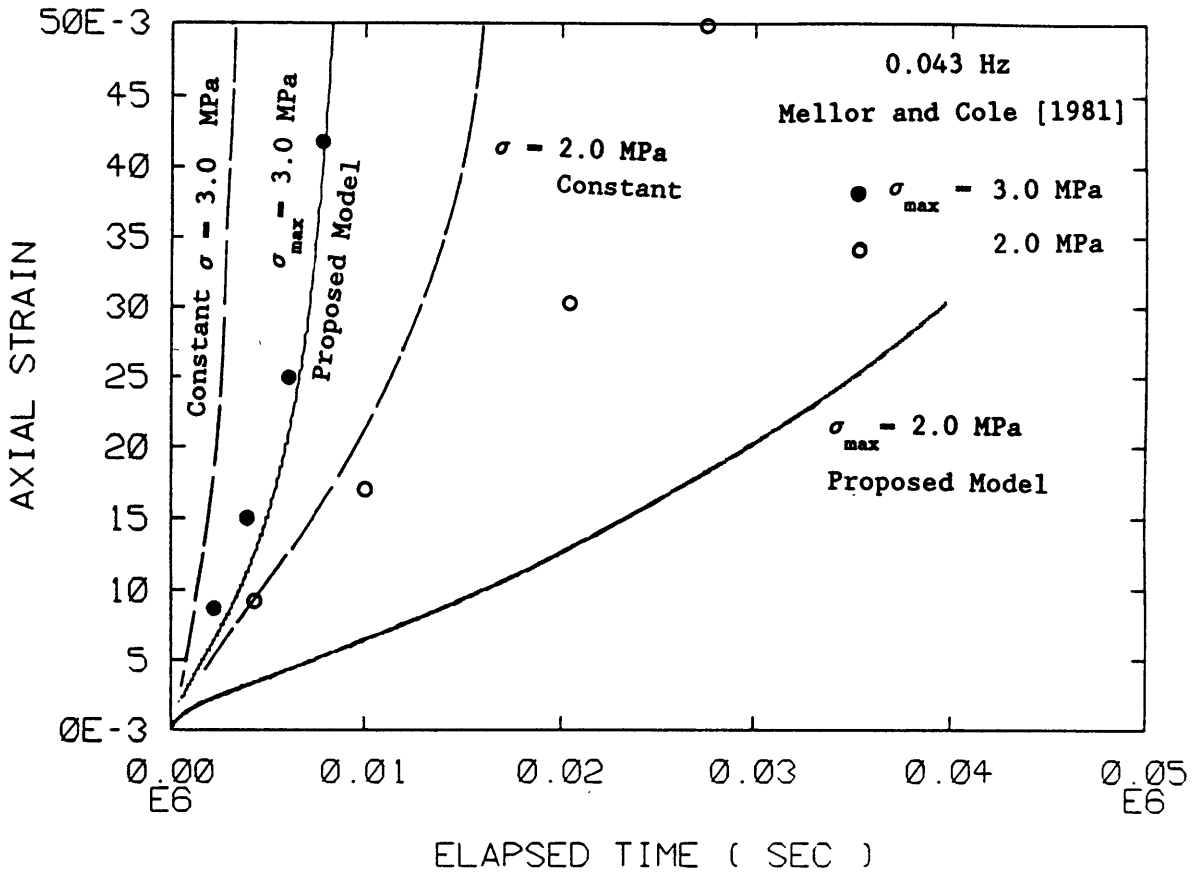

Figure 6.16 a) Creep Strain versus Time Plots. Data points (circles) are from Mellor and Cole [1983]. Dashed lines denote constant stress creep curves.

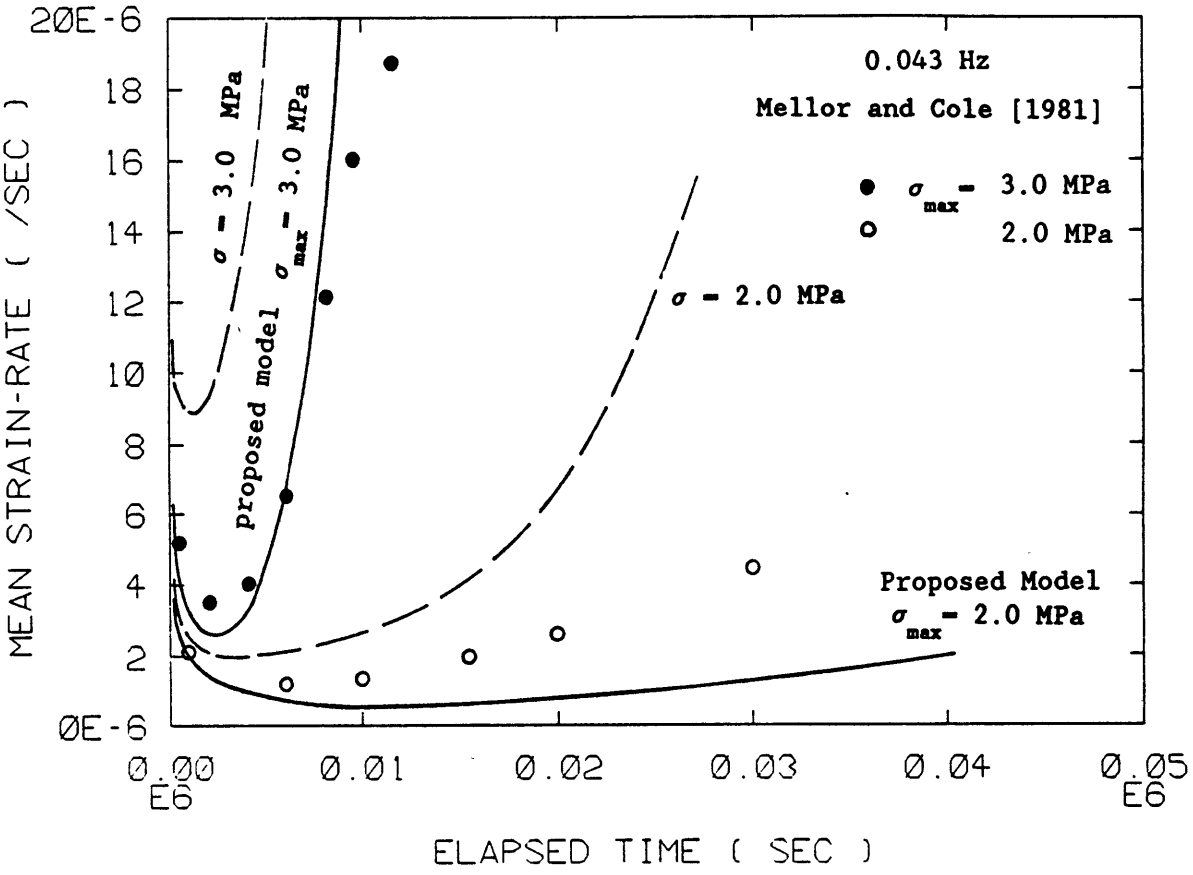

Figure 6.16 b) Mean Strain-rate vs. Time Plots in Linear Scale.
Data points (circles) are from Mellor and Cole [1983].
Dashed lines denote constant stress creep curves.

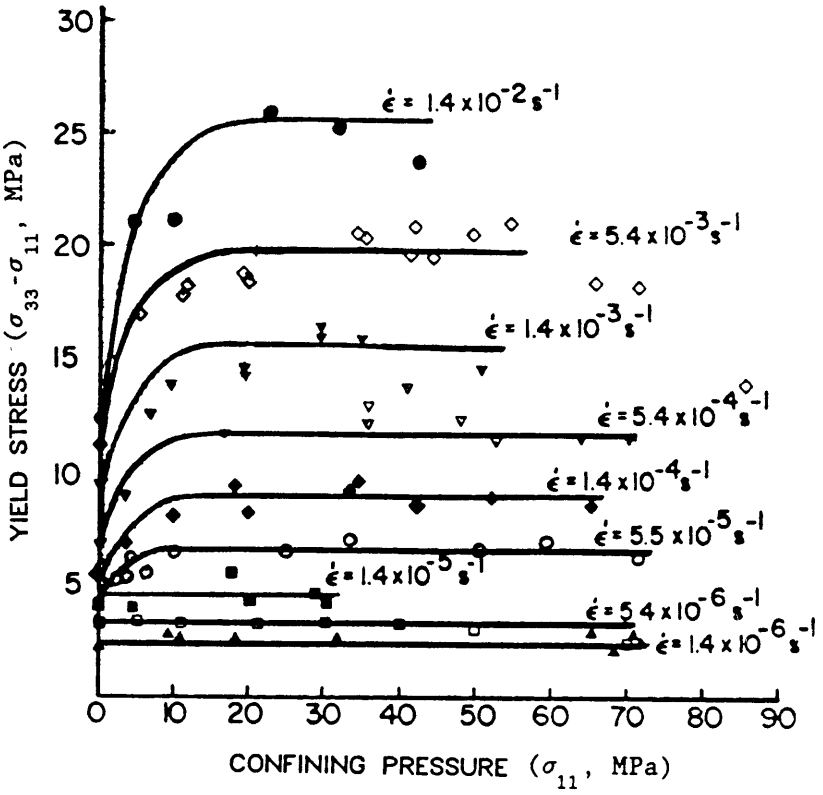

Figure 6.17 Failure Stress plotted against Confining Pressure for Different Strain-rates [Jordaan, 1986]. Data are from Jones [1982].

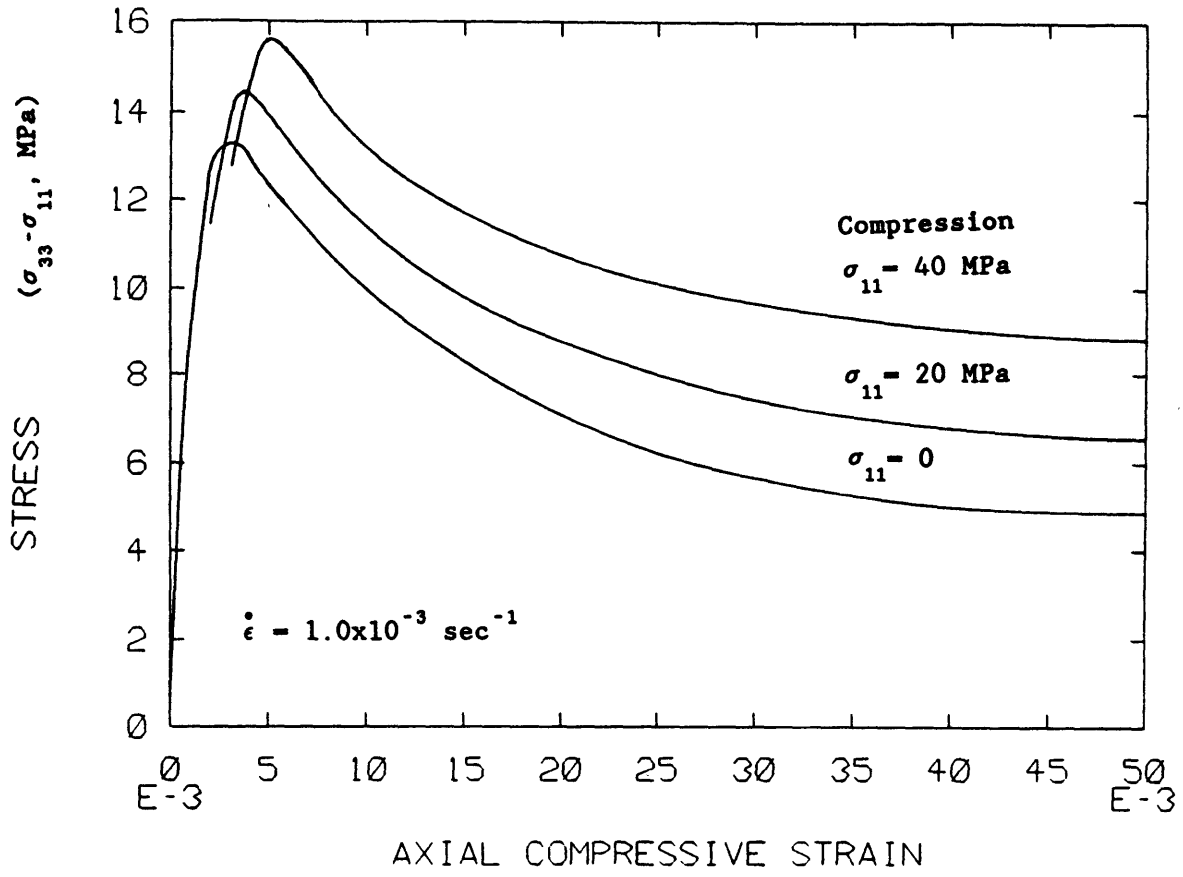

Figure 6.18 Stress-strain Curves for Different Confining Pressures.

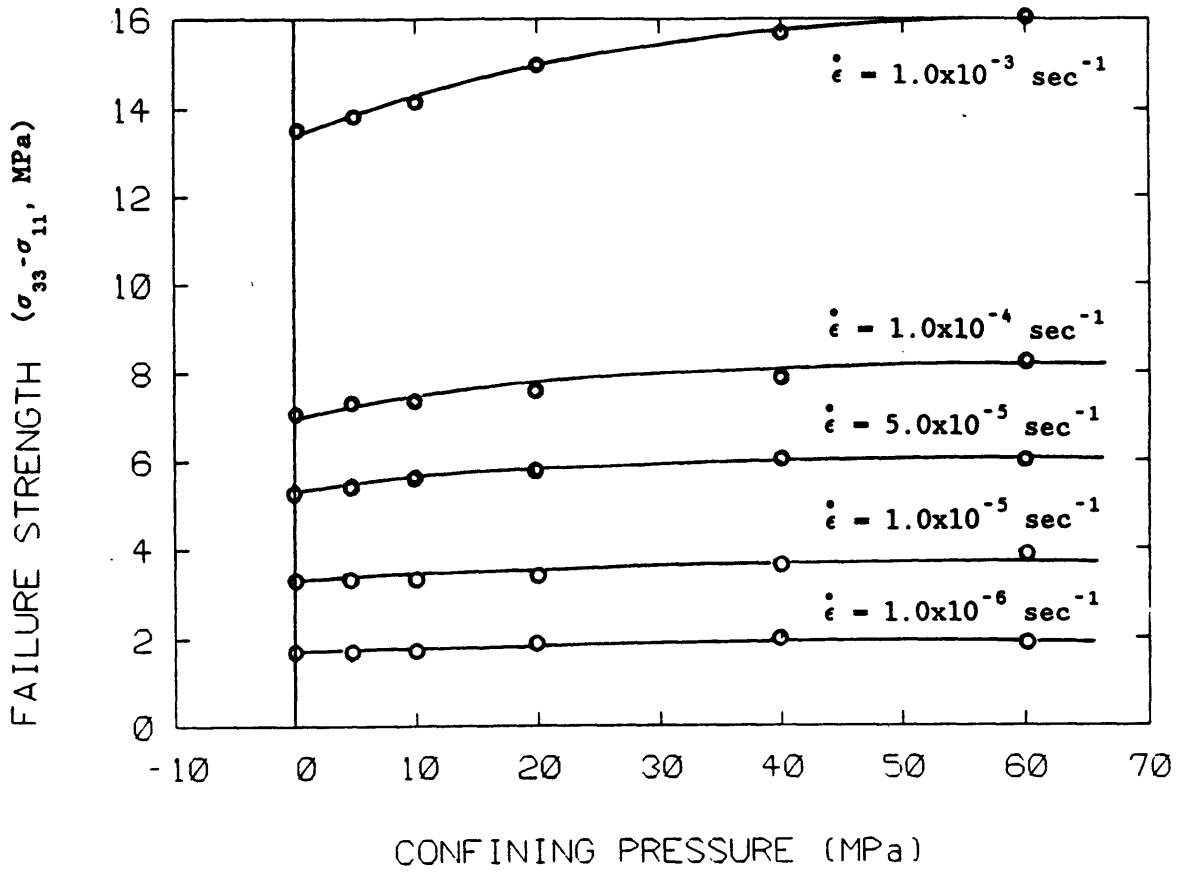

Figure 6.19 Deviatoric Failure Strength plotted against Confining Pressure.

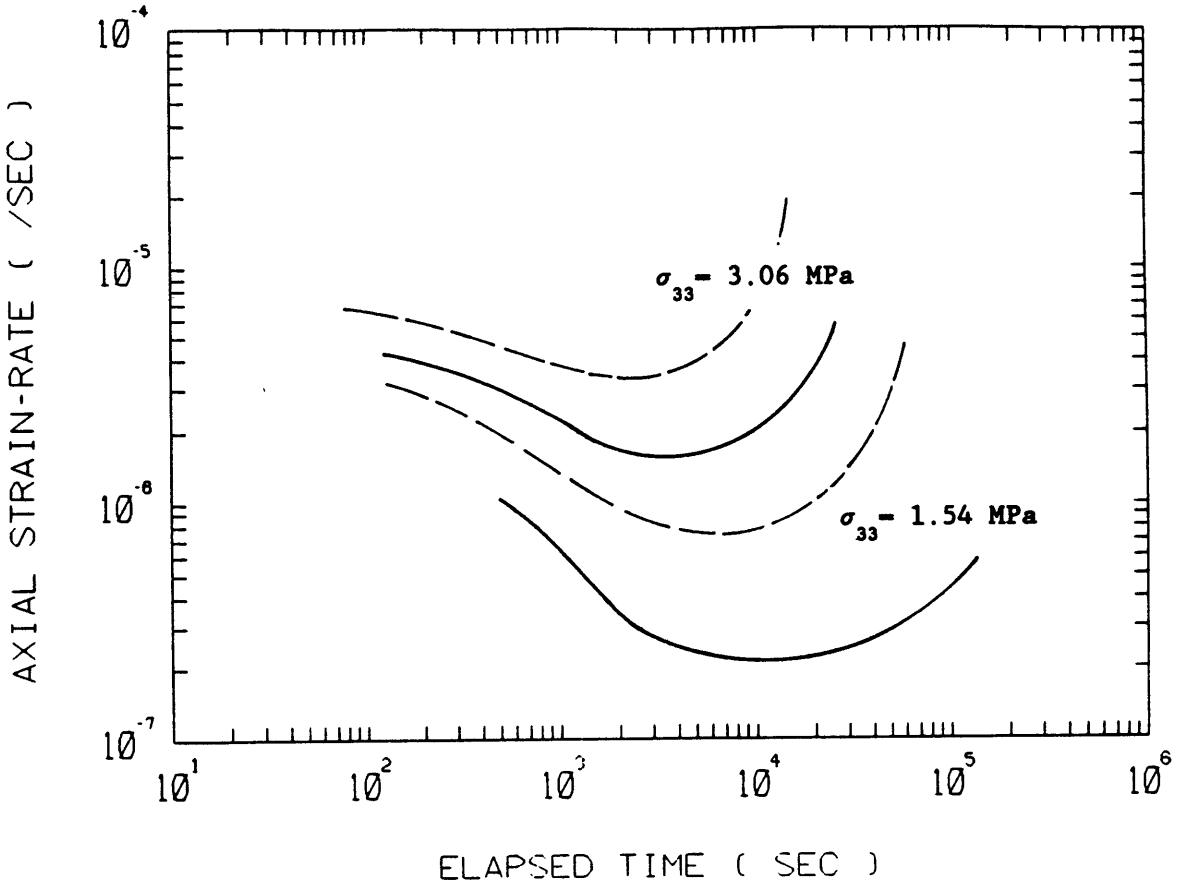

Figure 6.20 Effect of Confining Pressure on the Creep Responses. Dashed lines show unconfined pressure case and solid lines represent confined case with σ_{11}= σ_{22}= 0.5 MPa in compression.

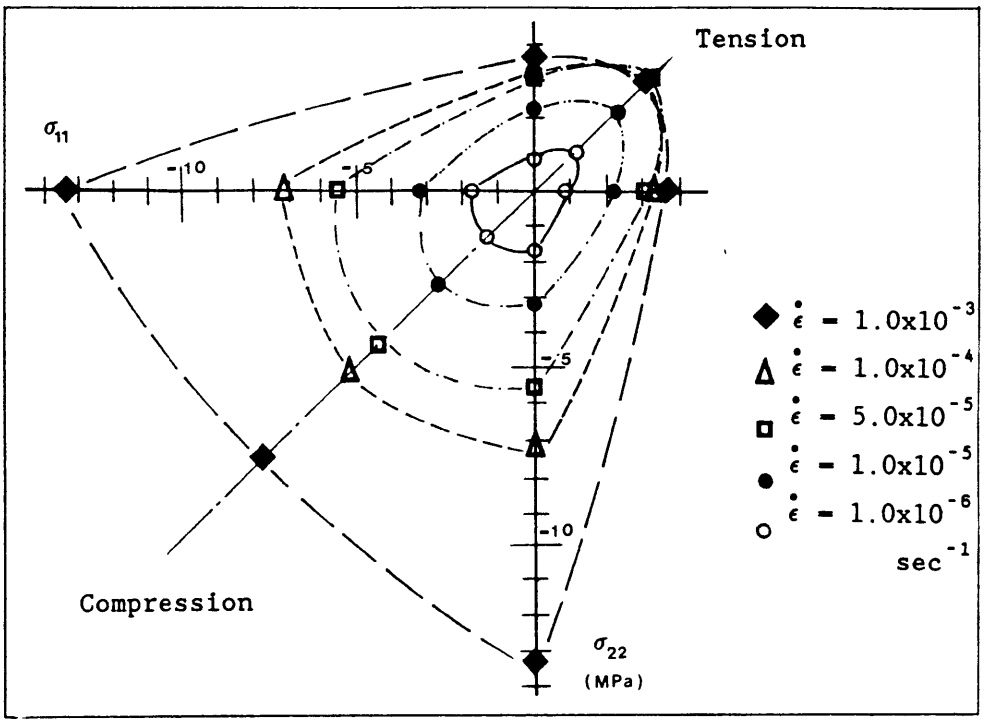

Figure 6.21 Prediction of the Biaxial Failure Envelopes for Polycrystalline Ice under Constant Strain-rate.

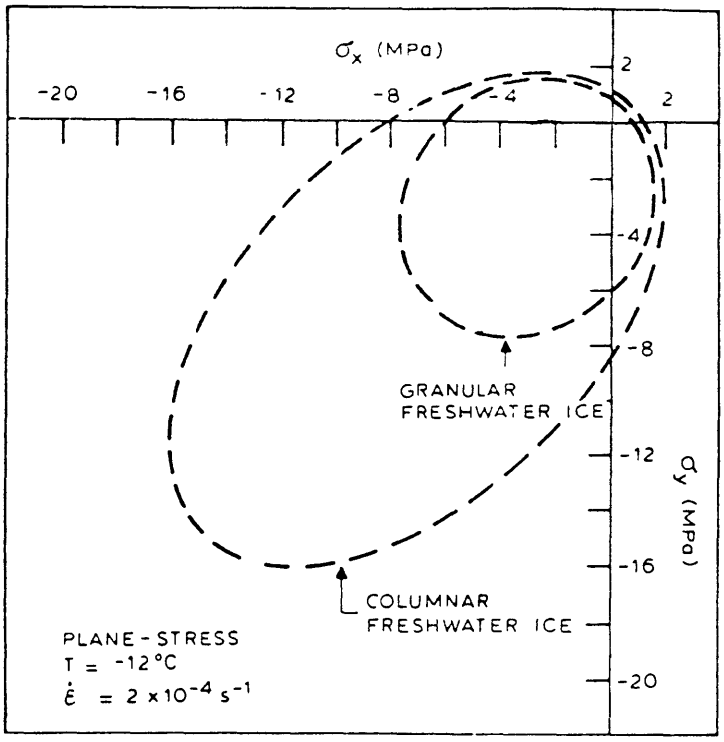

Figure 6.22 Failure Envelopes suggested by Timco and Frederking [1984] for various types of Ice.

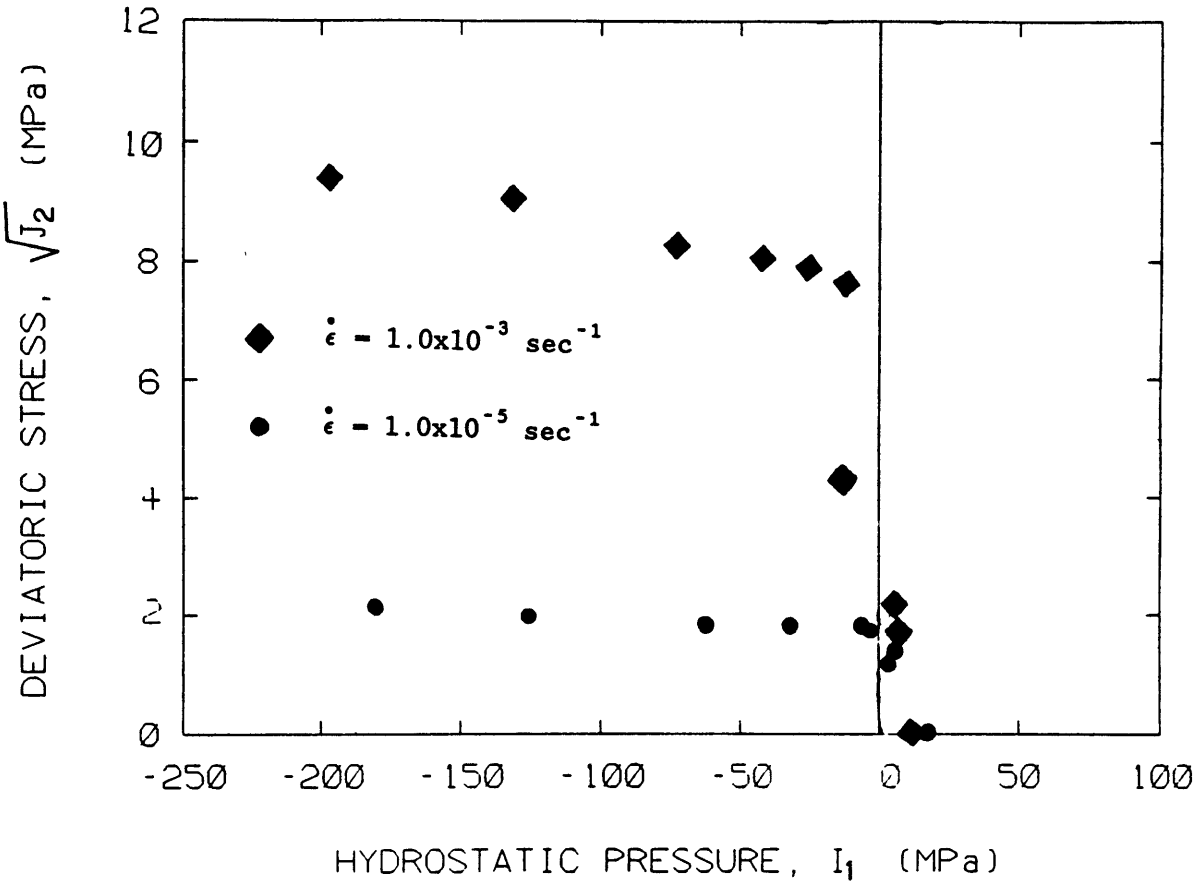

Figure 6.23 I_1- $\sqrt{J_2}$ Plots for Constant Strain-rate.

CHAPTER 7

CONCLUSIONS AND RECOMMENDATIONS FOR FUTURE STUDY

7.1 SUMMARY OF THE CONSTITUTIVE MODEL

The proposed constitutive model for describing polycrystalline isotropic ice deformation is based on continuum damage mechanics theory where damage evolution is formulated on the basis of the mathematical description of physical aspects of microcracking development. The mathematical nature of damage parameter is selected based on the anisotropic behavior of microcrack fields and its dependency on strain-rate and stress and therefore a tensorial representation of damage is appropriate. The main contribution of the thesis lies in the formulation of damage evolution laws where the damage growth is expressed by local resolved normal stress and strains for two different microcracking mechanisms, grain boundary cracking and transgranular cracking. The new concept is adopted for derivation of multiaxial damage evolution laws in terms of delayed elastic strain and total strain respectively.

The stress-strain relations are derived from a thermodynamic potential where the effects of damage are incorporated into strain components through an effective stress concept. The applicability of the present constitutive model is illustrated for several loading conditions and a wide range of strain-rates and stresses. Agreement between theoretical predictions and macroscopic observations is within an acceptable level. However some limitations should be noted on the

present theory. In the development of the continuum damage theory numbers of assumptions are introduced. As seen in several references [e.g. Krajcinovic and Fonseka, 1981] the theory is based on a representation of flat, planar microcracks rather densely distributed with favored orientations. Moreover small displacement and small rotations are assumed in the changes of microcrack growth. This approach is suitable for predicting small deformation behaviors commonly observed in ice. However it may not be appropriate to model the behavior at fairly large deformation stages where cracks may significantly change their shapes and totally different deformation mechanisms may take place. In fact at this stage of deformation the ice specimen deforms so much and discrete cracks are known to develop.

Another restriction of the present continuum damage model is the assumption that no single isolated cracks dominate the deformation process. Therefore there is always assumed to exist a uniform degradation of material while in real situations the material may fail before it reaches a continuum strength by sudden fracture due to material imperfection or stress localization in the experiments. This can make a difference between the observation and theoretical prediction especially in tensile loading conditions with high stress or high strain-rate. Also crack interaction should be incorporated in the constitutive formulation to deal with a large amount of microcrack distribution.

7.2 CONCLUSIONS

The continuum damage model developed in the present research is capable of describing microcracking effects related with various familiar phenomena observed in ice deformation. With tensorial representation of anisotropic damage nature, the model can predict the general multiaxial loading behavior over a wide range of deformation regimes without adjusting material parameters. The difference in tensile and compressive behaviors can be predicted and constant stress and constant strain-rate deformations are obtained. From the model predictions and experimental observations, the following specific conclusions are drawn:

1) The constitutive model can capture the strain-rate effect on the failure strength of ice. The rate sensitivity of the model is to a large extent attributed to the rate-type strain component and damage evolution law. The parameters in the damage evolution equations are also strongly dependent on applied strain-rates. An increase in strain-rate results in an increase of peak stress in uniaxial compression and also in uniaxial tension. Strain-rate increase also accelerates damage accumulation and the damage accumulation is faster in tension. The model can predict the smooth strain softening curve after a peak stress in compression. The strain softening is more significant in high strain-rate tests, which can be explained by faster material degradation due to damage accumulation. In tension strain softening can be seen, however the softening curve is not smooth at all.

2) Ice deformation behavior differs significantly below and above the stain-rate, $10^{-5}sec^{-1}$, as an approximate threshold. The failure strength data plotted against strain-rate variation show that there is a trend in strain-rate for ductile-to-brittle transition (Figure 6.3). This threshold can be identified again in the failure strain versus strain-rate plot (Figure 6.4). Both experiments and model predictions show that at low strain-rates the material behaves basically in a ductile mode while at high strain-rates in brittle mode. In view of low strain-rate ranges in constant stress creep tests, it is expected that creep behavior is essentially the same as that of low constant strain-rate tests and this is verified by the fact that the failure strain and failure stress are about the same level in both constant stress and constant strain-rate tests.

3) For very high strain-rates, the continuum damage model may not be valid. Since specimen inertia effect is critical in the experimentation and a small perturbation of material homogeneity or load application can cause a macrocrack initiation, a fracture criterion should be considered in conjunction with continuum damage model. At high strain-rates the propagating macrocrack dominates the deformation process which is not accounted for in the formulation of the present model.

4) Mellor and Cole [1982, 1983] regarded 1% failure strain as a characteristics in the ice deformation behavior in both constant strain-rate and constant stress tests. Although this is mostly true at low strain-rate and low stress states, the deviation of observed and predicted results from 1% failure strain gets bigger at high strain-rates. As explained before the ice deformation behavior

changes across $\dot{\epsilon} = 10^{-5}sec^{-1}$.

5) According to the proposed model the strain ratio (apparent Poisson's ratio) is a function of strain-rate along with damage accumulation. At high strain-rates basic deformation modes are elastic, i.e., brittle while at low strain-rate it is ductile hence the viscous strain component is much larger than the elastic components. As a consequence the strain ratio grows from a dynamic value (in this study 0.35) to a perfectly plastic limit 0.5. Apparent Poisson's ratio or simply strain ratio reflects the amount of these strain components which are continuously varying with strain-rate. Volumetric strain also reflects the change of strain components as we see a dilatancy phenomenon in Figure 6.7.

6) The proposed model captures the ideal creep behaviors including primary, secondary and damage-driven tertiary creep strains. The failure strain at minimum strain-rate is a distinguished point for all stress levels and is aligned near 1% strain line. Since the strain-rates in constant stress tests fall on the low strain ranges (below $10^{-5}sec^{-1}$), basically creep behavior is similar to that of low strain-rate tests at constant strain-rates. Experimental evidence supports this conclusion.

7) Nondimensional variables suggested by Ashby and Duval [1985] can be used in a log-scale plot of creep data. The master curves derived by them may be useful but the use of single master curve representation of creep data regardless of stress, temperature or grain size is strictly limited to low stress creep data. Due to damage accumulation, nondimensionalized creep curves deviate from Ashby and Duval's master creep curves. For high stress creep tests

represented in nondimensional variables, damage effect should be included.

8) In cyclic loading conditions the proposed damage model can describe the salient features of cyclic creep response of ice including hysteresis loops in stress-strain plots which is more significant as strain increases. The frequency of the cyclic load, maximum stress and possibly minimum stress affect the responses directly. But it is not yet clear what microstructural changes can occur in addition to microcracking during the cyclic loading. Further study is required.

9) Confining pressure greatly affects the mechanical properties of ice through the reduction of material damage. In general high confining pressure inhibits the opening of microcracks hence increases ductile behavior and also the strength of ice. The pressure sensitive behavior can not be seen at low strain-rate tests while at high strain-rate tests the strength of ice continously increases as confining pressure increases until an asymptotic value is attained. The model predicts that the deviatoric strengths under high confining pressure approach a maximum asymptotic values regardless of the magnitude of confining pressure for different strain-rates.

10) Biaxial failure envelopes in Figure 6.21 show rate dependent behavior in strength of ice where the failure strength in biaxial compression and biaxial tension tends to follow a von Mises yield criterion at low strain-rates but still compressive strength is slightly larger than tensile strength. At high strain-rates tensile strength slightly decreases with increase of strain-rate however the difference is very small so basically tensile strength reaches a

maximum value regardless of strain-rate. Compressive strength at high strain-rates shows a different behavior: the failure curve looks like a bell shape rather than a shifted oval shape usually seen in brittle materials.

7.3 RECOMMENDATIONS FOR FUTURE RESEARCH

Many aspects in the derivation of present constitutive model related to the prediction of ice deformation behavior need further study and experimental verification. A key development in this thesis lies in the multiaxial damage representation which can capture the general loading responses without much difficulty, however the model was applied here to somewhat simple loading conditions such as axisymmetric cases. Analysis of more complex stress paths may be undertaken in the future in conjunction with proper experimental efforts. Following recommendations are suggested for future research on the areas covered in this thesis:

1) In the area of practical application of the constitutive modelling, additional efforts should be directed on several structural problems including beam bending test, pure shear test, general biaxial test, and plane strain test etc. Proper definition on stress path should be established for constant strain-rate and constant stress tests.

2) The damage model should consider the effects of temperature, grain size variation whose profound influences are commonly observed in the natural state of ice. The present constitutive equations are

derived on the basis of constant temperature and uniform grain size assumption and the parameters of damage model are identified from experimental results. Formal thermodynamic formulation may be expanded to include these effects through additional internal variables.

3) The identification of damage parameters is a formidable task unless a systematic procedure for determination of parameters through a series of tests is developed. A simplified model using one damage mechanism is sought to reduce the number of parameters but some physical meaning may be lost.

4) A major effort in future study should be concentrated to extend the proposed continuum damage model to be implemented in the numerical computer program for solving various structural boundary value problems. The continuum behavior as well as the fracture characteristics must be considered in the modification.

References

Argon, A.S. ed., 1975, *Constitutive Equations in Plasticity*, The MIT Press, Cambridge.

Ashby, M.F., and Duval, P., 1985, "The Creep of Polycrystalline Ice," *Cold Regions Science and Technology*, Vol.11, pp. 285-300.

Ashby, M.F., and Frost, H.J., 1975, "The Kinetics of Inelastic Deformation above 0°K," *Constitutive Equations in Plasticity*, ed., A.S. Argon, pp. 117-147.

Betten, J., 1980, "Representation of Constitutive Equations in Creep Mechanics of Isotropic and Anisotropic Materials," *3rd IUTAM Symposium on Creep in Structures*, ed., A.R.S. Ponter and D.R. Hayhurst, Leicester, Great Britain, pp. 179-201.

Betten, J., 1981, "Damage Tensor in Continuum Mechanics," *147th European Mechanics Colloquium on Damage Mechanics*, Cachan, France, ed., J. Lemaitre.

Betten, J., 1986, "Applications of Tensor Functions to the Formulation of Constitutive Equations involving Damage and Initial Anisotropy," *Engineerring Fracture Mechanics*, Vol.25, pp. 573-584.

Bodner, S.R., 1981, "A Procedure for Including Damage in Constitutive Equations for Elastic-Viscoplastic Work-Hardening Materials," *IUTAM Symposium on Physical Nonlinearities in Structural Analysis*, ed., J. Hult, pp. 21-28.

Bodner, S.R., 1985, "Evolution Equations for Anisotropic Hardening and Damage of Elastic-Viscoplastic Materials," *Plasticity Today - Modelling, Methods and Applications*, ed., A. Sawczuk, pp. 471-482.

Bodner, S.R., and Chan, K.S., 1986, "Modeling of Continuum Damage for Application in Elastic-Viscoplastic Constitutive Equations," *Engineering Fracture Mechanics*, Vol.25, pp. 705-712.

Bodner, S.R., and Partom, Y., 1975, "Constitutive Equations for Elastic-Viscoplastic Strain-Hardening Materials," *Journal of Applied Mechanics*, Vol.42, pp. 385-389.

Broberg, H., 1974, "A New Criterion for Brittle Creep Rupture," *Journal of Applied Mechanics*, Vol.41, pp. 809-811.

Brown, R.L., 1987, "A Constitutive Equation for Sea Ice based on Microstructure and Irreverible Thermodynamics," *Proceedings of the 6th International Offshore Mechanics and Arctic Engineering Symposium*, Houston, Texas, Vol.IV, pp. 209-213.

Budiansky, B., and O'Connell, R.J., 1976, "Elastic Moduli of a Cracked Solid," *International Journal of Solids and Structures*, Vol.12, pp. 81-97.

Burt, N.J., and Dougill, J.W., 1977, "Progressive Failure in a Model Heterogeneous Medium," *ASCE Engineering Mechanics Division*, Vol.103, pp. 365-376.

Chaboche, J.-L., 1978, "Description Thermodynamique et Phénoménologique de la Viscoplasticité Cyclique avec Endommagement, Thèse, O.N.E.R.A.

Chaboche, J.-L., 1979, "Le Concept de Contrainte Effective Appliqué à l'Élasticité et à la Viscoplasticité en Présence d'un Endommagement Anisotrope," *Proceeding of the 115th European Mechanics Colloquium on Mechanical Behavior of Anisotropic Solids*, ed., J.P. Boehler, (in French) pp. 737-760.

Chaboche, J.-L., 1982, "Lifetime Predictions and Cumulative Damage under High-Temperature Conditions," *Symposium on Low-Cycle Fatigue and Life Prediction*, Firminy, France, ASTM STP 770, ed., C. Amzallag et al., pp. 81-104.

Chaboche, J.-L., 1984, "Anisotropic Creep Damage in the Framework of Continuum Damage Mechanics," *Nuclear Engineering and Design*, Vol.79, pp. 309-319.

Chen, W.F., and Saleeb, A.F., 1982, *Constitutive Equations for Engineering Materials*, Wiley and Sons, New York.

Chow, C.L., and Wang, J., 1987, "An Anisotropic Theory of Continuum Damage Mechanics for Ductile Fracture," *Engineering Fracture Mechanics*, Vol.27, pp. 547-558.

Cole, D.M., 1983, "The Relationship between Creep and Strength Behavior of Ice at Failure," *Cold Regions Science and Technology*, Vol.8, pp. 189-197.

Cole, D.M., 1985, "Grain Size and the Compressive Strength of Ice," *Proceedings of 4th International Offshore Mechanics and Arctic Engineering Symposium*, Dallas, Texas, Vol.II, pp. 220-226.

Cole, D.M., 1986, "Effect of Grain Size on the Internal Fracturing of Polycrystalline Ice," Cold Regions Research and Engineering Laboratory, Hanover, New Hampshire, Report 86-5.

Coleman, B.D., and Noll, W., 1963, "The Thermodynamics of Elastic Materials with Heat Conduction and Viscosity," *Archive for Rational Mechanics and Analysis*, Vol.4, pp. 167-178.

Coleman, B.D., and Gurtin, M.E., 1967, "Thermodynamics with Internal State Variables," *Journal of Chemical Physics*, Vol.47, pp. 597-613.

Cordebois, J.P., and Sidoroff, F., 1979, "Damage Induced Elastic Anisotrpy," *Proceedings of the 115th European Mechanics Colloquium on Mechanical Behavior of Anisotropic Solids*, ed., J.P. Boehler, pp. 761-774.

Currier, J.H., and Schulson, E.M., 1982, "The Tensile Strength of Ice as a Function of Grain Size," *Acta Metallurgica*, Vol.30, pp. 1511-1514.

Davison, L., and Stevens, A.L., 1972, "Continuum Measures of Spall Damage," *Journal of Applied Physics*, Vol.43, pp. 988-994.

Davison, L., and Stevens, A.L., 1973, "Thermomechanical Constitution of Spalling Elastic Bodies," *Journal of Applied Physics*, Vol.44, pp. 668-674.

Desai, C.S., and Siriwardane, H.J., 1984, *Constitutive Laws for Engineering Materials with Emphasis on Geologic Materials*, Prentice-Hall, Englewood Cliffs, New Jersey.

Dieter, G.E., 1961, *Mechanical Metallurgy*, McGrow-Hill, New York.

Dillon, O.W. Jr., 1976, "Some Experiments in Thermoviscoplasticity," *Constitutive Equations in Viscoplasticity: Phenomenological and Physical Aspects*, ed., K.C. Valanis, ASME Winter Annual Meeting, New York.

Domaschuk, L., Shields, D.H., and Rahman, M.G., 1987, "Effect of Hydrostatic Stress on Creep of a Frozen Sand," *Proceedings of the 6th International Offshore Mechanics and Arctic Engineering Symposium*, Houston, Texas, Vol.IV, pp. 119-124.

Dougill, J.W., 1975, "Some Remarks on Path Independence in the Small in Plasticity," *Quarterly of Applied Mathematics*, Vol.33, pp. 233-243.

Dougill, J.W., Lau, J.C., and Burt, N.J., 1976, "Towards a Theoretical Model for Progressive Failure and Softening in Rock, Concrete, and Similar Materials," *ASCE Engineering Mechanics Division*, University of Waterloo Press (1977), pp. 335-355.

Dragon, A., 1980, "Dilatational Creep in Rock-like Solids," *3rd IUTAM Symposium on Creep in Structures*, ed., A.R.S. Ponter and D.R. Hayhurst, Leicester, Great Britain, pp. 352-361.

Dragon, A., and Mroz, Z., 1979, "A Continuum Model for Plastic-Brittle Behavior of Rock and Concrete," *International Journal of Engineering Science*, Vol.17, pp. 121- 137.

Duval, P., 1981, "Creep and Fabrics of Polycrystalline Ice under Shear and Compression," *Journal of Glaciology,* Vol.27, pp. 129-140.

Dyson, B.F., Verma, A.K., and Szkopiak Z.C., 1981, "The Influence of Stress State on Creep Resistance: Experiments and Modelling," *Acta Metallurgica*, Vol.29, pp. 1573-1580.

Epifanov, V.P., 1984, "Failure Mechanisms of Ice in Relation to Temperature and Loading Rate," *Izv. AN SSSR., Mekhanika Tverdogo Tela*, Vol.19, pp. 188-196 (Mechanics of Solids, pp. 187-195, translated from Russian)

Fish, A.M., 1983, "Thermodynamic Model of Creep at Constant Stresses and Constant Strain Rates," Cold Rregions Research and Engineering Laboratory, Hanover, New Hampshire, Report 83-33.

Gao, Y.C., 1986, "Microcrack Damage," *Mechanics Research Communications*, Vol.13, pp. 231-237.

Glen, J.W., 1955, "The Creep of Polycrystalline Ice," *Proceeding of the Royal Society*, Series A, Vol.228, No.175, pp. 519-538.

Gold, L.W., 1958, "Some Observations on the Dependence of Strain on Stress of Ice," *Canadian Journal of Physics*, Vol.36, pp. 1236-1273.

Gold, L.W., 1960, "The Cracking Activity of Ice during Creep," *Canadian Journal of Physics*, Vol.38, pp. 1137-1148.

Gold, L.W., 1970, "Process of Failure in Ice," *Canadian Geotechnical Journal*, Vol.7, pp. 405-413.

Gold, L.W., 1972, "The Failure Process in Columnar-grained Ice," National Research Council, Canada, Technical paper No.369.

Hamza, H., 1985, "A Numerical Algorithm to Predict the Visco-Elastic Response of Ice under Different Loading Conditions," *Proceedings of the 4th International Offshore Mechanics and Arctic Engineering Symposium*, Dallas, Texas, Vol.II, pp. 177-185.

Hawkes, I., and Mellor, M., 1972, "Deformation and Fracture of Ice under Uniaxial Stress," *Journal of Glaciology*, Vol.11, pp. 103-131.

Hayhurst, D.R., 1972, "Creep Rupture under Multiaxial States of Stress," *Journal of the Mechanics and Physics of Solids*, Vol.20, pp. 381-390.

Hayhurst, D.R., and Felce, I.D., 1986, "Creep Rupture under Tri-Axial Tension," *Engineering Fracture Mechanics*, Vol.25, pp. 645-664.

Hayhurst, D.R., and Leckie, F.A., 1973, "The Effect of Creep Constitutive and Damage Relationships upon the Rupture Time of a Solid Circular Torsion Bar," *Journal of the Mechanics and Physics of Solids*, Vol.21, pp. 26-31.

Hayhurst, D.R., Trampczynski, W.A., and Leckie, F.A., 1980, "Creep Rupture under Non-proportional Loading," *Acta Metallurgica*, Vol.28, pp. 1171 -1183.

Haynes, F.D., 1973, "Tensile Strength of Ice under Triaxial Stresses," Cold Regions Research and Engineering Laboratory, Hanover, New Hampshire, Report 312.

Heverly, J.R., 1949, "Supercooling and Crystallization," *Transaction of American Geological Union*, Vol.30, pp. 205-210.

Holcomb, D.J., and Costin, L.S., 1986, "Detecting Damage Surfaces in Brittle Materials using Acoustic Emissions," *Journal of Applied Mechanics*, Vol.53, pp. 536-544.

Horii, H., and Nemat-Nasser, S., 1983, "Overall Moduli of Solids with Microcracks: Load-induced Anisotropy," *Journal of the Mechanics and Physics of Solids*, Vol.31, pp. 155-171.

Hooke, R.L. et al., 1980, "Mechanical Properties of Polycrystalline Ice: An Assessment of Current Knowledge and Priorities for Research," *Cold Regions Science and Technology*, Vol.3, pp. 263-275.

Hult, J., 1974, "Creep in Continua and Structures," *Topics in Applied Continuum Mechanics*, ed., J.L. Zeman and F. Zigler, Springer-Verlag, Wien, pp. 137-155.

Iwan, W.D., 1967, "On a Class of Models for the Yielding Behavior of Continuous and Composite Systems," *Journal of Applied Mechanics*, Vol.34, pp. 612-617.

Jacka, T.H., 1984, "The Time and Strain required for Development of Minimum Strain Rates in Ice," *Cold Regions Science and Technology*, Vol.8, pp. 261-268.

Jacka, T.H., and Maccagnan, M., 1984, "Ice Crystallographic and Strain Rate changes with Strain in Compression and Extension," *Cold Regions Science and Technology*, Vol.8, pp. 269-286.

Janson, J., and Hult, J., 1977, "Fracture Mechanics and Damage Mechanics, A Combined Approach," *Journal de Mécanique appliquée*, Vol.1, pp. 69-84.

Jones, S.J., 1978, "Triaxial Testing of Polycrystalline Ice," *Proceedings of the 3rd International Conference on Permafrost*, Edmonton, Canada, Vol.1, pp. 671-674.

Jones, S.J., 1982, "The Confined Compressive Strength of Polycrystalline Ice," *Journal of Glaciology*, Vol.28, pp. 171-176.

Jordaan, I.J., 1986, "Numerical and Finite Element Techniques in Calculation of Ice-structure Interaction," *Proceedings of IAHR Symposium on Ice*, Iowa City, Iowa, Vol.II, pp. 405-441.

Kachanov, L.M., 1958, "Time of the Rupture Process under Creep Conditions," *Izv. AN SSSR., Otd. Tekh. Nauk.*, No.8, pp. 26-31. (in Russian)

Kachanov, L.M., 1986, *Introduction to Continuum Damage Mechanics*, Martinus Nijhoff, Dordrecht.

Kachanov, M., 1984, "On a Continuum Modelling of Damage," *Proceedings of NATO Advanced Research Workshop on Application of Fracture Mechanics on Cementitious Composites*, Northwestern University, Evanstons, Illinois, ed., S.P. Shah, Dordrecht, Netherlands, pp. 521-531.

Karr, D.G., 1984, "Applications of Continuous Damage Models in Ice Mechanics," *Proceedings of the 4th International Conference on Applied Numerical Modeling*, Taiwan, pp. 73-77.

Karr, D.G., 1985, "A Damage Mechanics Model for Uniaxial Deformation of Ice," *Journal of Energy Resources Technology*, Vol.107, pp. 363-368.

Kestin, J., and Bataille, J., 1977, "Irreversible Thermodynamics of Continua and Internal Variables," *Continuum Models of Discrete Systems*, ed., J.W. Provan, University of Waterloo Press, pp. 39-67.

Kildow, J.T., 1984, "Arctic Policy I, Introduction," *Arctic Technology and Policy*, ed., I.Dyer and C. Chryssostomidis, Hemisphere Pub. Corp., pp. 41-44.

Krajcinovic, D., 1979, "Distributed Damage Theory of Beams in Pure Bending," *Journal of Applied Mechanics*, Vol.46, pp. 592-596.

Krajcinovic, D., 1983a, "Creep of Structure - A Continuous Damage Mechanics Approach," *Journal of Structural Mechanics*, Vol.11, pp. 1-11.

Krajcinovic, D., 1983b, "Constitutive Equations for Damaging Materials," *Journal of Applied Mechanics*, Vol.50, pp. 355-360.

Krajcinovic, D., 1984a, "Continuum Damage Mechanics," *Applied Mechanics Reviews*, Vol.37, pp. 1-6.

Krajcinovic, D., 1984b, "Mechanics of Solids with a Progressively Deteriorating Structure," *Proceedings of NATO Advanced Research Workshop on Application of Fracture Mechanics to Cementitious Composites*, Northwestern University, Evanstons, Illinois, ed., S.P. Shah, Dordrecht, Netherlands, pp. 453-479.

Krajcinovic, D., 1985, "Continuous Damage Mechanics Revisited: Basic Concepts and Definitions," *Journal of Applied Mechanics*, Vol.52, pp. 829-834.

Krajcinovic, D., and Fonseka, G.U., 1981, "The Continuous Damage Theory of Brittle Materials, Part 1: General Theory, Part 2: Uniaxial and Plane Response Modes, *Journal of Applied Mechanics*, Vol.48, pp. 809-824.

Krajcinovic, D., and Ilankamban, R., 1985, "Mechanics of Solids with Defective Microstructure," *Journal of Structural Mechanics*, Vol.13, pp. 267-282.

Krajcinovic, D., and Selvaraj, S., 1983, "Constitutive Equations for Concrete," *Proceedings of the International Symposium on Constitutive Laws for Engineering Materials: Theory and Applications*, Tucson, Arizona, pp. 399-406.

Krajcinovic, D., and Silva, M.A.G., 1982, "Statistical Aspects of the Continuous Damage Theory," *International Journal of Solids and Structures*, Vol.18, pp. 551-562.

Kratochvil, J., and Dillon, O.W. Jr., 1969, "Thermodynamics of Elastic-Plastic Materials as a Theory with Internal State Variables," *Journal of Applied Physics*, Vol.40, pp. 3207-3218.

Langdon, T.G., 1973, "Creep Mechanisms in Ice," *Physics and Chemistry of Ice*, ed., E. Whalley, pp. 356-361.

Leckie, F.A., 1978, "The Constitutive Equations of Continuum Creep Damage Mechanics," *Creep of Engineering Materials and of the Earth, Royal Society of London, Philosophical Transaction,* Series A, Vol.288, pp. 27-47.

Leckie, F.A., 1986, "The Micro- and Macromechanics of Creep Rupture," *Engineering Fracture Mechanics*, Vol.25, pp. 505-521.

Leckie, F.A., and Hayhurst, D.R., 1974, "Creep Rupture of Structure," *Royal Society of London, Proceedings*, Series A, Vol.340, pp. 323-347.

Leckie, F.A., and Hayhurst, D.R., 1977, "Constitutive Equations for Creep Rupture," *Acta Metallurgica*, Vol.25, pp. 1059-1070.

Leckie, F.A., and Onat, E.T., 1981, "Tensorial Nature of Damage Measuring Internal Variables," *IUTAM Symposium on Physical Nonlinearities in Structural Analysis*, ed., J. Hult, pp. 140-155.

Lee, R.W., and Schulson, E.M., 1986, "The Strength and Ductility of Ice under Tension," *Proceedings of the 6th International Offshore Mechanics and Arctic Engineering Symposium*, Houston, Texas, Vol.IV, pp. 298-302.

Legendre, D., and Mazars, J., 1984, "Damage and Fracture Mechanics for Concrete (A Combined Approach)," *International Conference on Fracture (ICF6)*, New Delhi, India, *Advances in Fracture Research*, ed., S.R. Valluri et al., Pergamon, New York, Vol.4, pp. 2841-2848.

Lemaitre, J., 1984, "How to use Damage Mechanics" *Nuclear Engineering and Design*, Vol.80, pp. 233-245.

Lemaitre, J., 1985, "A Continuous Damage Mechanics Model for Ductile Fracture," *Journal of Engineering Materials and Technology*, Vol.107, pp. 83-89.

Lemaitre, J., 1986, "Local Approach of Fracture," *Engineering Fracture Mechanics*, Vol.25, pp. 523-537.

Lemaitre, J., and Chaboche, J.-L., 1974, "A Nonlinear Model of Creep-Fatigue Damage Cumulation and Interaction," *Proceedings of IUTAM Symposium on Mechanics of Viscoelastic Media and Bodies*, Springer Verlag, Gothenburg.

Lemaitre, J., and Chaboche, J.-L., 1978, "Phenomenological Approach of Damage Rupture," *Journal de Mécanique appliquée*, Vol.2, No.3, pp. 317-365.

Levy, A.J., 1985, "A Physically Based Constitutive Equation for Creep-Damaging Solids," *Journal of Applied Mechanics*, Vol.52, pp. 615-620.

Loland, K.E., 1980, "Continuous Damage Model for Load-Response Estimation of Concrete," *Cement and Concrete Research*, Vol.10, pp. 395-402.

Malvern, L.E., 1969, *Introduction to the Mechanics of a Continuous Medium*, Prentice-Hall, Englewood Cliffs, New Jersey.

Mazars, J., 1981, "Mechanical Damage and Fracture of Concrete Structures," *International Conference on Fracture (ICF5)*, Cannes, France, *Advances in Fracture Research*, ed., D. Francois, Pergamon, New York, Vol.4, pp. 1499-1506.

Mazars, J., 1986, "A Description of Micro- and Macroscale Damage of Concrete Structures," *Engineering Fracture Mechanics*, Vol.25, pp. 729-737.

Mazars, J., and Lemaitre, J., 1984, "Application of Constitutive Damage Mechanics to Strain and Fracture Behavior of Concrete," *Proceedings of NATO Advanced Research Workshop on Application of Fracture Mechanics on Cementitious Composites*, Northwestern University, Evanstons, Illinois, ed., S.P. Shah, Dordrecht, Netherlands, pp. 507-520.

Mellor, M., 1983, "Mechanical Behavior of Sea Ice," Cold Regions Research and Engineering Laboratory, Hanover, New Hampshire, Monograph 83-1.

Mellor, M., and Cole, D.M., 1981, "Cyclic Loading and Fatigue in Ice," *Cold Regions Science and Technology*, Vol.4, pp. 41-53.

Mellor, M., and Cole, D.M., 1982, "Deformation and Failure of Ice under Constant Stress or Constant Strain-rate," *Cold Regions Science and Technology*, Vol.5, pp. 201-219.

Mellor, M., and Cole, D.M., 1983, "Stress/Strain/Time Relations for Ice under Uniaxial Compression," *Cold Regions Science and Technology*, Vol.6, pp. 207-230.

Michel, B., 1978a, "A Mechanical Model for Creep of Polycrystalline Ice," *Canadian Geotechnical Journal*, Vol.15, pp. 155-170.

Michel, B., 1978b, *Ice Mechanics*, Les Presses De L'universite Laval, Quebec, Canada.

Michel, B., and Ramseier, R., 1971, "Classification of River and Lake Ice," *Canadian Geotechnical Journal*, Vol.8, pp. 38-45.

Morland, L.W., and Spring, U., 1981, "Viscoelastic Fluid Relation for the Deformation of Ice," *Cold Regions Science and Technology*, Vol.4, pp. 255-268.

Mroz, Z., and Angelillo, M., 1982, "Rate-dependent Degradation Model for Concrete and Rock," *International Symposium on Numerical Models in Geomechanics*, Zurich, Swiss, pp. 208-217.

Murakami, S., 1983, "Notion of Continuum Damage Mechanics and its Application to Anisotropic Creep Damage Theory," *Journal of Engineering Materials and Technology*, Vol.105, pp. 99-105.

Murakami, S., 1988, "Mechanical Modelling of Material Damage," *Journal of Applied Mechanics*, Vol.55, pp. 280-286.

Murakami, S., and Ohno, N., 1981, "A Continuum Theory of Creep and Creep Damage", *3rd IUTAM Symposium on Creep in Structures*, eds., A.R.S. Ponter and D.R. Hayhurst, Springer-Verlag, pp. 422-444.

Murakami, S., and Sanomura, Y., 1985, "Creep and Creep damage of Copper under Multiaxial States of Stress," *Plasticity Today - Modelling, Methods and Applications*, ed., A. Sawczuk, pp. 535-551.

Murakami, S., and Sanomura, Y., 1986, "Analysis of the Coupled Effect of Plastic Damage and Creep Damage in Nimonic 80A at Finite Deformation," *Engineering Fracture Mechanics*, Vol.25, pp. 693-704.

Murakami, S., Sanomura, Y., and Hattori, M., 1985, "Modelling of the Coupled Effect of Plastic Damage and Creep Damage in Nimonic 80A," *International Journal of Solids and Structures*, Vol.22, pp. 373-386.

Murat, J.R., and Lainey, L.M., 1982, "Some Experimental Observations on the Poisson's Ratio of Sea Ice," *Cold Regions Science and Technology*, Vol.6, pp. 105-113.

Nadai, A., 1950, *Theory of Flow and Fracture of Solids*, McGrow-Hill, Vol.1 and 2, revised edition, New York.

Nadreau, J.-P., and Michel, B., 1986, "Yield and Failure Envelope for Ice under Multiaxial Compressive Stresses," *Cold Regions Science and Technology*, Vol.13, pp. 75-82.

Nilsson, L., 1979, *Impact Loading on Concrete Structures*, Chalmers University of Technology, Publication 79:1.

Ohno, N., Murakami, S., and Ueno, T., 1985, "A Constitutive Model of Creep Describing Creep Recovery and Material Softening Caused by Stress Reversals," *Journal of Engineering Materials and Technology*, Vol.107, pp. 1-6.

Onat, E.T., 1982, "Representation of Inelastic Behavior in the Presence of Anisotropy and of Finite Deformations," *Recent Advances in Creep and Fracture of Engineering Materials and Structures*, eds., B. Wilshire and D.R.J. Owen, Pineridge Press, Swansea, UK, pp. 231-264.

Onat, E.T., 1986, "Representation of Mechanical Behavior in the Presence of Internal Damage," *Engineering Fracture Mechanics*, Vol.25, pp. 605-614.

Pipkin, A.C., and Rivlin, R.S., 1959, "The Formulation of Constitutive Equations in Continuum Physics I," *Archive of the Rational Mechanics and Analysis*, Vol.4, pp. 129-144.

Polar Research Board, 1985, *National Issues and Research Priorities in the Arctic*, National Research Council, Washington.

Rabotnov, Y.N., 1963, "On the Equations of State for Creep," *Progress in Applied Mechanics*, Prager Anniversary Volume, MacMillan, New York, pp. 307-315.

Rabotnov, Y.N., 1969, *Creep Problems in Structural Members*, North-Holland, Amsterdam.

Rabotnov, Y.N., 1971, "Creep Rupture under Stress Concentration," *Advances in Creep Design*, ed., A.I. Smith and A.M. Nicolson, pp. 3-19.

Rice, J.R., 1971, "Inelastic Constitutive Relations for Solids: An Internal Variable Theory and its Application to Metal Plasticity," *Journal of the Mechanics and Physics of Solids*, Vol.19, pp. 433-455.

Rice, J.R., 1975, "Continuum Mechanics and Thermodynamics of Plasticity in Relation to Microscale Deformation Mechanics," *Constitutive Equations in Plasticity*, ed., A.S. Argon, pp. 23-79.

Richter-Menge, J.A., 1987, "Confined Compressive Strength of Horizontal First-year Sea Ice Samples," *Proceedings of the 6th International Offshore Mechanics and Arctic Engineering Symposium*, Houston, Texas, Vol.IV, pp. 197-207.

Schulson, E.M., 1979, "An Analysis of the Brittle to Ductile Transition in Polycrystalline Ice under Tension," *Cold Regions Science and Technology*, Vol.1, pp. 87-91.

Schulson, E.M., and Cannon, N.P., 1984, "The Effect of Grain Size on the Compressive Strength of Ice," *Proceedings of the IAHR Symposium on Ice*, Hamburg, Germany, pp. 29-38.

Schulson, E.M., Lim, R.N., and Lee, R.W., 1984, "A Brittle to Ductile Transition in Ice under Tension," *Philosophical Magazine,* Series A, Vol.49, pp. 353-363.

Sidoroff, F., 1981, "Description of Anisotropic Damage Application to Elasticity," *IUTAM Symposium on Physical Nonlinearities in Structural Analysis*, ed., J. Hult, pp. 237-244.

Sinha, N.K., 1977, "Dislocations in Ice as Revealed by Etching," *Philosophical Magazine*, Vol.36, pp. 1385-1404.

Sinha, N.K., 1978a, "Rheology of Columnar-grained Ice," *Experimental Mechanics*, Vol.18, pp. 464-470.

Sinha, N.K., 1978b, "Short-Term Rheology of Polycrystallice Ice," *Journal of Glaciology*, Vol.21, pp. 457-473.

Sinha, N.K., 1979, "Grain Boundary Sliding in Polycrystalline Materials," *Philosophical Magazine*, Series A, Vol.40, pp. 825-842.

Sinha, N.K., 1982a, "Acoustic Emission and Microcracking in Ice," *Proceedings of the SESA, Japan Society of Mechanical Engineering*, pp. 767-772.

Sinha, N.K., 1982b, "Delayed Elastic Strain Criterion for First Cracks in Ice," *IUTAM conference on Deformation and Failure of Granular Materials*, Delft, Netherlands, pp. 323-330.

Sinha, N.K., 1984a, "Intercrystalline Cracking, Grain-Boundary Sliding and Delayed Elasticity at High Temperatures," *Journal of Materials Science*, Vol.19, pp. 359-376.

Sinha, N.K., 1984b, "Delayed-Elastic Model for Initiation and Accumulation of Creep Cavitation at High Temperatures," *Proceedings of the 6th International Conference on Fracture, Advances in Fracture Research*, New Delhi, India, Pergamon Press, pp. 2295-2302.

Sinha, N.K., 1987, "Effective Poisson's Ratio of Isotropic Ice," *Proceedings of the 6th International Offshore Mechanics and Arctic Engineering Symposium*, Houston, Texas, Vol.IV, pp. 189-195.

Sjölind, S.-G., 1987, "A Constitutive Model for Ice as a Damaging Visco-Elastic Material," *Cold Regions Science and Technolgoy*, Vol.41, pp. 247-262.

Spring, U., and Morland, L.W., 1982, "Viscoelastic Solid Relations for the Deformation of Ice," *Cold Regions Science and Technology*, Vol.5, pp. 221-234.

St. Lawrence, W.F., and Cole, D.M., 1982, "Acoustic Emissions from Polycrystalline Ice," *Cold Regions Science and Technology*, Vol.5, pp. 183-199.

Suaris, W., 1983, "Dynamic Behavior of Concrete," Ph.D. dissertation, Northwestern University.

Suaris, W., and Shah, S.P., 1984, "Rate-Sensitive Damage Theory for Brittle Solids," *ASCE Journal of Engineering Mechanics*, Vol.110, pp. 985-997.

Szyszkowski, W., Dost, S., and Glockner, P.G., 1985, "A Nonlinear Constitutive Model for Ice," *International Journal of Solids and Structures*, Vol.21, pp. 307-321.

Szyszkowski, W., and Glockner, P.G., 1987, "Modelling the Mechanical Properties of Ice," *Preceedings of the 6th International Offshore Mechanics and Arctic Engineering Symposium*, Houston, Texas, Vol.IV, pp. 159-165.

Tai, W.H., and Yang, B.X., 1986, "A New Microvoid-Damage Model for Ductile Fracture," *Engineering Fracture Mechanics*, Vol.25, pp. 377-384.

Talreja, R., 1983, "A Continuum Mechanics Characterization of Damage in Composite Materials," The Danish Center for Applied Mathematics and Mechanics, Report No.268.

Timco, G.W., and Frederking, R.M.W., 1984, "An Investigation of the Failure Envelope of Granular/Discontinuous Columnar Sea Ice," *Cold Regions Science and Technology*, Vol.9, pp. 17-27.

Timco, G.W., and Frederking, R.M.W., 1986, "Confined Compression Tests: Outlining the Failure Envelope of Columnar Sea Ice," *Cold Regions Science and Technology*, Vol.12, pp. 13-28.

Ting, S.-K., and Shyam Sunder, S., 1985, "Constitutive Modelling of Sea Ice with Applications to Indentation Problems," MIT SCEOE Research Report No.3.

Tomin, M.J., Cheung, M., Jordaan, I.J., and Cormeau, A., 1986, "Anaysis of Failure Modes and Damage Processes of Freshwater Ice in Indentation Tests," *Proceedings of the 5th International Offshore Mechanics and Arctic Engineering Symposium*, Tokyo, Japan, Vol.IV, pp. 453-460.

Traetteberg, A., Gold, L.W., and Frederking, R.M.W., 1975, "The Strain-rate and Temperature Dependence of Young's Modulus of Ice," *Proceedings of the 3rd IAHR International Symposium on Ice Problems*, Hanover, New Hampshire, pp. 479-486.

Vakulenko, A.A., and Kachanov, M.L., 1971, "Continual Theory of a Medium with Cracks," *Izv. AN SSSR., Mekhanika Tverdogo Tela,* Vol.6, pp. 159-166, (Mechanics of Solids, pp. 145-151, traslated from Russian).

Vinogradov, A.M., 1987, "Constitutive Modeling of Ice," *Proceedings of the 6th International Offshore Mechanics and Arctic Engineering Symposium*, Houston, Texas, Vol.IV, pp. 181-188.

Wang, Y.S., 1981, "Uniaxial Compression Testing of Arctic Sea Ice," *Proceedings of the 6th International Conference on Port and Ocean Engineering under Arctic Conditions*, Quebec, Canada, Vol.1, pp. 346-355.

Wang, Y.S., 1982, "A Rate-dependent Stress-strain Relationship for Sea Ice," *Proceedings of the 1st Offshore Mechanics/ Arctic Engineering/ Deepsea Systems Symposium*, New Orleans, Lousiana, Vol.II, pp. 243-248.

Weeks, W.F., and Assur, A., 1968, "Fracture of Lake and Sea Ice," *Fracture - An Advanced Treatise*, ed., H. Liebowitz, Vol.7, pp. 879-978.

Weertman, J., 1973, "Creep of Ice," *Physics and Chemistry of Ice*, ed., E. Whalley, pp. 320-337.

Wu, M.S., 1986, "Continuum Modelling of Sea Ice," Master thesis, Massachusetts Institute of Technology.

APPENDIX

A.1 GENETIC CLASSIFICATION OF ICE

The microstructure and textures of ice samples can be observed from thin sections placed under polarized light. The grain size and crystallographic orientation of the c-axis greatly influence the mechanical properties of ice [from Michel and Ramselier, 1971; Michel, 1978b].

Primary Ice (ice formed initially)

P1 (calm surface, small temperature gradient)
c-axis preferred vertical; crystal size large to extra large; crystal boundaries of irregular shape.

P2 (calm surface, large temperature gradient)
c-axis orientation random to preferred vertical superimposed on random; crystal size medium to extra large; crystal shape tabular or needle.

P3 (agitated surface, nucleated from frazil)
c-axis orientation random; crystal size fine to medium; crystal shape tabular and equiaxed.

P4 (initiated by snow)
c-axis orientation random; crystal size fine to medium; crystal shape equiaxed.

Secondary Ice (developed from the primary ice)

S1 columnar grained; c-axis orientation vertical; crystal size increases with depth, usually large to extra large; grain shape irregular.

S2 columnar grained; c-axis orientation preferred horizontal; grain size fine to large, increasing more rapidly with depth than S1 ice.

Tertiary Ice (superimposed on top of the primary ice)

T1 (snow ice)

c-axis orientation random; grains equiaxed; grain size fine to medium.

Grain Size

fine grain diameter less than 1 mm.

medium grain diameter between 1 and 5 mm.

large grain diameter between 5 and 20 mm.

extra large grain diameter greater than 20 mm.